Activation of molecules by mono and multimetallic complexes! : A theoretical approach

Yan Yang

Université Fédérale
Toulouse Midi-Pyrénées

THÈSE

En vue de l'obtention du
DOCTORAT DE L'UNIVERSITÉ DE TOULOUSE

Délivré par l'Université Toulouse 3 - Paul Sabatier

Présentée et soutenue par

Yan YANG

Le 17 décembre 2021

Activation de molécules par des complexes mono et multimétalliques ! Une approche théorique

Ecole doctorale : **SDM - SCIENCES DE LA MATIERE - Toulouse**

Spécialité : **Physico-Chimie Théorique**

Unité de recherche :
LPCNO-IRSAMC - Laboratoire de Physique et Chimie des Nano-Objets

Thèse dirigée par
Laurent MARON et Iker DEL ROSAL

Jury

M. Marc Visseaux, Rapporteur
M. Christophe Thomas, Rapporteur
Mme Blanca Martin-Vaca, Examinatrice
M. Laurent MARON, Directeur de thèse

Résumé

Au cours de cette thèse, nous sommes intéressés à l'étude théorique de l'activation de petites molécules telles que CO_2, H_2, N_2 par des complexes métalliques impliquant des métaux s, d ou encore f. Ce travail a été réalisé en proche collaboration avec des groupes expérimentaux. Le contrôle de la réactivité de ces petites molécules reste un challenge important pour l'industrie chimique mais aussi d'un point de vue sociétal avec par exemple le réchauffement climatique. Nous avons utilisé des techniques de calcul théoriques de mécanisme réactionnels basés sur la théorie de la fonctionnelle de la densité afin de comprendre, expliquer voire prédire l'activité de complexes métalliques vis-à-vis de ces petites molécules. Nous avons par exemple pu montrer que la réduction de O_2 par des complexes bimétalliques de fer(II) pouvait se réaliser sous des conditions expérimentales douces par un transfert monoélectronique de chacun des deux centres métalliques. Ce travail a été réalisé en collaboration avec l'équipe du Professeur LaPierre à Atlanta. En collaboration avec le groupe du Professeur Piers à l'université de Calgary, nous avons pu montrer qu'une simple modification d'un ligand sur des complexes de fer ou de cobalt pouvait conduire soit à l'activation facile de la molécule de dioxygène soit à l'activation de la molécule d'ammoniaque (NH_3). Ces deux résultats ont marquants car ils montrent que l'on peut facilement moduler la réactivité de complexes de métaux de transition pour permettre ou non d'activer des molécules aussi inertes que O_2 ou NH_3. Nous avons aussi pu montrer en collaboration avec l'équipe du Professeur Okuda d'Aachen qu'un complexe bimétallique d'hydrure de calcium pouvait réagir avec la molécule de CO et ainsi le fonctionnaliser. Ce travail est une première approche d'une réaction de type Fischer-Tropsch à partir de composé moléculaire.

Mots clés: Activation de petites molécules, Théorie fonctionnelle de la densité, Complexes métalliques, Réactivité

Abstract

During this thesis, we are interested in the theoretical study of the activation of small molecules such as CO_2, H_2, N_2 by metal complexes involving s, d or f metals. This work has been done in close collaboration with experimental groups. The control of the reactivity of these small molecules remains an important challenge for the chemical industry but also from a societal point of view with for example the global warming. We have used theoretical calculation techniques of reaction mechanisms based on density functional theory to understand, explain and even predict the activity of metal complexes towards these small molecules. For example, we were able to show that the reduction of O_2 by bimetallic iron(II) complexes could be achieved under mild experimental conditions by a monoelectronic transfer of each of the two metallic centers. This work was carried out in collaboration with the team of Professor LaPierre in Atlanta. In collaboration with Professor Piers' group at the University of Calgary, we were able to show that a simple modification of a ligand on iron or cobalt complexes could lead to either the easy activation of the oxygen molecule or the activation of the ammonia (NH_3) molecule. These two results are significant because they show that the reactivity of transition metal complexes can be easily modulated to allow or not the activation of molecules as inert as O_2 or NH_3. We were also able to show in collaboration with the team of Professor Okuda from Aachen that a bimetallic complex of calcium hydride could react with the CO molecule and thus functionalize it. This work is a first approach of a Fischer-Tropsch type reaction starting from a molecular compound.

Keywords: Small molecule activation, Density functional theory, Metal complexes, Reactivity

Achnowledgements

On the completion of this doctoral thesis, I would like to express my sincerest gratitude to my supervisor, experimental collaborators, colleagues, friends, and relatives who have helped me in scientific research and daily life.

First of all, I would like to sincerely thank my supervisor, Prof. Laurent Maron. When I first left China for my PhD in France with anxiety, it was Laurent's kindness and friendliness that allowed me to start my research life step by step in an orderly way. Laurent's kindness and friendliness allowed me to start my research life step by step in an orderly manner, and I have been grateful for Laurent's patience in guiding my project every day for three years. However 2019 covid came out of nowhere and everyone's life was disrupted, leaving me in a bad place mentally. Without Laurent, I think I would have had a hard time finishing my PhD. I would like to send my sincere thanks to Laurent.

I would also like to thank all the experimental collaborators I have worked with. It was their perfect experimental results that gave me the computational possibilities. In particular, our collaborator Prof. Professor Jaroschik Jaroschik, who not only gave me a lot of advice during the research, but also gave me advice for my thesis.

I would also like to thank every lab colleagues who have helped me so much, whether in life, research, or language. Every one of them is so friendly and warm.

I would like to thank my parents most of all for their continuous trust and support that allowed me to study abroad for my PhD. Their love has always been with me. And my boyfriend Luo, who takes care of me in daily life and comforts me with delicious meals. And all of my friends I met in Toulouse, Yifan, Bingqian, Weilei, Xiner and orthers, they gave me a lot of support.

Finally, I would like to thank the China Scholarship Council for funding me.

CONTENTS

Chapter I

Introduction

I.1. Research and development of coordination complexes

Coordination complexes are widely used in daily life, industrial production and life science research. The study of these complexes is one of the most active and growing frontier disciplines in chemis[1] because of its multidisciplinarity and the wide range of subjects it covers. Its main research content is the characteristics of metal ions reacting with inorganic/organic ions/molecules to form coordination complexes, as well as the studies of their bonding, structure, reaction, classification and preparation. It is generally believed that a complex is a compound formed by a certain composition and spatial configuration of ligands such as ions (Cl^-, CN^-, …) or molecules (NH_3, H_2O,...) around a central metal atoms/ions [1, 3, 4]. Because of their various spatial structures, valence bonds and peculiar physical, chemical and biological properties, the coordination complexes are of great importance to the further development of both fundamental and applied chemistry[1].

In general, according to the nature of the ligands surrounding the central metal atom, we can classify the complex into conventional (inorganic), organometallic, and bioinorganic complexes. Inorganic complexes mainly refer to compounds whose ligands are ions or molecules bounded to the metal center through an electron lone pair donation of one or more ligand atoms[3]. Organometallic complexes generally refer to compounds with metal-carbon bonds and the ligands are organic groups[5-7]. Finally, as an interdisciplinary subject, bioinorganic chemistry is a major research direction. In bioinorganic complex, the ligands around the metal center are of natural origin such as metalloenzymes, porphyrins, ...[8]

Historically, coordination chemistry is a very important branch developed on the basis of inorganic chemistry. In 1798, Tazzaret in France accidentally discovered that cobalt salt could be converted into $CoCl_3 \cdot 6NH_3$ in NH_4Cl and $NH_3 \cdot H_2O$ solution. Tazzaret's original experimental scheme was to form cobalt hydroxide precipitation from cobalt divalent ions, and then recombustion cobalt hydroxide to form cobalt oxide to measure the content of Co^{2+}. When NaOH was replaced by $NH_3 \cdot H_2O$, he inadvertently found that orange crystal $[Co(NH_3)_6]Cl_3$ was generated. The appearance of orange crystal marks the gradual entry of coordination chemistry into people's sight[1,

9]. In the following 100 years, people used the method of measuring molar conductivity to study the properties of such substances, thereby deriving the number of ions contained in each compound molecule. During this period, the accumulation of many experiments laid the foundation for coordination chemistry, but it has not been explained theoretically. Until 1893, Werner proposed coordination theory. The true meaning of coordination chemistry has since been established. However, Werner's theory is still unable to explain well the nature of the primary valence state and secondary valence state. Then Sidgwick proposed the Effective Atomic Number (EAN) rule in 1923. That is, the sum of the number of valence electrons of the central atom and the number of electrons donated by the ligand should be equal to the atomic number of the inert atom following it in the periodic table. It revealed the main relationship between the electron number and the coordination number of the central atom, further enriching the coordination theory[10].

In 1951, the research of Pauson and Miller broke the boundary between traditional inorganic and organic compounds and synthesized ferrocene, from which coordination chemistry has gradually leaped from inorganic complexes to a new field of metal-organic chemistry[1, 2]. The development of organometallic chemistry in the 60's of the 20th century surpasses the traditional boundary between inorganic chemistry and organic chemistry, making the great barrier between the traditional organic chemistry and inorganic chemistry gradually dissolve. Metal-organic complexes with various structural forms and unique physical and chemical properties have been synthesized and widely usedin pharmaceutical synthesis and chemical production., mainly as catalysts to increase the rate of such reactions.

With the development of many new characterization methods (such as X-ray crystal diffraction, nuclear magnetic resonance (NMR), mass spectrometry (MS), photoelectron spectroscopy (PES), electron spin resonance (ESR) or electron paramagnetic resonance (EPR) spectroscopy, etc.), the characterization and application of complexes conditions are created[12]. At the same time, it also brings development prospects to emerging research fields such as nanocoordination chemistry, photocoordination chemistry, and coordination supramolecular chemistry. Therefore, the study of complexes has been gradually expanded to polydentate chelates (β-

diketone complexes), polynuclear complexes, organometallic π-complexes (Zeise salts), metal clusters, macrocyclic complexes, and even all kinds of biomimics complexes[12].

Based on the experimental study of complexes, some simple theories emerged, such as: the simple Lewis acid-base concept, the valence bond theory, the ligand field theory[13-15], and semi-empirical and ab initio molecular orbital theory[16, 17]. Moreover, some theories can help us to study the reaction mechanism of complexes from the perspective of thermodynamics and kinetics, such as the electron transfer theory of Taube and Marcus[18-21], the rapid reaction study of Eigen[22, 23], the substitution mechanism of Basolo and Pearson[24], and the photochemical study of Adamson et al.[25-27].

With the development of science and technology, functional complexes with peculiar properties will be paid more and more attention by chemists. There are a wide variety of complexes with excellent properties, especially in [1, 28-30].:

- Analytical chemistry : can be used as ion exchanger, titrant, precipitating agent, extraction agent, chromogenic agent, masking agent and metal indicator, ...
- Catalytic chemistry : can be used as an effective catalyst for a variety of reactions
- Energy chemistry : such as the development of the solar energy conversion, molecular optoelectronic devices and battery research
- Materials chemistry : such as magnetic materials, superconducting materials, excellent nonlinear optical materials and nonlinear conductive material, ...
- Biochemistry : mainly studies reveal the interaction between metal ions and biological systems, such as protein markers of fluorescent probe design
- Pharmaceutical chemistry : such as marine design synthesis of coordination compound drugs, cancer drugs and new medical preparations such as MRI contrast agents
- Important application in the field of electroplating industry, etc

And various metal complexes have huge research content in each different field, especially in the field of catalytic chemistry. But from the perspective of green

chemistry, the activation of small molecules such as hydrogen molecules, oxygen molecules, carbon monoxide, and carbon dioxide is particularly important.

I.2. Small molecule activation catalyzed by metal complexes

The essence of chemical reaction is the rearrangement of bonding electrons to break old bonds and form new bonds. How to achieve the rupture and synthesis of chemical bonds with high activity and selectivity is the pursuit of researchers for a long time. However, small molecules usually have very high bond dissociation energy, such as inorganic or organic small molecules containing C≡O, N≡N, C = O, O=N, C-H, C-C, O-H and H-H bonds. Therefore, how to activate small molecules has become an interesting research field. Thus these kinds of small molecules can be used as basic precursors of chemical products or basic reagents of chemical reactions, and become more and more important in the development of green chemical industry and energy economy.

Therefore, activation of small molecules is widely used in pharmaceutical chemistry and chemical synthesis. For example, acetylene and propyne in petroleum cracked gas can be partially hydrogenated through catalyst to produce high-purity ethylene and propylene; or as the most important carbon source in the chemical industry, carbon monoxide and carbon dioxide are activated to generate methanol, methane, formic acid, and carbon. Green energy products such as acid salts. Due to the different structures and application fields of each small molecule, the activation of each small molecule has its own characteristics, and there is no unified activation mode. For example, the use of carbon dioxide in industrial applications remains rare due to the low reactivity of this molecule. Few reactions involving CO_2 are thermodynamically feasible. A very promising approach to promote its activation is its coordination to transition metal complexes. Indeed, the coordination of CO_2 to metal centers decreases the activation energy necessary to perform many catalytic reactions. It is therefore possible to transform this "inert" molecule into useful chemicals. Although we are unable to make a systematic generalization of a unified reaction model for small molecule activation, we can nevertheless understand the reactions that can take place between these molecules and metal complexes.

I.2.1. Oxidative addition reaction

The oxidative addition reaction of metal complex refers to the reaction of a molecule X-Y with a metal complex M^nL_m to form $XM^{(n+2)}YL$. In this reaction, the original X-Y bond breaks, resulting in the formation of new M-X and M-Y bonds . Then the valence state of the metal increases by 2 and the coordination number also increases by 2 (scheme 1.1). Thus, in order to perform the oxidative addition process, the starting metal complex must be electronically and coordinatively unsaturated or formed by the dissociation of a two-electron donor ligand prior to the oxidative addition step and the metal must have a stable oxidation state that is two units higher. A high variety of substrates, including both electrophilic and non-electrophilic molecules, are susceptible to be used in oxidative addition processes. The higher the electron cloud density is, the more favorable the oxidation addition reaction is[31-33].

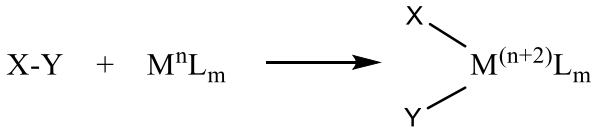

Scheme 1.1 Oxidative addition reaction

Oxidation addition reactions can also occur on binuclear metal complexes. In this case, each of the two metals changes its oxidation state, electron count and coordination number by 1 unit instead of 2. The total number of electrons in the coordination layer of the metal atom remains unchanged (Eq2).

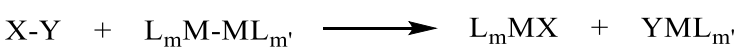

Scheme 1.2 Oxidative addition reaction on bimetallic complex

I.2.2. Insertion reaction

The reaction in which the unsaturated group Y is inserted into the adjacent metal-ligand bond is called the insertion reaction. The insertion reaction is reversible. An insertion reaction is actually the migration of an adjacent group on the metal to an unsaturated group, and the forming a vacancy, which is supplemented by other ligands,

as shown in the following equation[34-36]. Among them, Y=CO, C_2H_4, C_2H_2, C_6H_6 and cyclopentadienyl, etc.; X=H, R and C(O)R, etc.; L=Lewis base, solvent, PR_3, NR_3 and R2O, etc. (Eq3)

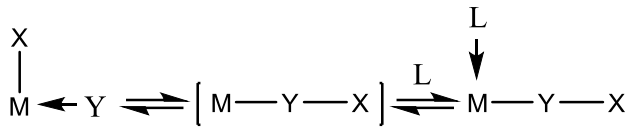

Scheme 1.3 Insertion reaction

There are two common insert geometrys **1,1** and **1,2**, of which **1,2** insert is more popular.

1, 1 insert:

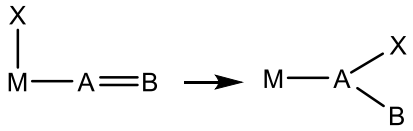

Scheme 1.4 1,1 insertion reaction

1, 2 insert:

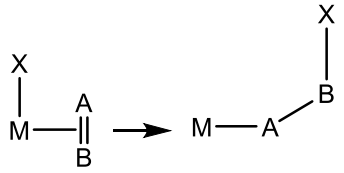

Scheme 1.5 1,2 insertion reaction

The characteristic of the insertion reaction is that the oxidation state of the central metal does not change. The migration and insertion groups must be on ortho position; The insertion reaction results in the creation of a vacancy; If the migration group X is chiral, its configuration stays the same[36, 37].

I.2.3. Reductive elimination reaction

Reductive elimination is the reverse reaction of oxidative addition. In this case, the oxidation state of the metal is reduced by two (or one, in a bimetallic reaction). By

reduction elimination, the complex removes two cis-ligands from the central metal atom be combining it to form a stable compound. [31, 33, 38].

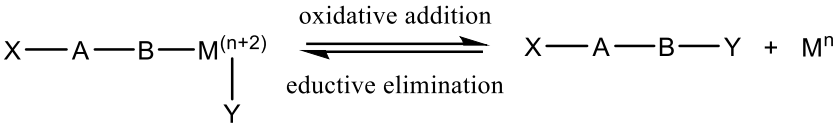

Scheme 1.6 Reductive elimination reaction

I.2.4. Coordination and dissociation of ligands

Ligand coordination refers to the process in which ligands with a pair of electrons form coordination bonds with metal. Ligand dissociation is the process by which the ligand detach from the metal with a pair of electrons. Different ligands can be exchanged in two ways:

- Associative mechanism in which the new ligand binds and then the old one leaves.

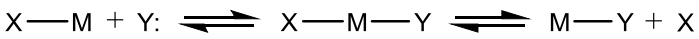

Scheme 1.7 Associative mechanism

- Dissociative mechanism in which the old ligand leaves and then the new one binds.

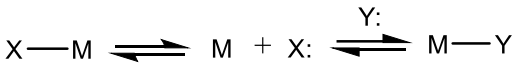

Scheme 1.8 Dissociative mechanism

In homogeneous complexation catalytic reactions, metal complexes often dissociate to form a coordination site as shown in Schem1.8, and then the substrate molecules are activated by coordination[39-41].

I.3. Overview of the activation of small molecules by different metal complexes

With the further development of science and technology, the research topics in coordination chemistry have broadened and their content has expanded and enriched. From the original simple low-dimensional study to the current multidimensional topology, organic ligands have also developed from the original simple organic molecules to now contain heteroatom molecules. Metal center atoms or ions have also developed from the initial d^{10} electronic structure of transition metals or rare earth metals to the current alkali (alkaline earth) metals and the other main group metals, especially in recent decades. This is because due to the specificity of d orbital valence electrons, chemists once believed that the activation of small molecules must be completed by d/f-block metal compounds. But now chemists have also found effective main group elements to activate small molecules, like alkali (alkaline earth) metals. Therefore, this thesis focuses on several d-block, f-block and s-block metal complexes catalyzing the activation of small molecules. The rapid development of X-ray single-crystal diffractometers and the wide application of quantum mechanics theory in recent decades have broken through the bottleneck that it was difficult to determine the spatial structure of the complexes by conventional spectroscopy. As a result, thousands of novel complexes structures are reported every year.

Ligands and metal centers play a very important role in the study of metal complexes. The diversity of ligands and the tunability of metal centers have led to the great enrichment applications in chemistry, materials, biomedicine and other fields. This is because the properties of metal complexes are not only determined by the properties of the metal itself, but also by the ligand.

Ligands can change the catalyst properties by changing the electron density and stereoscopic properties of metal complexes. Generally speaking, according to the different atoms contained, ligands can be divided into nitrogen ligands, oxygen ligands and carbon ligands, etc.. According to the number of coordination atoms, the ligands can be divided into mono-dentate, bidentate and multi-dentate ligands, etc.. According to the ligand and metal coordination form, the ligands can be divided into chelate ligand and amphiphilic ligand, etc.

The complexes can divide into transition metals (d-block metals and f-block metals) and main group metals (alkali metals, alkaline earth metals, other main group metals) by the different types of metal centers.

I.3.1. d-block metal complexes

According to the properties of metal-ligands, there are covalent σ bonds and π antibonds between transition metals and ligands. Transition metal elements with partially filled valence layer d orbital or empty d orbital can be used as electrophiles to provide vacant orbital or nucleophile to provide lone pair electrons when participating in chemical reactions, thus reducing the activation energy of the reaction and speeding up the reaction. Among them, d-block metal catalysts have strong reactivity, high selectivity and chemical stability, so they are very important for energy materials, chemical synthesis, environmental engineering and petrochemical industry. Transition metals as intermediates have generated a large number of reports due to the diversity of their ligands. In this section, several d-block metal complexes involved in small molecule activation reactions will be briefly described.

I.3.1.1. Dianionic Pentadentate Ligand B_2Pz_4Py

As early as 1997, Professor Jonas and Stack[42] designed and synthesized an Iron complex including a tetrapod pentadentate ligand able to activate the weak C-H bond on cyclohexadiene. Polypyridyl (PY_5) consists of five pyridine subunits that bind to a single metal in a nearly idealized pyramidal geometry, leaving a coordination site that can be used to complex a monodentate exogenous ligand, such as: $[Fe^{II}(PY_5)(X)]^{n+}$, X = MeOH, H_2O, MeCN, pyridine, Cl^-, OBz^-, MeO, PhO^- and CN^- [43]. The combination of this ligand with molybdenum or cobalt has been successfully used to reduce water to hydrogen by electrochemical or photochemical catalysis [44]. Then a new pentatentate ligand, tetra (tyrazolyl) lutidine (Pz_4lut), was synthesized [45]. The electronic properties indicate that the new ligand is a slightly stronger-field donor to the metal center than a related pentadentate ligand with five pyridyl donors. On this basis, Professor Warren E. Piers and Michael L. Neidig introduced boron to replace the carbon atoms linked to pyridine and pyrazole to generate a new dianionic ligand B_2Pz_4Py. The iron imido complex formed with this dianionic ligand proved to be a good acceptor of

H atoms[46].

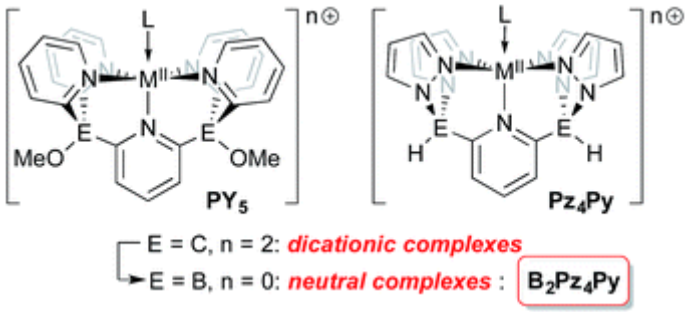

Scheme 1.9 Dianionic Pentadentate Ligand B_2Pz_4Py

Dr. Nurdin [47] reported the cobalt (II) complex with tetrapod pentatentate B_2Pz_4Py ligand and its reaction with organoazides (Scheme 1.10). The formation of Co imido derivatives was indicated by N_2 escape, and Co(III) amido was formed by C-C bond dimerization of the ortho carbons of the aryl group on the azide. DFT calculations verified the electronic structure of d^6 Co(III) radical complex, and indicated that the spin density was located on imido nitrogen and imido aryl group. Analysis of the singly occupied molecular orbital (SOMO) confirms a lack of Co−N π bonding and shows that it is highly localized on the aryl imido group, mainly associated with the imido nitrogen, but also delocalized into the ortho and para positions of the aryl ring(Figure 1.1). The delocalization of spin density onto the aryl ring also explains the tendency of these compounds to dimerize via C−C bond formation through the ortho positions.

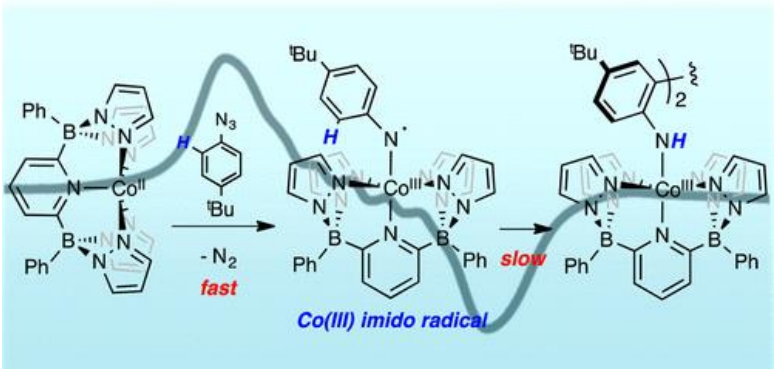

Scheme 1.10 The reaction of Co complexes and organoazides

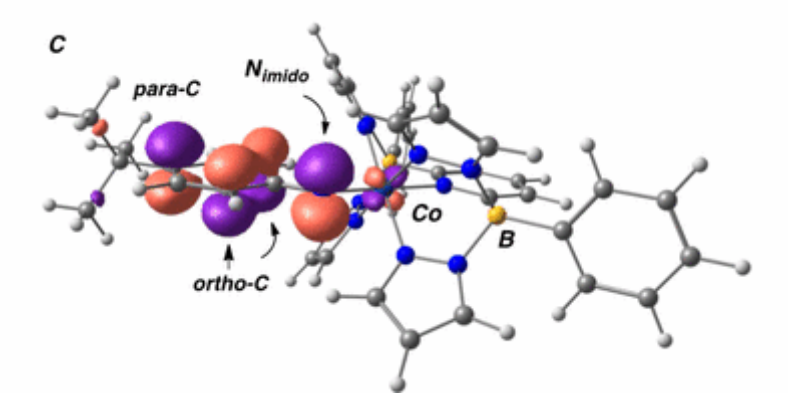

Figure 1.1 The SOMO of Co(III) imido radical

On this basis, Doctor. Nurdin et al. also studied the catalytic reduction of O_2 by cobalt (III) in a dianionic pentadentate ligand system(Scheme 1.11). The peroxo complex Co(III)-O-O-Co(III), as important known intermediates, are prone to occur O-O bond cleavage, resulting in the highly reactive Co(IV) oxyl cation. The protonation of Co(III)-O-O-Co(III) complex is more likely to produce H_2O due to the properties of pentagonal dianions of ligands[48].

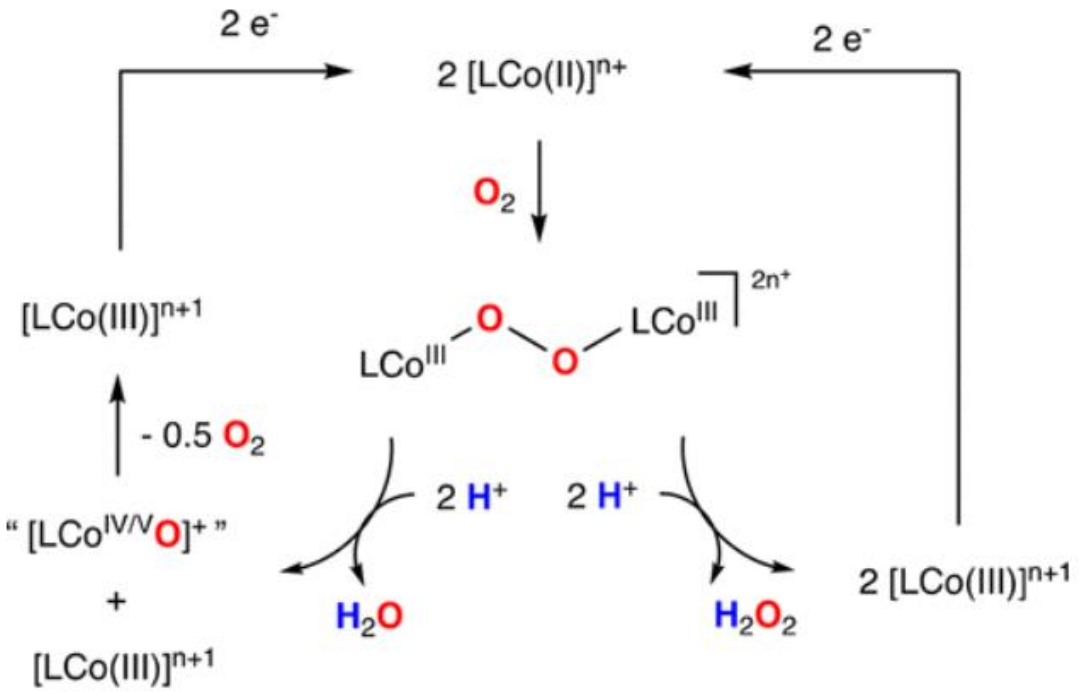

Scheme 1.11 Diprotonation of Co(III)–O–O–Co(III) Complexes

It follows that this dianion pentadentate ligand is suitable for exploring small molecule activation reactions throughout the d block. Doctor Daniel and Professor

Warren applied the B_2Pz_4Py ligand to hydrido and methyl complexes of group III metal scandium and explored the mechanism of its reaction with CO_2.(Figure 1.2). The mechanisms were studied via density function theory and distinct transition states for insertion of CO_2 into the Sc-R (R = H, CH_3) were found, with the insertion into the Sc-CH_3 being more enthalpically difficult (by 18 kcal mol-1) than insertion into Sc-H. The slow rate of reaction between $[(B_2Pz_4Py)ScH]_2$ and CO_2 is attributed to the barrier associated with dimer dissociation[49].

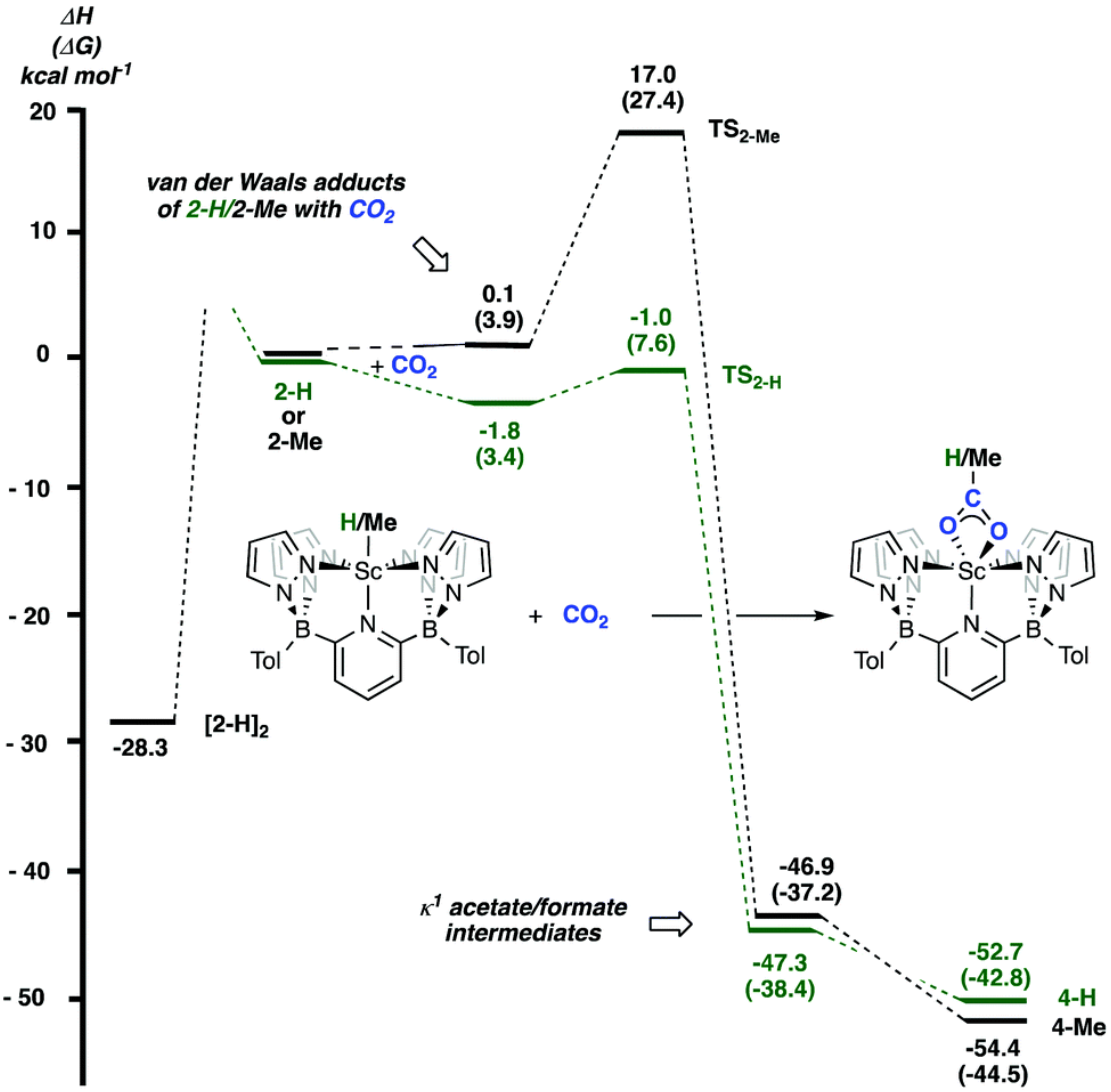

Figure 1.2 Computed energy profile (DFT, B3PW91) for the insertion of CO_2 into the Sc–H and Sc–C bonds.

I.3.1.2. Homoleptic imidophosphorane ligand

Professor Dehnicke and Weller discovered and studied imidophosphorane ligands (as 1σ,2π donors)[50, 51]. This ligand is bonded to the metal through a single donor atom and can control the steric effect through a substituent group on the phosphorus. In

the early years, a series of wolfram, vanadium, and molybdenum complexes supported by homoleptic imidophosphorane ligands with alkyl or aryl substituents were synthesized and studied by Kurt Dehnicke et al[52-54]. In recent years, Professor Pierre's group presented a tris(piperidinyl)imidophosphorane ligand, $[NP(pip)_3)]^{1-}$ (pip = piperidinyl, a six-member ring -$N(C_5H_{10})$)[55]. Here the piperidine substituent amplifies the zwitterionic character. Their reports on such ligands in the last three years have mainly focused on Ce complexes. For example, they found that the covalent interactions between Ce and ligands give significant stability to tetravalent cerium[56]. And the tris(piperidinyl)imino orthophosphine ligand $[NP(pip)_3)]^{1-}$ provided the most reductive trivalent cerium complex $K(Et_2O)_2[Ce(NP(pip)_3)_4]$[55]. In addition to these transition metal homoleptic imidophosphorane complexes applied in addition to f-block metals, the Ag and Cu tetramer complexes supported by imidophosphorane ligand demonstrate the redox stability of these ligands to oxidizing salts[57].

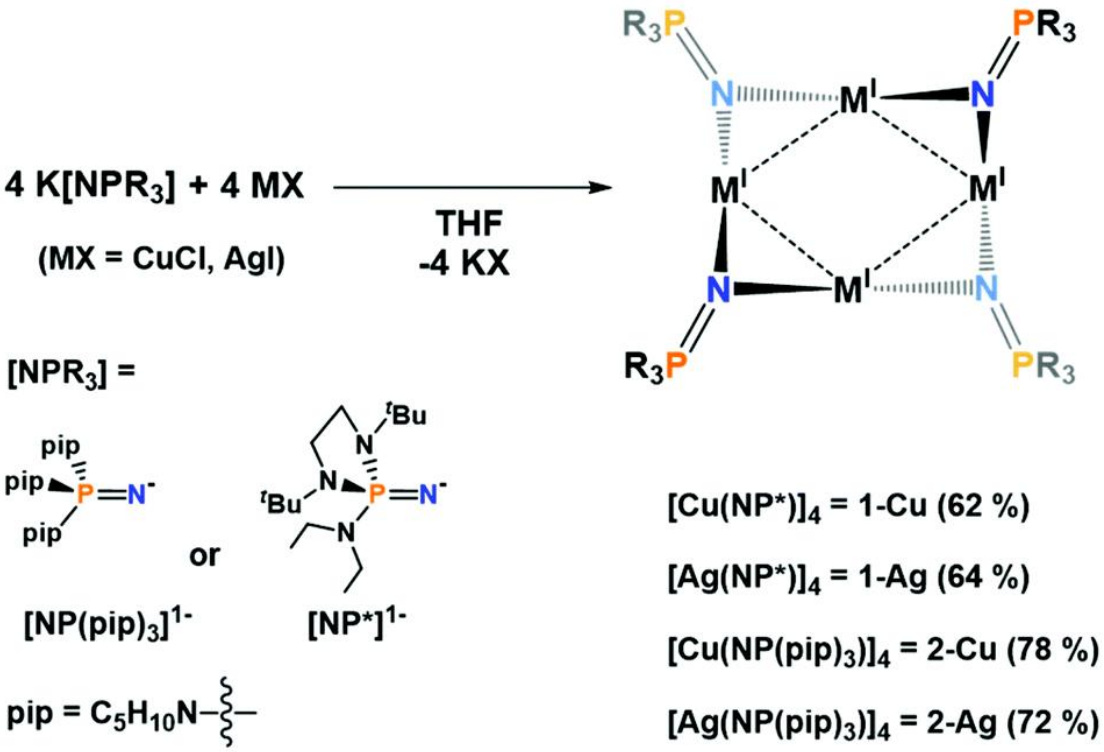

Scheme 1.12 Synthesis of **1-Cu**, **1-Ag**, **2-Cu**, and **2-Ag**.

Although there have been many studies on the synthesis and properties of such transition metal complexes supported by imidophosphorane ligand, the catalytic properties of such complexes have rarely mentioned. Professor Bai et al. proposed a homoleptic iron (II) and cobalt (II) bis(phosphoranimide) complexes (Scheme **1.13**) . The Fe(II) complexes can catalyze the hydroboration of aldehydes and ketones effectively. Co(II) complexes are used as hydrogenation catalyst for alkenes and

alkynes under mild conditions[58]. However, piperidine has not been reported as a substituent in these Fe or Co complexes. Professor Luis M. Aguirre Quintana recently used this weak-field ligand-supported bimetallic Fe complex to study the reactivity of nitrous oxide.

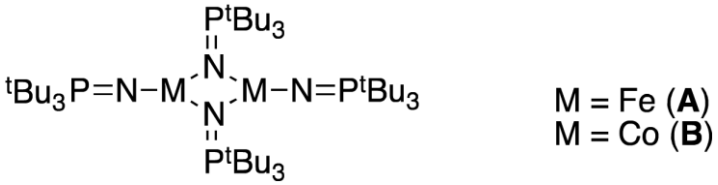

Scheme 1.13 Tri-t-butyl-phosphoranimidometal(II) dimers.

I.3.2. f-block metal complexes

The lanthanides and actinides are both located in the f block in the periodic table of elements, and their electron configuration is $(n-2)f^{1-14}$ $(n-l)d^{1}$ ns^{2}, with equal number of outer shall electrons. For different elements, the electron will fill the (n-2)f orbitals while the nuclear charge is added. The first element of the lanthanide series, lanthanum (La), has an electron configuration of $6s^{2}5d^{1}$ and is the only lanthanide element that does not contain f electrons. The lanthanides and actinides have similar electronic configurations, similar atomic and ionic radii. Similar ionic radius contraction phenomenon exists, and chemical differences decrease gradually with increasing atomic number. The unique electronic configuration is responsible for the stability of the physicochemical properties of the lanthanides such as oxidation states, redox potentials and ionic radii. All elements show a stable +3 oxidation state. In the lanthanides, elements that can reach the $4f^{0}$, $4f^{7}$ or $4f^{14}$ configuration deviate from the +3 oxidation state, and the +2 or +4 oxidation state is stable in these cases.

The coordination numbers of lanthanide metals range from 3 to 12, depending on the steric hindrance requirements of the ligands, with 8 and 9 being the most common coordination numbers. The synthesis of lanthanide metal complexes with specific properties is challenging due to the variable coordination numbers of lanthanide metal ions and the difficult to control coordination environment. In this section, several lanthanide metal complexes will be introduced, including those possessing N-heterocyclic carbene, polydentate tris(tertbutoxy) siloxide, and Lanthanide halogenates.

I.3.2.1. Lanthanide halogenates

Among the many theoretical works on lanthanides, halides are very important. On the one hand, halide as a complex, it has fewer atoms comparing to the organometallic complex, so that the theoretical calculation of halide complex is less difficult. And also, it has abundant experimental data for reference, so it can make a rigorous evaluation of the theoretical results.

SmI_2 is a versatile single electron transfer agent that can be used for reductive transformations. Therefore, it is usually used in many different reactions, such as couplings[59], cleavages[60] and cyclizations[61]. They can be well applied to the development of new complex catalysts, such as bidentate ligands containing two N atoms coordinated to metals. 1,10-phenanthrolines are one of these versatile ligands, Professor Jeremy Weitgenant has used the reaction of an aldehyde or ketone with SmI_2 to establish an efficient form of ligand library in which the hydroxyalkyl substituent in the product can be bi-functionalized or coupled to provide a large number of phenanthroline derivatives[62](Schme 1.14).

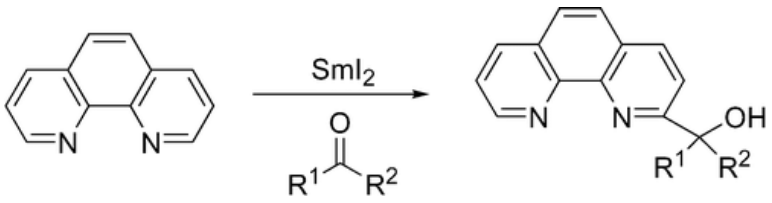

Scheme 1.14 The reaction of SmI_2 and aldehyde or ketone

Professor Kato and his co-workers previously reported a SmI_2-promoted cleavage of alkoxides on 2-(1-acetoxypropyl)phenanthroline and a completed reductive coupling with ketone to generate 2-propylphenanthroline[63]. To further test the scope and limits of the reductive coupling, Professor Weitgenant et al. tested different substituted substrates such as isoquinoline, pyridine, bipyridine, quinoline, and 1,10-phenanthroline analogues instead of propylphenanthroline. In the presence of SmI_2, these substrates were coupled to aldehydes or ketones to produce hydroxyalkyl[64](Scheme 1.15).

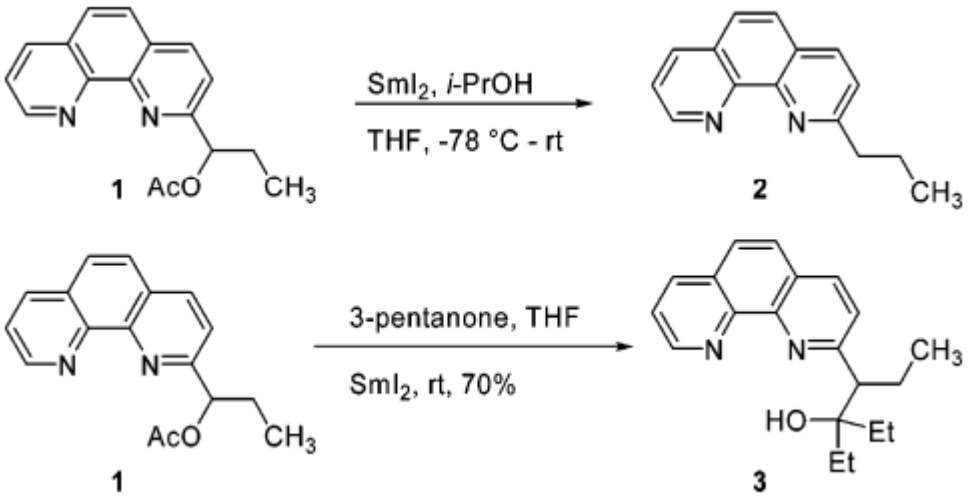

Scheme 1.15 SmI_2-promoted cleavage of alkoxides and reductive coupling with ketone

Lanthanide metals are also used in the activation of organic C-F bonds. Organofluorides are a class of organic compounds in which the C-H bond is replaced by a C-F bond. The F atom has a very strong electronegativity, which makes the C-F bond strongly polar and the largest bond dissociation energy in nature(130kal/mol). The bond energy of C-F bonds is much higher than that of C-H, C=O bonds, and other common chemical bonds in organic compounds, so researchers expect to find the better ways to activate C-F bonds efficiently. For metal-organic chemistry, the use of metal complexes to participate in the activation and functionalization of C-F bonds in aromatic and aliphatic fluorides is a hot topic today. Professor Hilmersson have demonstrated the reduction cleavage of C-F bonds by SmI_2, and the products vary with the solvent and Sm sources [65]. Professor Deacon and Junk found that [La $(CF_3Form)_3$] (CF_3Form=N,N′-bis(2-trifluoromethylphenyl)formamidine) could activate all the F on the CF_3 group[66]. In this paper, the C-F bond activation and the effect on selective addition of aldehydes to trifluoromethylated benzofulvenes involved in LaI_3 are studied.

I.3.2.2. N-Heterocyclic Carbene

N-Heterocyclic Carbene (NHC), as a special lewis base catalyst and an effective metal catalyst ligand, has attracted extensive attention in organic synthesis experiments and metal-organic chemistry. Compared with conventional electron-deficient carbenes, n-heterocyclic carbenes are electron-rich nucleophilic compounds, more stable than electron-deficient carbenes. From the perspective of an induction effect, this is mainly

due to the high electronegativity of nitrogen atoms connected with carbene carbon atoms, and the electron density of C-N bond is biased towards nitrogen atoms by the electron-withdrawing effect of nitrogen, thus stabilizing the lone pair of Carbene carbon atoms. Considering the conjugation effect, the p orbital of nitrogen atom has a pair of unbonded lone electrons, which can provide electrons for the empty p orbital of carbon atom, forming a three-center four-electron conjugated system. Secondly, the conjugated system with the presence of a C=C bond can also stabilize the carbene. There is a lone pair of electrons in the sp^2 hybrid orbital of the carbene carbon atom, which makes the nitrogen heterocyclic carbene have strong nucleophilicity. According to its unique electronic properties, nitrogen-heterocyclic carbene exhibits both strong σ electron-donor and weak π acceptor properties.

Professor Muthukumaran has synthesized and characterized a new o-aryloxide-n-heterocyclic Carbene ligand. Moreover, it has been proved to be an effective catalyst for transamidation of carboxamides with amines on transition metal center catalysts[67]. F-block metal complexes with n-heterocyclic Carbene as ligands also can be involved in catalytic activation of many small molecules. For example, Professor Arnold, Kühn and Smith used cerium n-heterocyclic carbene complexes to selectively catalyze the activation of CO_2 and heteroallene[68](Scheme1.16). The cerium complexes cleanly and quantitatively insert carbon dioxide exclusively into all three cerium carbene bonds, forming $Ce(L^R{\cdot}CO_2)_3$. The insertion is reversible only for the mesityl-substituted complex $Ce(L^{Mes})_3$. Analysis of the capacity of $Ce(L^R)_3$ to insert a range of heteroallenes that are isoelectronic with CO_2 reveals the solvent and ligand size dependence of the selectivity. This is important because only the complexes capable of reversible CO_2-insertion are competent catalysts for catalytic conversions of CO_2. The reversibility of the CO_2 insertion appears to be crucial for further reactivity as only $Ce(L^{Mes}{\cdot}CO_2)_3$ is an active catalyst for the conversion of propylene oxide to propylene carbonate. In the last few years that Ce(III) catalyst was demonstrated to be a great catalyst for a lot of really nice organic transformation including C-C bond formation, C-H activation under mild condition or under UVA. This complex exhibits brilliant orange color under UV irradiation.

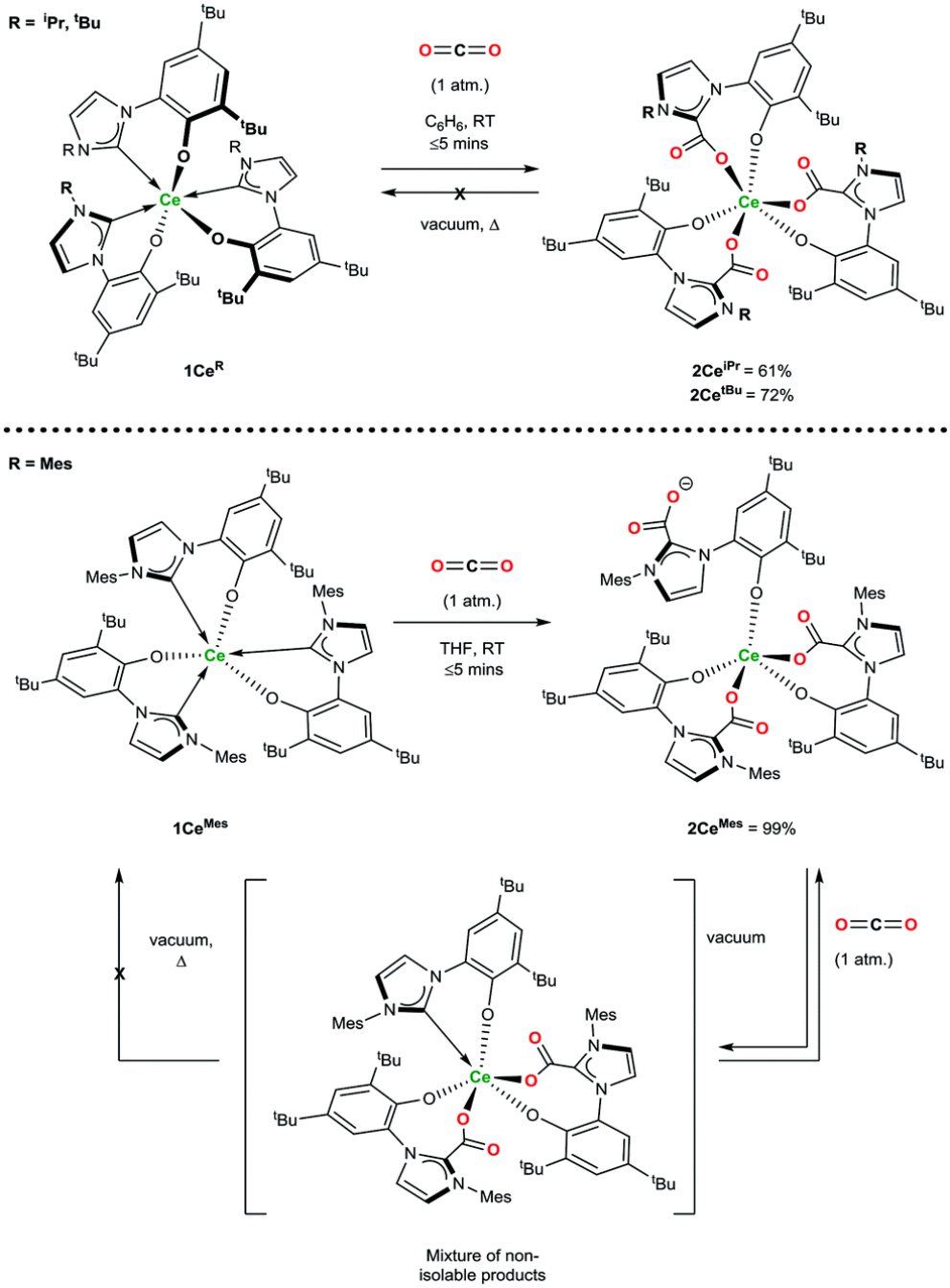

Scheme 1.16 Reactivity of **1Ce^{R}** with CO_2 that forms the triply CO_2–NHC inserted adducts irreversibly (**2Ce^{iPr}** and **2Ce^{tBu}**) and reversibly (**2Ce^{Mes}**).

I.3.2.3. Tris(tert-butoxy)siloxide ligands

In fact, most of the reported small molecule activation reactions are focused on d-block metals. f-block metal-mediated small molecule transformations are limited to a small amount of reactions, such as the reductive capture of dinitrogen, the reduction of carbon dioxide or carbon disulfide, etc[69-76].

Professor Anwander's group has successively synthesized a series of bulky divalent lanthanide ions complexes supported by electron-rich tris(tert-butoxy)siloxide ligands, $[Ln^{II}(OSi(O^tBu)_3)_4K_2]$, and investigated their catalytic properties for the reduction reactions of PhNNPh, CS_2 and CO_2 . Siloxanes are not often used as auxiliary ligands in lanthanide chemistry, and such ligands can impart stability to homogeneous metal complexes and enhance the binding of reduction products. The tris(tert-butoxy)siloxide ligands play an important role in CO_2 reduction. Thus, the Yb complexes formed (Figure 1.3) allow the formation of oxalate and carbonate products.[77-80]. Numerous experiments and theoretical calculations have also been performed to confirm the reaction mechanism on Sm and U. In general , this reaction take places through the formation of a key intermediate in which the CO_2 molecule is doubly reduced . Then, a free CO_2 molecule is added to the system to form an oxalate product, or a carbonate product when CO is removed(scheme 1.17) [81-87].

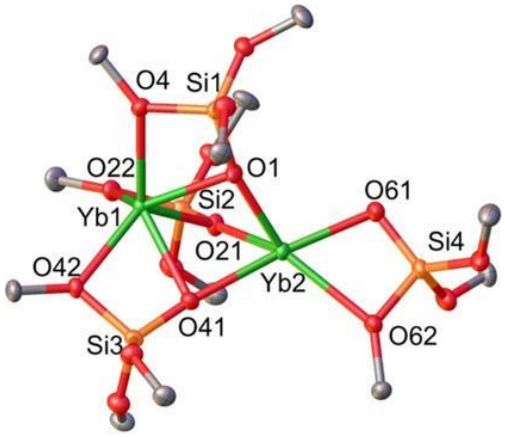

Figure 1.3 The Yb complex with tris(tert-butoxy)siloxide ligands

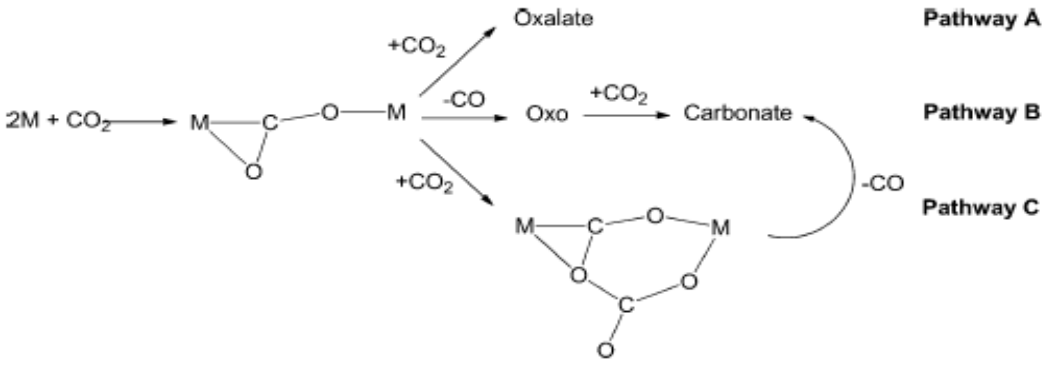

Scheme 1.17 Different pathways for the CO_2 reduction

I.3.3. s-block metal complexes

Among the main group metals, most of the complexes mainly used for catalytic small molecule activation are focused on the reports for alkali and alkaline earth metals, such as magnesium and calcium complexes supported by mutidentate N ligand.

I.3.3.1. Mutidentate N ligand

Generally, ligands can be classified into monodentate and multidentate ligands depending on the number of coordination atoms (scheme 1.18). In the field of metal-organic complex research, multidentate N ligands have received much attention because of their properties in stabilizing multiple metal complexes. This is because the presence of several N atoms as Lewis acidic donors can lead to ligands with multiple coordination sites.

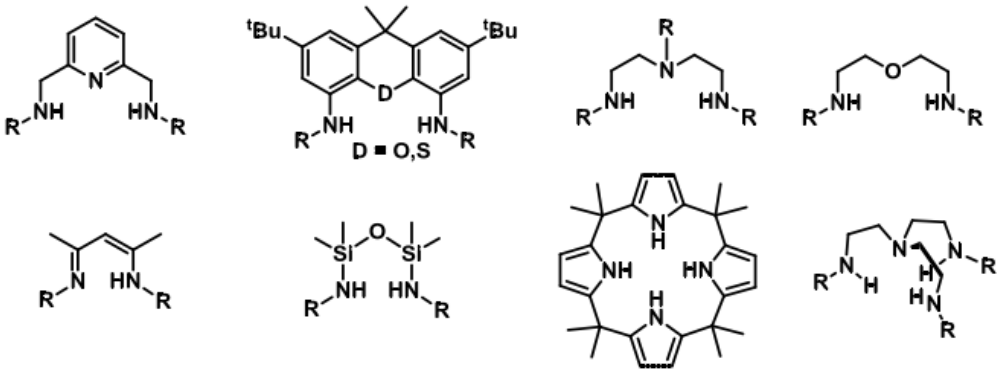

Scheme 1.18 Different Mutidentate N ligand

In 1961, Professor Hall synthesized silica-azatricycles by the alcoholysis of trihydroxyethylamines with trialkoxysilanes and confirmed their structures by X-ray diffraction, with silicon atoms in a five-coordination mode and containing axial reaction sites[88]. Subsequently, the concept of atranes was proposed, and they were classified into three major groups, atrane, quasi-atrane and pro-atrane, according to the presence or absence of coordination interactions between the central atom E (the main group elements) and N center (scheme 1.19).

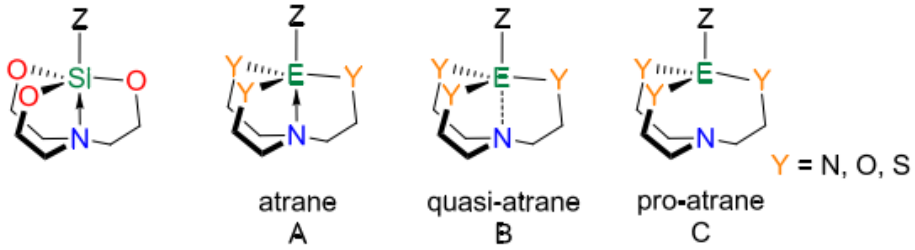

Scheme 1.19 The structure of atrane, quasi-atrane and pro-atrane

On this basis, Professor Davidson and Mahon first reported tris(2-dimethylaminoethyl)amine (Me_6TREN) supported s-block metal complexes with an η^4 coordination mode[89]. Through a series of synthesis and characterization of Li and Na complexes, the coordination chemistry of Me_6TREN for s-block metals was established. Professor Ajay Venugopal's group started working on this basis a cationic butylmagnesium complex $[Me_6TREN\text{-}Mg\text{-}n\text{-}Bu][B(C_6F_5)_4]$ (scheme 1.20). The β-CH functional group on the butylmagnesium cation can be used for the effective alkylation of CO_2 and the quantitative reduction of benzophenone[90]. Then they synthesized and characterized a kind of cationic magnesium amides. And the reaction of benzophenone, CO_2 insertion into β-SiH bond was also studied[91].

Scheme 1.20 The alkylation of CO_2 and reduction of benzophenone for Mg complex

Another NNNN-type macrocyclic ligand used for dicalcium trihydride cation , $[Ca_2H_3(Me_4TACD)_2](SiPh_3)$, was first reported by Professor Okuda (scheme 1.21) [92]. Professor Okuda and Maron then investigated the catalytic properties of NNNN-type macrocyclic cation $[CaH]^+$ for the catalytic properties of selective hydrogenation of olefins[93].

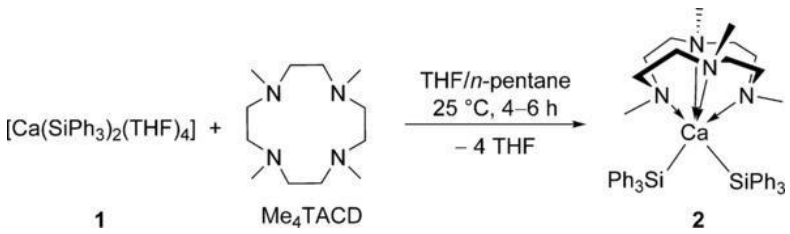

Scheme 1.21 The Ca complex with NNNN-type macrocyclic ligand

In this thesis, DFT calculations will be used to study the activation of small molecules catalyzed by d/f/s-block complexes with different ligands.

For d-block metals center, there are two kinds of ligands: 1) A pentadentate ligand is proposed that can adjust the charge of the ligand by adding or subtracting boron atoms, namely B_2Pz_4Py and BPz_2Py_3. With these ligands, the interconversion of hydroxyl and oxo using scandium complexes, and activation of ammonia and hydrazine using iron complexes are studied. 2) A tris(dialkylamido)-imidophosphoranes ligand is coordinated with iron center. With this ligand, reduction of N_2O to N_2 using Fe complexes is studied.

For f-block metals center, there are three kinds of complexes: 1) the mechanism of the regioselective addition reaction of benzaldehyde using pentadienyl lanthanum metal complex; 2) the mechanism of direct coupling of benzophenone and N-heterocycle (such as pyridine and phenanthroline) to form methanol using SmI_2; 3) the reduction mechanism of CO_2 and CS_2 on a bimetallic coordination complexes (samarium or ytterbium).

For s-block metals center, there are two kinds of complexes :1) the mechanism of CO reduction using calcium complexes supported by NNNN-type macrocyclic ligands; 2) the mechanism of ketone hydroboration using Magnesium complexes supported by multi-dentate N heterocyclic ligands.

References:

1. [a]Lawrance, G.A., *Introduction to coordination chemistry*. 2013: John Wiley & Sons; [b]Miller, S.A., J.A. Tebboth, and J.F. Tremaine, *114. Di cyclo pentadienyliron.* Journal of the Chemical Society (Resumed), 1952: p. 632-635.
2. [a]McNaught, A.D. and A. Wilkinson, *Compendium of chemical terminology*. Vol. 1669. 1997: Blackwell Science Oxford; [b]Kealy, T. and P. Pauson, *A new type of organo-iron compound.* Nature, 1951. **168**(4285): p. 1039-1040.
3. Busch, D.H., *The complete coordination chemistry-one practioner's perspective.* Chemical reviews, 1993. **93**(3): p. 847-860.
4. Greenwood, N.N. and A. Earnshaw, *Chemistry of the Elements*. 2012: Elsevier.
5. Favre, H.A., *Nomenclature of Organic Chemistry : IUPAC Recommendations 2012 and Preferred IUPAC Names.* 2011.
6. Kealy, T. and P. Pauson, *A new type of organo-iron compound.* Nature, 1951. **168**(4285): p. 1039-1040.
7. Whisnant, D.M., *Evolution of Bonding Theory: The Werner-Jorgenson Controversy*. 1989, ACS Publications.
8. You Xiaozeng, Meng Qingjin, and Han Wanshu, Advances in Coordination Chemistry. Higher Education Press, Beijing, 2000. 121: p. 131.
9. Von Zelewsky, A., *Stereochemistry of coordination compounds*. Vol. 3. 1996: John Wiley & Sons.
10. Bensaude-Vincent, B. and I. Stengers, *A history of chemistry*. 1996: Harvard University Press.
11. Berg, J.M., *Principles of bioinorganic chemistry*. 1994: University Science Books.
12. Bertini, I., et al., *Bioinorganic chemistry*. 1994: University science books.
13. Gerloch, M., J.H. Harding, and R.G. Woolley, *The context and application of ligand field theory*, in *Inorganic Chemistry*. 1981, Springer. p. 1-46.
14. Griffith, J. and L. Orgel, *Ligand-field theory.* Quarterly Reviews, Chemical Society, 1957. **11**(4): p. 381-393.
15. Atanasov, M., C. Daul, and C. Rauzy, *A DFT based ligand field theory.* Optical spectra and chemical bonding in inorganic compounds, 2004: p. 97-125.
16. You Xiaozeng, Structure and properties of coordination compounds. 1992: Science Press.
17. Zaera, F., *Preparation and reactivity of alkyl groups adsorbed on metal surfaces.* Accounts of chemical research, 1992. **25**(6): p. 260-265.
18. Marcus, R.A., *Electron transfer reactions in chemistry. Theory and experiment.* Reviews of Modern Physics, 1993. **65**(3): p. 599.
19. Marcus, R.A., *On the theory of oxidation-reduction reactions involving electron transfer. I.* The Journal of chemical physics, 1956. **24**(5): p. 966-978.
20. Marcus, R., *On the theory of oxidation-reduction reactions involving electron transfer. II. Applications to data on the rates of isotopic exchange reactions.* The Journal of Chemical Physics, 1957. **26**(4): p. 867-871.
21. Marcus, R., *On the theory of oxidation-reduction reactions involving electron transfer. III. Applications to data on the rates of organic redox reactions.* The Journal of Chemical Physics, 1957. **26**(4): p. 872-877.
22. Eigen, M. and P. Schuster, *The hypercycle: a principle of natural self-organization*. 2012: Springer Science & Business Media.
23. Eigen, M. and P. Schuster, *A principle of natural self-organization.*

Naturwissenschaften, 1977. **64**(11): p. 541-565.
24. Katakis, D. and G. Gordon, *Mechanisms of inorganic reactions.* 1987.
25. Adamson, A.W. and A.P. Gast, *Physical chemistry of surfaces*. Vol. 150. 1967: Interscience publishers New York.
26. Wegner, E.E. and A.W. Adamson, *Photochemistry of complex ions. III. Absolute quantum yields for the photolysis of some aqueous chromium (III) complexes. Chemical actinometry in the long wavelength visible region.* Journal of the American Chemical Society, 1966. **88**(3): p. 394-404.
27. Boyd, G., A. Adamson, and L. Myers Jr, *The exchange adsorption of ions from aqueous solutions by organic zeolites. II. Kinetics1.* Journal of the American Chemical Society, 1947. **69**(11): p. 2836-2848.
28. Jurisson, S., et al., *Coordination compounds in nuclear medicine.* Chemical reviews, 1993. **93**(3): p. 1137-1156.
29. Hauser, A., *Intersystem crossing in Fe (II) coordination compounds.* Coordination Chemistry Reviews, 1991. **111**: p. 275-290.
30. Huang, C.-H., *Rare earth coordination chemistry: fundamentals and applications*. 2011: John Wiley & Sons.
31. Stahl, S.S., *Organotransition Metal Chemistry: From Bonding to Catalysis*. 2010, ACS Publications.
32. Shriver, D.F., P.W. Atkins, and C.H. Langford, *Inorganic chemistry*. 1999, Oxford University Press Oxford.
33. Crabtree, R.H., *The organometallic chemistry of the transition metals*. 2009: John Wiley & Sons.
34. Brown, I.D., *Bond valences—A simple structural model for inorganic chemistry.* Chemical Society Reviews, 1978. **7**(3): p. 359-376.
35. Brown, I.D., *The chemical bond in inorganic chemistry: the bond valence model*. Vol. 27. 2016: Oxford University Press.
36. Metzler-Nolte, N. and H. Kraatz, *Concepts and models in bioinorganic chemistry*. 2006: Wiley-VCH.
37. Purcell, K.F. and J.C. Kotz, *Inorganic chemistry.* Holt-Saunders International Editions, 1977.
38. Gillie, A. and J. Stille, *Mechanisms of 1, 1-reductive elimination from palladium.* Journal of the American Chemical Society, 1980. **102**(15): p. 4933-4941.
39. Bailar, J.C. and H. Itatani, *Homogeneous Catalysis in the Reactions of Olefinic Substances. 1a VI. Selective Hydrogenation of Methyl Linoleate and Isomerization of Methyl Oleate by Homogeneous Catalysis with Platinum Complexes Containing Triphenylphosphine,-arsine, or-stibine1b.* Journal of the American Chemical Society, 1967. **89**(7): p. 1592-1599.
40. Itatani, H. and J.C. Bailar Jr, *Homogenous catalysis in the reactions of olefinic substances. V. Hydrogenation of soybean oil methyl ester with triphenylphosphine and triphenylarsine palladium catalysts.* Journal of the American Oil Chemists' Society, 1967. **44**(2): p. 147-151.
41. Brintzinger, H., *Hydride, alkyl, and alyl complexes of bis (. pi.-cyclopentadienyl) thitanium (III).* Journal of the American Chemical Society, 1967. **89**(26): p. 6871-6877.
42. Jonas, R.T. and T. Stack, *C− H bond activation by a ferric methoxide complex: a model for the rate-determining step in the mechanism of lipoxygenase.* Journal of the American Chemical Society, 1997. **119**(36): p. 8566-8567.
43. Goldsmith, C.R., et al., *A spectrochemical walk: single-site perturbation within*

a series of six-coordinate ferrous complexes. Inorganic chemistry, 2002. **41**(18): p. 4642-4652.
44. Zee, D.Z., et al., *Metal–polypyridyl catalysts for electro-and photochemical reduction of water to hydrogen.* Accounts of chemical research, 2015. **48**(7): p. 2027-2036.
45. Morin, T.J., et al., *First-Row Transition-Metal Complexes of a New Pentadentate Ligand, α, α, α′, α′-Tetra (pyrazolyl) lutidine.* Inorganic chemistry, 2008. **47**(17): p. 7468-7470.
46. Spasyuk, D.M., et al., *Facile hydrogen atom transfer to iron (III) imido radical complexes supported by a dianionic pentadentate ligand.* Chemical science, 2016. **7**(9): p. 5939-5944.
47. Nurdin, L., et al., *Reactions of Neutral Cobalt (II) Complexes of a Dianionic Tetrapodal Pentadentate Ligand: Cobalt (III) Amides from Imido Radicals.* Inorganic chemistry, 2017. **56**(7): p. 4157-4168.
48. Nurdin, L., et al., *Oxygen–oxygen bond cleavage and formation in Co (II)-mediated stoichiometric O2 reduction via the potential intermediacy of a Co (IV) oxyl radical.* Journal of the American Chemical Society, 2018. **140**(47): p. 16094-16105.
49. Beh, D.W., et al., *Scandium alkyl and hydride complexes supported by a pentadentate diborate ligand: reactions with CO 2 and N 2 O.* Dalton Transactions, 2018. **47**(38): p. 13680-13688.
50. Dehnicke, K., M. Krieger, and W. Massa, *Phosphoraneiminato complexes of transition metals.* Coordination chemistry reviews, 1999. **182**(1): p. 19-65.
51. Dehnicke, K. and F. Weller, *Phosphorane iminato complexes of main group elements.* Coordination chemistry reviews, 1997. **158**: p. 103-169.
52. Rhiel, M., et al., *Tetrakis (trimethylphosphaniminato) molybdän-dichlorid,[Mo (NPMe3) 4] Cl2/Tetrakis (trimethylphosphoraneiminato) molybdenum Dichloride,[Mo (NPMe3) 4] Cl2.* Zeitschrift für Naturforschung B, 1996. **51**(10): p. 1419-1422.
53. Rentschler, E., et al., *[W (NPPh3) 4] Cl2—Ein Phosphaniminato-Komplex mit einem Wolfram-Dikation.* Zeitschrift für anorganische und allgemeine Chemie, 1993. **619**(6): p. 999-1003.
54. Anfang, S., et al., *Phosphaniminato-Komplexe Seltener Erden. Synthese und Kristallstrukturen von [M2 (C5H5) 3 (NPPh3) 3]· 3 C7H8 mit M= Y, Dy und Er. Magnetische Eigenschaften von [Dy2 (C5H5) 3 (NPPh3) 3]· 3 C7H8.* Zeitschrift für anorganische und allgemeine Chemie, 1998. **624**(1): p. 159-166.
55. Rice, N.T., et al., *Homoleptic imidophosphorane stabilization of tetravalent cerium.* Inorganic chemistry, 2019. **58**(8): p. 5289-5304.
56. Rice, N.T., et al., *Design, isolation, and spectroscopic analysis of a tetravalent terbium complex.* Journal of the American Chemical Society, 2019. **141**(33): p. 13222-13233.
57. Quintana, L.M.A., et al., *Coinage metal tris (dialkylamido) imidophosphorane complexes as transmetallation reagents for cerium complexes.* Dalton Transactions, 2020. **49**(17): p. 5420-5423.
58. Bai, T., T. Janes, and D. Song, *Homoleptic iron (II) and cobalt (II) bis (phosphoranimide) complexes for the selective hydrofunctionalization of unsaturated molecules.* Dalton Transactions, 2017. **46**(37): p. 12408-12412.
59. Fier, P.S. and J.F. Hartwig, *Selective CH fluorination of pyridines and diazines inspired by a classic amination reaction.* Science, 2013. **342**(6161): p. 956-960.
60. Concellón, J.M., J.A. Pérez-Andrés, and H. Rodríguez-Solla, *Synthesis of (E)-*

α, β-Unsaturated Amides with High Selectivity by Using Samarium Diiodide. Chemistry–A European Journal, 2001. **7**(14): p. 3062-3068.
61. Chatterjee, S., et al., *Indium trichloride catalyzed sp3 C–H bond functionalization of 2-alkyl azaarenes under microwave irradiation.* Tetrahedron Letters, 2014. **55**(49): p. 6680-6683.
62. Weitgenant, J.A., et al., *Samarium-promoted coupling of 1, 10-phenanthroline with carbonyl compounds for synthesis of new ligands.* The Journal of organic chemistry, 2004. **69**(8): p. 2809-2815.
63. Kunishima, M. and S. Tani, *Generation and reactions of samarium carbanions mediated by samarium iodide.* Journal of Synthetic Organic Chemistry, Japan, 1999. **57**(2): p. 127-135.
64. Weitgenant, J.A., J.D. Mortison, and P. Helquist, *Samarium-promoted coupling of pyridine-based heteroaryl analogues of benzylic acetates with carbonyl compounds.* Organic letters, 2005. **7**(17): p. 3609-3612.
65. Janjetovic, M., et al., *Solvent dependent reductive defluorination of aliphatic C–F bonds employing Sm (HMDS) 2.* Chemical Communications, 2013. **49**(18): p. 1826-1828.
66. Deacon, G.B., P.C. Junk, and D. Werner, *Lanthanoid induced C–F activation of all fluorine atoms of one CF3 group.* European Journal of Inorganic Chemistry, 2015. **2015**(9): p. 1484-1489.
67. Nirmala, M., et al., *An attractive route to transamidation catalysis: Facile synthesis of new o-aryloxide-N-heterocyclic carbene ruthenium (II) complexes containing trans triphenylphosphine donors.* Journal of Molecular Catalysis A: Chemical, 2015. **403**: p. 15-26.
68. Arnold, P.L., et al., *Selective and catalytic carbon dioxide and heteroallene activation mediated by cerium N-heterocyclic carbene complexes.* Chemical science, 2018. **9**(42): p. 8035-8045.
69. Lam, O.P., F.W. Heinemann, and K. Meyer, *C□ C Bond Formation through Reductive Coupling of CS2 to Yield Uranium Tetrathiooxalate and Ethylenetetrathiolate Complexes.* Angewandte Chemie International Edition, 2011. **50**(26): p. 5965-5968.
70. Mougel, V., et al., *Siloxides as Supporting Ligands in Uranium (III)-Mediated Small-Molecule Activation.* Angewandte Chemie International Edition, 2012. **51**(49): p. 12280-12284.
71. Brennan, J.G., R.A. Andersen, and A. Zalkin, *Chemistry of trivalent uranium metallocenes: electron-transfer reactions with carbon disulfide. Formation of [(RC5H4) 3U] 2 [. mu.-. eta. 1. eta. 2-CS2]*. Inorganic Chemistry, 1986. **25**(11): p. 1756-1760.
72. Ren, W., et al., *A bipyridyl thorium metallocene: synthesis, structure and reactivity.* Dalton Transactions, 2012. **41**(19): p. 5965-5973.
73. Summerscales, O.T., et al., *Reductive disproportionation of carbon dioxide to carbonate and squarate products using a mixed-sandwich U (III) complex.* Chemical communications, 2008(2).
74. Lam, O.P., et al., *Formation of a uranium trithiocarbonate complex via the nucleophilic addition of a sulfide-bridged uranium complex to CS2.* Inorganic chemistry, 2012. **51**(2): p. 781-783.
75. Evans, W.J., C.A. Seibel, and J.W. Ziller, *Organosamarium-Mediated Transformations of CO2 and COS: Monoinsertion and Disproportionation Reactions and the Reductive Coupling of CO2 to [O2CCO2] 2.* Inorganic Chemistry, 1998. **37**(4): p. 770-776.

76. Heitmann, D., et al., *Low coordinate lanthanide (II) complexes supported by bulky guanidinato and amidinato ligands.* Dalton Transactions, 2010. **39**(7): p. 1877-1882.
77. Zimmermann, M., et al., *Homoleptic Rare-Earth Metal (III) Tetramethylaluminates: Structural Chemistry, Reactivity, and Performance in Isoprene Polymerization.* Chemistry–A European Journal, 2007. **13**(31): p. 8784-8800.
78. Michel, O., et al., *Surface Organobarium and Organomagnesium Chemistry on Periodic Mesoporous Silica MCM-41: Convergent and Sequential Approaches Traced by Molecular Models.* Chemistry–A European Journal, 2011. **17**(42): p. 11857-11867.
79. Elvidge, B.R., et al., *Synthesis, structure and hydrosilylation activity of neutral and cationic rare-earth metal silanolate complexes.* Dalton Transactions, 2006(7): p. 890-901.
80. Andrez, J., et al., *Tuning Lanthanide Reactivity Towards Small Molecules with Electron-Rich Siloxide Ligands.* Angewandte Chemie, 2014. **126**(39): p. 10616-10620.
81. Castro, L., et al., *Insights into the Mechanism of Reaction of [(C5Me5) 2SmII (thf) 2] with CO2 and COS by DFT Studies.* Chemistry–A European Journal, 2012. **18**(25): p. 7886-7895.
82. Schmidt, A.C., et al., *Activation of SO2 and CO2 by trivalent uranium leading to sulfite/dithionite and carbonate/oxalate complexes.* Chemistry–A European Journal, 2014. **20**(42): p. 13501-13506.
83. Louyriac, E., P.W. Roesky, and L. Maron, *SO 2 and SO 3 reactions with [(C 5 Me 5) 2 Sm-O-Sm (C 5 Me 5) 2]: a DFT investigation and comparison with CO 2 reactivity.* Dalton Transactions, 2017. **46**(24): p. 7660-7663.
84. Castro, L., et al., *Activation of Heteroallenes COxS2–x (x= 0–2): Experimental and Theoretical Evidence of the Synthetic Versatility of a Bulky Guanidinato SmII Complex*. 2016, Wiley Online Library.
85. Cooper, O., et al., *Multimetallic cooperativity in uranium-mediated CO2 activation.* Journal of the American Chemical Society, 2014. **136**(18): p. 6716-6723.
86. Castro, L., et al., *Carbonate formation from CO2 via oxo versus oxalate pathway: theoretical investigations into the mechanism of uranium-mediated carbonate formation.* Organometallics, 2010. **29**(21): p. 5504-5510.
87. Castro, L. and L. Maron, *Insight into the Reaction Mechanisms of (MeC5H4) 3U with Isoelectronic Heteroallenes CS2, COS, PhN3, and PhNCO by DFT Studies: A Unique Pathway that Involves Bimetallic Complexes.* Chemistry–A European Journal, 2012. **18**(21): p. 6610-6615.
88. Frve, C.L., G.E. Vogel, and J.A. Hall, *Triptych-siloxazolidines: pentacoordinate bridgehead silanes resulting from transannular interaction of nitrogen and silicon.* Journal of the American Chemical Society, 1961. **83**(4): p. 996-997.
89. Cousins, D.M., et al., *Tris (2-dimethylaminoethyl) amine: a simple new tripodal polyamine ligand for Group 1 metals.* Dalton Transactions, 2010. **39**(35): p. 8278-8280.
90. Banerjee, S., A. Andrews, and A. Venugopal, *A disguised hydride in a butylmagnesium cation.* Chemical Communications, 2018. **54**(45): p. 5788-5791.
91. Banerjee, S., et al., *Amidomagnesium cations.* Dalton Transactions, 2019. **48**(21): p. 7313-7319.

92. Leich, V., et al., *Molecular Calcium Hydride: Dicalcium Trihydride Cation Stabilized by a Neutral NNNN-Type Macrocyclic Ligand.* Angewandte Chemie International Edition, 2016. **55**(15): p. 4794-4797.
93. Schuhknecht, D., et al., *Calcium Hydride Cation [CaH]+ Stabilized by an NNNN-type Macrocyclic Ligand: A Selective Catalyst for Olefin Hydrogenation.* Angewandte Chemie International Edition, 2017. **56**(40): p. 12367-12371.

Chapter II

Theoretical Backgroud

II.1. Quantum mechanics method

The preparation and study of a variety of metal complexes and their derivatives have demonstrated that they can act as effective catalysts for many reactions, speeding up the reaction rate by reducing the activation energy. These metal-centered reactions often contain one or more radical reactions, such as substitution, oxidative addition, reductive elimination, migratory insertion, oxygen exchange, transfer, bond complexation, and nucleophilic addition. To understand these fundamental transformations, scientists have conducted numerous experimental and theoretical studies. The ability to predict them through computer technology is particularly important when experimental phenomena and certain important intermediates cannot be explained with current characterization tools and experimental equipment[1-5] [6].

The impact of quantum chemistry is mainly in two aspects: (1) A conceptual aspect, such as the concept of orbitals, the concept of bonding and antibonding, the concept of electron density, the concept of energy levels, etc. These concepts have become an important part of the understanding of the electronic structure of molecules, geometric structure and chemical reactions. (2) The computational aspect, which can be calculated to understand and predict the properties of molecules and the principles of chemical reactions, etc. .

At present, the key to real chemical reaction mechanism calculation and material design calculation is to solve Schrödinger's equation, which is what we call the first principle calculation (ab-initio calculation)[6]. The system consists of N particles, assuming that the nucleus is at the coordinate origin and that infinity is zero potential energy. Hartree and Fock et al. separated the electron and nuclear motions in the stationary Schrödinger equation and decomposed the multi-electron problem into several single-electron problems to obtain the Hartree-Fock equation[7-11].

$$H\hat{}\psi(\vec{x_1},\vec{x_2}\ldots,\vec{x_N}) = E\psi(\vec{x_1},\vec{x_2}\ldots,\vec{x_N}) \qquad (2.1)$$

where $\psi(\vec{x_1},\vec{x_2}\ldots,\vec{x_N})$ denotes the wave function of the ground state of the system, and $\vec{x_i}$ denotes the spatial coordinates $\vec{r_i}$ of the electron i and the corresponding spin $\vec{\sigma_i}$.

The Hamiltonian $H\hat{}$ inside the equation is shown in equation (2.2) below:

$$\widehat{H} = -\frac{\hbar^2}{2m_e}\sum_i \nabla_{r_i}^2 - \sum_{i,j}\frac{Ze^2}{|r_i - R_j|} + \frac{1}{2}\sum_{j,j'}\frac{Z^2e^2}{|R_j - R_{j'}|} - \sum_j \frac{\hbar^2}{2M_j}\nabla_{R_j}^2 + \frac{1}{2}\sum_{i,i'}\frac{e^2}{|r_i - r_{i'}|} \quad (2.2)$$

where the coordinates of the nucleus and electron are denoted by R and r respectively, m_e is the mass of the electron and M_j is the mass of the nucleus.

The right-hand side of the formula is, in order, the kinetic energy term of the electron, the interaction energy term of the electron and the nucleus, the nucleus-nucleus interaction energy term, the kinetic energy term of the nucleus, and the oulomb interaction force term between the electron and the electron.

II.1.1. Density Functional Theory (DFT)

Density Functional Theory (DFT) is a method of studying the electronic structure of multielectronic systems using electron density distribution as a basic variable. It is widely used in the field of physics and chemistry, especially for studying the properties of molecules and condensed matter, and is one of the most commonly used methods in the field of computational chemistry and condensed matter physics.

In 1927, Thomas-Fermi's theory[12-14] first studied the multielectron system as a basic variable in calculating the structure of electrons in atoms, thus giving a simplified method of processing. If it can be proved that the distribution of the base electron density of any electronic system solely determines the situation of the electronic system, a new theoretical framework for calculating the structure of the electron can be established, which is the starting point for expressing density functional theory.

In 1951, Slater[14, 15] proposed to express the Hartree-Fock exchange energy by density functional in order to solve the problem of calculating the exchange term too slowly. Although the Hartree-Fock method can accurately express the exchange terms, it ignores the correlation effect. And with the increase of the number of electrons in the system, the Hartree-Fock method using the one-electron approximation will be difficult to accurately solve the system dealing with more wave functions due to the large amount of calculation.

In 1964, Hohenberg and Kohn[16, 17] demonstrated that the system's base energy and other properties can be expressed by electron density, which mathematically, means

that energy and other attributes are density dunctional theory, a theory that transforms the solution of Schrödinger's equations into the search for optimal electron density.

However the H-K theory has encountered serious difficulties in its practical implementation. The exchange association, which is primarily an interactive electronic system, can be obtained precisely. In order for the DFT theory to be put into practice, Kohn and Sham[16-18] proposed a local density approximation (LDA). Although the K-S equation is simple and computationally only at the level of the Hartree equation, it contains much more profound physical content. One important conceptual result is that the solution of the polymorphic base state is accurately reduced to the solution of the base state density distribution, which is given by the Schrödinger equation of a single particle. Thus, the valid potential in the equation in principle includes all the interaction effects, i.e. Hartree potential, exchange potential (the potential generated by the interaction determined by the Pauli principle) and correlation potential (the potential generated by the influence of a given electron on the entire charge distribution). In this sense, it is much superior to the Hartree-Fock equation.

The main density flooding theories based on electron density include Thomas-Fermi model, Slater and Hohenberg-Kohn as the three main underlying theories. Due to the difficulty of DFT in finding the exact general function, the total energy of the system can be decomposed as:

$$E(\rho) = E^T(\rho) + E^V(\rho) + E^J(\rho) + E^{EC}(\rho) \qquad (2.3)$$

where E^T, E^V, E^J, E^{EC} denote the electron kinetic energy, the external field energy, the coulomb interaction energy and the exchange-correlation energy, respectively.

The classical coulomb interactions E^V and E^J can be obtained directly. The remaining two terms, E^T and E^{XC}, need to be improved. In order to obtain E^{XC} closer to the real system, it is often necessary to introduce a density gradient into the general function, which can be expressed as：

$$E^{XC}(\rho) = \int f\left(\rho_\alpha(\vec{r}), \rho_\beta(\vec{r}), \nabla\rho_\alpha(\vec{r}), \nabla\rho_\beta(\vec{r})\right) d^3\vec{r} \qquad (2.4)$$

where ρ_α and ρ_β denote the spin densities of α and β respectively.

The exchange-correlation energy term E^{XC} is usually decomposed into the correlation functional E^{C} and the exchange functional E^{X}.

$$E^{XC}(\rho) = E^{X}(\rho) + E^{C}(\rho) \qquad (2.5)$$

The B3LYP functional was developed from the exchange functional proposed by Becke and the related functional proposed by Lee, Weitao Yang and Parr[19-25], and is one of the most widely used computational methods to date, belonging to the generalized gradient approximation density functional.

$$E_{B3LYP}^{XC} = E_{LDA}^{X} + c_o(E_{HF}^{X} - E_{LDA}^{X}) + c_X(E_{CGA}^{X} - E_{LDA}^{X}) + E_{LDA}^{C} + c_C(E_{CGA}^{C} - E_{LDA}^{C}) \qquad (2.6)$$

where c_o=0.20, c_x=0.72, c_c=0.81. E_{CGA}^{X} and E_{CGA}^{C} are generalized gradient approximations of the exchange and correlation functionals, which each use the Becke 88 exchange functional[26] and LYP correlation functional expressions[25], while the local correlation functional E_{LDA}^{C} uses the VWN functional III form[27]. B3LYP is able to accurately calculate properties such as molecular geometry, energy, frequency, etc.

Therefore, DFT can solve many problems in atomic molecular physics, such as the calculation of ionization potential, vibration spectrum research, chemical reaction problems, the structure of biomolecules, the properties of catalytic active positions, and so on.

II.1.2. Basis set

Basis set is a mathematical description of the orbitals in the system. Most programs use a linear combination of atomic orbitals (LCAO) to construct molecular orbitals, known as:

$$\psi_i = \sum_{\mu-1}^{N} c_{\mu i}\chi_\mu \qquad (2.7)$$

where $c_{\mu i}$is the molecular orbital combination coefficient. (χ_μ, μ=1, 2, 3,…,N) is the set of atomic orbital basis functions, including Slater Type orbital (STO) and Gaussian Type orbital (GTO) functions.

In order to combine the advantages of these two functions, several GTOs are generally used to fit one STO. The basis function formed by the linear fitting of the GTO function is called the Contracted Gaussian basis function. STO-KG basis sets, that

is, use K (K=3~6) GTOs to fit one STO, and then use one STO to fit an atomic orbital[28, 29]. Increasing the number of basis functions in the valence layer can increase the flexibility of the basis set. This basis set is called the split-valence basis sets. The commonly used split-valence basis sets are 3-21G[30-32]and 6-31G[33-35].

For small systems, in order to improve the calculation accuracy, the outer orbitals with higher angular quantum numbers are often added to the inner orbitals and valence orbitals. This is called the polarization basis set, which is represented by "*" or "**". In addition, there is a diffuse basis set that adds a diffuse function, which is represented by "+" or "++". For example, 6-31G** and 6-311+G** are mainly used in this paper[34, 35].□

For systems with heavy atoms, the inner electrons of heavy atoms have little influence when they participate in chemical reactions, but a larger number of inner electrons require more basis functions, which leads to more calculations and significant relativistic effects. Therefore, in order to solve this problem, Effective Core Potentials[36-38] is introduced into the calculation, that is to say, the nucleus and inner electrons are treated as one nucleus. For example, the SDD used in this paper[39].

II.1.3. Transition State Theory

The transition state theory is a theory proposed by A.G Evans and M. Polanyi in the 1930s to study the elementary reaction mechanism and reaction rate[40]. The basis of this theory is that the reactants will pass through the transition state during the process of forming the product, and the formation of the transition state requires a certain activation energy. If the basic physical quantities such as the vibration frequency of the molecule, the mass of the molecule, and the distance between the nuclei are known, the extreme points of the curved surface on the potential energy surface in the chemical reaction can be found through mathematical analysis. The structures corresponding to the extreme points are reactants, transition states, and products[41, 42].

In the actual chemical reaction process, the reactants, transition states and products can be connected by the minimum energy reaction path on the potential energy surface. In the calculation to verify whether the transition state is the correct structure, the

intrinsic reaction coordinate[43, 44] and Gonzales-Schlegel integration[45, 46] methods are generally used. If the reactant and product are connected to the two ends of the transition state, it means that the transition state is the correct configuration. In general, the configuration and energy changes of reactants, products, transition states and intermediates can also be obtained from the IRC reaction path[47, 48].

As shown in scheme 2.1, reactant generates product through the high-energy transition state TS1. When the reaction is in the transition state, some chemical bonds in the reactant molecules are broken, and some chemical bonds are formed in the product. The energy difference between TS1 and reactant is the energy barrier that must be crossed for the reaction to occur.

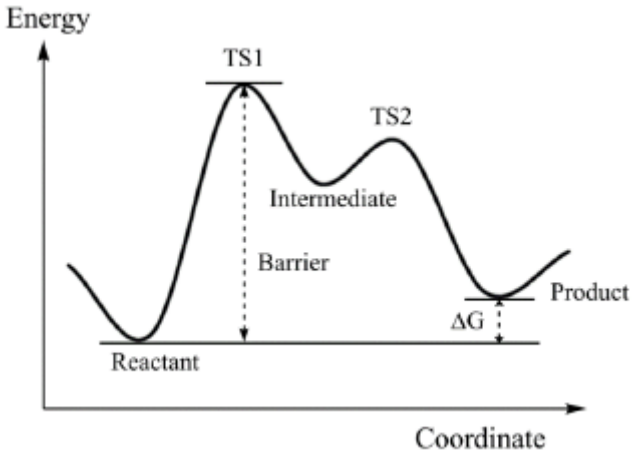

Scheme 2.1 Transition state theory illustration

II.1.4. Natural bond orbital

In the early 1950s, Lowdin first proposed the idea of natural orbitals—a single-electron basis function is used to represent a group of natural orbitals, and the multi-particle electron configuration can be represented by a linear combination of this basis function[49]. The research groups of Weinhold and Reed et al. [50, 51]expanded on this basis and put forward the concepts of natural spin orbitals, natural bond orbitals, and natural hybrid orbitals, and developed the NBO theory.

NBO is a theory based on the single-particle density matrix to study the multi-atom wave function and its bonding behavior. It transforms the regular multi-center molecular orbital into a set of regular single-center and double-center localized orbitals similar to Lewis-type nuclei, σ, π, and n orbitals, and a small amount of σ*, π* and

Rydberg orbitals. According to the perturbation theory, the second-order perturbation stabilization energy E(2) (the decrease in energy of the system caused by the superposition of bonding orbitals and antibonding orbitals) can be obtained by the following formula:

$$E(2) = E_{ij} = q_i \frac{F(i,j)^2}{\varepsilon_j - \varepsilon_i} \qquad (2.8)$$

where q_i is the number of electrons occupied by the donor orbital; ε_i, ε_j are the Fock diagonal elements (orbital energy) of NBO respectively; F (i, j) is Fock non-diagonal elements of NBO.

Reed A. E et al. called this orbital interaction the Lewis base-Lewis acid interaction. The theoretical analysis of NBO through the analysis of natural atomic orbital population, natural hybrid orbital analysis and electron transfer model analysis between electron Donor-Acceptor, can clearly give the type of bond between atoms, molecular orbital composition and its interaction. It is suitable for the analysis of neutral hydrogen bonding or non-hydrogen bonding complexes and intramolecular orbital interactions[52-55] .

II.1.5. Molecular orbital

Molecular orbital theory was proposed by German physicist Hund and American chemist Mulliken in 1932, and is one of the modern covalent bond theories. They used the theory to clarify the nature of molecular bonds and solved the problems that valence bond theory could not solve[56, 57].

Molecular orbital theory believes that after atoms form a molecule, the electrons in the molecule are no longer confined to the original atomic orbital, but move on the entire orbital of the recombined molecule, and its state of motion is represented by Ψ. Molecular orbitals are formed by linear combinations of atomic orbitals, and as many molecular orbitals as there are atomic orbitals, such as atomic orbitals φ1 and φ2, they can be combined into two molecular orbitals Ψ and Ψ'.

$$\Psi = C_1\varphi_1 + C_2\varphi_2$$

$$\Psi' = C_1\varphi_1 - C_2\varphi_2 \qquad (2.9)$$

Bonding orbital is formed by superposition of atomic orbitals with the same wave function signs, and the resulting molecular orbital energy is lower than the original atomic orbitals energy; while the antibonding orbital is formed by superimposion of atomic orbitals with opposite wave function signs, and the molecular orbital energy higher than the atomic orbitals. The linear combination of atomic orbitals into molecular orbitals needs to follow the three bonding principles, that is, the principle of symmetry matching, energy approximation, and maximum overlap. For the electron filling after combining the molecular orbitals, the molecular orbital theory believes that the filling should obey minimum energy principle, Pauli exclusion principle and Hund's rule.

In 1951, Japanese theoretical chemist Kenichi Fukui proposed Frontier Molecular Orbital Theory (FMO)[58]. In 1965, Woodward and Hoffmann proposed the principle of the Orbital Symmetry Conservation[59] . These two theories have a pivotal position in quantum chemistry, because their establishment marks that modern chemistry can no longer only study the static properties of molecules, but the dynamic processes of molecules can also be studied. The frontier orbital theory believes that the electron cloud around molecules can be subdivided into molecular orbitals of different energy levels according to their energy. When the electrons are arranged, they do not occupy the highest energy molecular orbital (Highest Occupied Molecular Orbital, HOMO), but occupy the lowest energy molecular orbital (Lowest Unoccupied Molecular Orbital, LUMO), and the others have little effect on the reaction. HOMO and LUMO are the frontier molecular orbital that play a decisive role in chemical reactions.

2.6 Electronic Excited State Theory

At present, many methods have been proposed to solve the problem of electronic excited state. There are roughly two methods that can be widely accepted: Transition-based and State-based. Among them, time-dependent density functional theory (TD-DFT) is a transition-based method that has developed rapidly and accurately in recent years. TD-DFT can give accurate electronic transition excitation energy through the calculation of exchange-correlation functional.

In 1978, Peukert first obtained the time-dependent Kohn-Sham equation, before that the traditional Kohn-Sham equation can only deal with ground-state molecules. So

the extended density functional method to deal with excited states has become a hot research topic[17, 60-64]. The time-dependent Schrödinger equation is:

$$i\frac{\partial}{\partial t}\Psi(t) = H\hat{}(t)\Psi(t) \qquad (2.10)$$

where the Hamiltonian function $H\hat{}$ includes the kinetic energy $T\hat{}$, the coulomb interaction $W\hat{}$ and the time-dependent external potential energy $V\hat{}(t)$:

$$H\hat{} = T\hat{} + W\hat{} + V\hat{}(t) \qquad (2.11)$$

When TD-DFT calculates the excitation energy, only the eigenvalues and orbitals of the ground state Kohn-Sham equation are used, and only one self-consistent field calculation is required. The above method is to solve the problem of excited state and multi-state structure within the DFT framework. Because of the low-frequency adiabatic approximation to the exchange correlation potential, it can give accurate results for single-electron low-lying states.

References:

1. Cances, E. and C. Le Bris, *On the convergence of SCF algorithms for the Hartree-Fock equations.* ESAIM: Mathematical Modelling and Numerical Analysis, 2000. **34**(4): p. 749-774.
2. Cancès, E. and C. Le Bris, *Can we outperform the DIIS approach for electronic structure calculations?* International Journal of Quantum Chemistry, 2000. **79**(2): p. 82-90.
3. Le Bris, C., *Computational chemistry from the perspective of numerical analysis.* Acta Numerica, 2005. **14**: p. 363-444.
4. Handy, N.C., J.D. Goddard, and H.F. Schaefer III, *Generalization of the direct configuration interaction method to the Hartree–Fock interacting space for doublets, quartets, and open-shell singlets. Applications to NO2 and NO2−.* The Journal of Chemical Physics, 1979. **71**(1): p. 426-435.
5. Koga, N. and K. Morokuma, *Ab initio molecular orbital studies of catalytic elementary reactions and catalytic cycles of transition-metal complexes.* Chemical Reviews, 1991. **91**(5): p. 823-842.
6. Hehre, W.J., *Ab initio molecular orbital theory.* Accounts of Chemical Research, 1976. **9**(11): p. 399-406.
7. Schuchardt, K.L., et al., *Basis set exchange: a community database for computational sciences.* Journal of chemical information and modeling, 2007. **47**(3): p. 1045-1052.
8. Fischer, C.F., T. Brage, and P. Jönsson, *Computational atomic structure: an MCHF approach*. 2019: Routledge.
9. Heine, V., *Hyperfine structure of paramagnetic ions.* Physical Review, 1957. **107**(4): p. 1002.
10. Lykos, P. and G. Pratt, *Discussion on the Hartree-Fock approximation.* Reviews of Modern Physics, 1963. **35**(3): p. 496.
11. Cohen, H.D. and C. Roothaan, *Electric Dipole Polarizability of Atoms by the Hartree—Fock Method. I. Theory for Closed-Shell Systems.* The Journal of chemical physics, 1965. **43**(10): p. S34-S39.
12. Thomas, L.H. *The calculation of atomic fields*. in *Mathematical proceedings of the Cambridge philosophical society*. 1927. Cambridge University Press.
13. KOMATSU, T., *Mathematical proceedings of the cambridge philosophical society.* a,..., a, 1927. **1000**(a2): p. a2.
14. Slater, J.C., *A simplification of the Hartree-Fock method.* Physical review, 1951. **81**(3): p. 385.
15. Slater, J., *Magnetic effects and the Hartree-Fock equation.* Physical Review, 1951. **82**(4): p. 538.
16. Baerends, E.J. and O.V. Gritsenko, *A quantum chemical view of density functional theory.* The Journal of Physical Chemistry A, 1997. **101**(30): p. 5383-5403.
17. Hohenberg, P. and W. Kohn, *Inhomogeneous electron gas.* Physical review, 1964. **136**(3B): p. B864.
18. Kohn, W. and L.J. Sham, *Self-consistent equations including exchange and correlation effects.* Physical review, 1965. **140**(4A): p. A1133.
19. Becke, A.D., *Density-functional thermochemistry. I. The effect of the exchange-only gradient correction.* The Journal of chemical physics, 1992. **96**(3): p. 2155-2160.

20. Becke, A.D., *Density-functional thermochemistry. V. Systematic optimization of exchange-correlation functionals.* The Journal of chemical physics, 1997. **107**(20): p. 8554-8560.
21. Becke, A.D., *Density-functional thermochemistry. II. The effect of the Perdew–Wang generalized-gradient correlation correction.* The Journal of chemical physics, 1992. **97**(12): p. 9173-9177.
22. Becke, A.D., *Density-functional thermochemistry. IV. A new dynamical correlation functional and implications for exact-exchange mixing.* The Journal of chemical physics, 1996. **104**(3): p. 1040-1046.
23. Zhao, Y. and D.G. Truhlar, *Density functionals with broad applicability in chemistry.* Accounts of chemical research, 2008. **41**(2): p. 157-167.
24. Zhao, Y. and D.G. Truhlar, *The M06 suite of density functionals for main group thermochemistry, thermochemical kinetics, noncovalent interactions, excited states, and transition elements: two new functionals and systematic testing of four M06-class functionals and 12 other functionals.* Theoretical chemistry accounts, 2008. **120**(1): p. 215-241.
25. Lee, C., W. Yang, and R.G. Parr, *Development of the Colle-Salvetti correlation-energy formula into a functional of the electron density.* Physical review B, 1988. **37**(2): p. 785.
26. Becke, A.D., *Density-functional exchange-energy approximation with correct asymptotic behavior.* Physical review A, 1988. **38**(6): p. 3098.
27. Vosko, S.H., L. Wilk, and M. Nusair, *Accurate spin-dependent electron liquid correlation energies for local spin density calculations: a critical analysis.* Canadian Journal of physics, 1980. **58**(8): p. 1200-1211.
28. Rauhut, G. and P. Pulay, *Transferable scaling factors for density functional derived vibrational force fields.* The Journal of Physical Chemistry, 1995. **99**(10): p. 3093-3100.
29. Zhou, M., et al., *Carbon dioxide fixation by copper and silver halide. Matrix-isolation FTIR spectroscopic and DFT studies of the XMOCO (X= Cl and Br, M= Cu and Ag) molecules.* The Journal of Physical Chemistry A, 2000. **104**(45): p. 10159-10164.
30. Fukui, K., *Recognition of stereochemical paths by orbital interaction.* Accounts of Chemical Research, 1971. **4**(2): p. 57-64.
31. Cordaro, J.G. and R.G. Bergman, *Dissociation of carbanions from acyl iridium compounds: an experimental and computational investigation.* Journal of the American Chemical Society, 2004. **126**(51): p. 16912-16929.
32. Versluis, L., T. Ziegler, and L. Fan, *A theoretical study on the insertion of ethylene into the cobalt-hydrogen bond.* Inorganic chemistry, 1990. **29**(22): p. 4530-4536.
33. Fukui, K., *The role of frontier orbitals in chemical reactions (Nobel Lecture).* Angewandte Chemie International Edition in English, 1982. **21**(11): p. 801-809.
34. Dunning, T.H. and P.J. Hay, *Gaussian basis sets for molecular calculations*, in *Methods of electronic structure theory*. 1977, Springer. p. 1-27.
35. Huzinaga, S., *Basis sets for molecular calculations.* Computer physics reports, 1985. **2**(6): p. 281-339.
36. Hay, P.J. and W.R. Wadt, *Ab initio effective core potentials for molecular calculations. Potentials for K to Au including the outermost core orbitals.* The Journal of chemical physics, 1985. **82**(1): p. 299-310.
37. Hay, P.J. and W.R. Wadt, *Ab initio effective core potentials for molecular calculations. Potentials for the transition metal atoms Sc to Hg.* The Journal of

chemical physics, 1985. **82**(1): p. 270-283.
38. Wadt, W.R. and P.J. Hay, *Ab initio effective core potentials for molecular calculations. Potentials for main group elements Na to Bi.* The Journal of Chemical Physics, 1985. **82**(1): p. 284-298.
39. Andrae, D., et al., *Energy-adjusted ab initio pseudopotentials for the second and third row transition elements.* Theoretica chimica acta, 1990. **77**(2): p. 123-141.
40. Truhlar, D.G., B.C. Garrett, and S.J. Klippenstein, *Current status of transition-state theory.* The Journal of physical chemistry, 1996. **100**(31): p. 12771-12800.
41. Eyring, H., *The activated complex and the absolute rate of chemical reactions.* Chemical Reviews, 1935. **17**(1): p. 65-77.
42. Janssens, S. and G. Van den Mooter, *Physical chemistry of solid dispersions.* Journal of Pharmacy and Pharmacology, 2009. **61**(12): p. 1571-1586.
43. Fukui, K., A. Tachibana, and K. Yamashita, *Toward chemodynamics.* International Journal of Quantum Chemistry, 1981. **20**(S15): p. 621-632.
44. Fukui, K., *Variational principles in a chemical reaction*, in *Frontier Orbitals And Reaction Paths: Selected Papers of Kenichi Fukui*. 1997, World Scientific. p. 461-470.
45. Gonzalez, C. and H.B. Schlegel, *Reaction path following in mass-weighted internal coordinates.* Journal of Physical Chemistry, 1990. **94**(14): p. 5523-5527.
46. Gonzalez, C. and H.B. Schlegel, *An improved algorithm for reaction path following.* The Journal of Chemical Physics, 1989. **90**(4): p. 2154-2161.
47. Fukui, K., *Formulation of the reaction coordinate.* The Journal of Physical Chemistry, 1970. **74**(23): p. 4161-4163.
48. Müller, K. and L.D. Brown, *Location of saddle points and minimum energy paths by a constrained simplex optimization procedure.* Theoretica chimica acta, 1979. **53**(1): p. 75-93.
49. Löwdin, P.-O., *Scaling problem, virial theorem, and connected relations in quantum mechanics.* Journal of Molecular Spectroscopy, 1959. **3**(1-6): p. 46-66.
50. Reed, A.E., R.B. Weinstock, and F. Weinhold, *Natural population analysis.* The Journal of Chemical Physics, 1985. **83**(2): p. 735-746.
51. Frank, J., *Introduction to computational chemistry.* Editorial Offices October, 1999.
52. Reed, A.E., L.A. Curtiss, and F. Weinhold, *Intermolecular interactions from a natural bond orbital, donor-acceptor viewpoint.* Chemical Reviews, 1988. **88**(6): p. 899-926.
53. Reed, A.E. and F. Weinhold, *Natural bond orbital analysis of near-Hartree–Fock water dimer.* The Journal of chemical physics, 1983. **78**(6): p. 4066-4073.
54. Hijikuro, I., T. Doi, and T. Takahashi, *Parallel synthesis of a vitamin D3 library in the solid-phase.* Journal of the American Chemical Society, 2001. **123**(16): p. 3716-3722.
55. Fock, V., *Näherungsmethode zur Lösung des quantenmechanischen Mehrkörperproblems.* Zeitschrift für Physik, 1930. **61**(1-2): p. 126-148.
56. Hückel, E., *Theory of free radicals of organic chemistry.* Transactions of the Faraday Society, 1934. **30**: p. 40-52.
57. Mulliken, R.S., *Spectroscopy, molecular orbitals, and chemical bonding*. 1967: Norstedt.
58. Fukui, K., T. Yonezawa, and H. Shingu, *A molecular orbital theory of reactivity*

in aromatic hydrocarbons. The Journal of Chemical Physics, 1952. **20**(4): p. 722-725.
59. Woodward, R.B. and R. Hoffmann, *The conservation of orbital symmetry*. 2013: Elsevier.
60. Runge, E. and E.K. Gross, *Density-functional theory for time-dependent systems.* Physical Review Letters, 1984. **52**(12): p. 997.
61. Perdew, J.P., *Density-functional approximation for the correlation energy of the inhomogeneous electron gas.* Physical Review B, 1986. **33**(12): p. 8822.
62. Tawada, Y., et al., *A long-range-corrected time-dependent density functional theory.* The Journal of chemical physics, 2004. **120**(18): p. 8425-8433.
63. Stratmann, R.E., G.E. Scuseria, and M.J. Frisch, *An efficient implementation of time-dependent density-functional theory for the calculation of excitation energies of large molecules.* The Journal of chemical physics, 1998. **109**(19): p. 8218-8224.
64. Petersilka, M., U. Gossmann, and E. Gross, *Excitation energies from time-dependent density-functional theory.* Physical review letters, 1996. **76**(8): p. 1212.

Chapter III

d-block metal complexes

Since many elements in the d-block have a number of single electrons in their electronic configuration that are easier to lose, these metals have variable valence states, such as iron. These metals can easily form complexes due to the presence of empty d-orbitals. Metallic elements adopt hybridized orbitals to accept electrons in order to reach a stable state of 16 or 18 valence electrons.

The d-block metals generate complexes with different molecules or groups that can be used to catalyze small molecule activation reactions. These partially filled d-orbitals and electrons give them special chemical properties: on the one hand, the empty d-orbitals can accept lone pairs of electrons from the substrate molecule, thus making the substrate molecule electron deficient and increasing its reactivity with nucleophilic reagents; on the other hand, the electrons on the d-orbitals can flow to the empty orbitals of the substrate molecule, making the substrate molecule electron rich and increasing its reactivity with electrophilic reagents. Through the interaction with the metal d-orbitals, the electronic properties of the substrate molecule change and activation is achieved, resulting in a higher value product. In this chapter we focus on two kinds of d-block metal complexes and their reactivity to small molecule activation.

III.1. Scandium complex and iron complex supported by pentadentate ligand

Research on d-metal complexes supported by pentadentate ligands *B_2Pz_4Py* or BPz_2Py_3 have been studied. The first row of transition metals has been coordinated and synthesized by such pentadentate ligands[1-5]. This chapter mainly discusses the different reaction properties brought by the diversity of the terminal metal linking groups of iron complexes and scandium complexes and the derivatives of the multi-bond mode.

III.1.1. Introduction

III.1.1.1. Interconversion of hydroxo and oxo using scandium complexes supported by the dianionic pentadentate ligand B_2Pz_4Py

Scandium alkyl complexes supported by the dianionic pentadentate ligand *B_2Pz_4Py* can react with proton reagents to form oxo complexes[3, 6] ， Even trace

amounts of water can trigger the hydrolysis of scandium complexes. This hydrolysis can generate the desired terminal metal hydroxyl complex L_nM-OH. This hydroxyl complex can be used to synthesize oxo bridged complexes L_nM-O-M'L_n with different metals. However, such transition metal complexes with terminal hydroxyl groups are rare in reports. The main reason is that the reaction rate of metal-alkyl groups to produce metal-hydroxy groups through hydrolysis is in competition with the reaction rate of metal-hydroxyl dehydration to form bridged oxo, and oxo complexes are favored in both kinetics and thermodynamics[7-9].

Recently, Professor Piers [10]found in experiments that only the μ-oxo compound can be observed when the alkyl scandium (*B_2Pz_4Py*)Sc-CH_3 reacts with water in a toluene solution. But when the solid sample is exposed to the atmosphere for a period of time, the μ-oxo compound [(*B_2Pz_4Py*)Sc]$_2$O and the dimeric hydroxyl substance Heating this mixed sample will find that [(*B_2Pz_4Py*)Sc(μ -OH)]$_2$ slowly disappears. This is because the hydroxyl group continues to react with water which remove during the conversion from [(*B_2Pz_4Py*)Sc(μ-OH)]$_2$ to (*B_2Pz_4Py*)Sc)$_2$O, and finally a completely hydrolyzed nitrogen (pyridyl) protonated product is formed. In this product, Sc has lost part of its multidentate coordination sites. Therefore, we calculated this transformation mechanism using DFT.

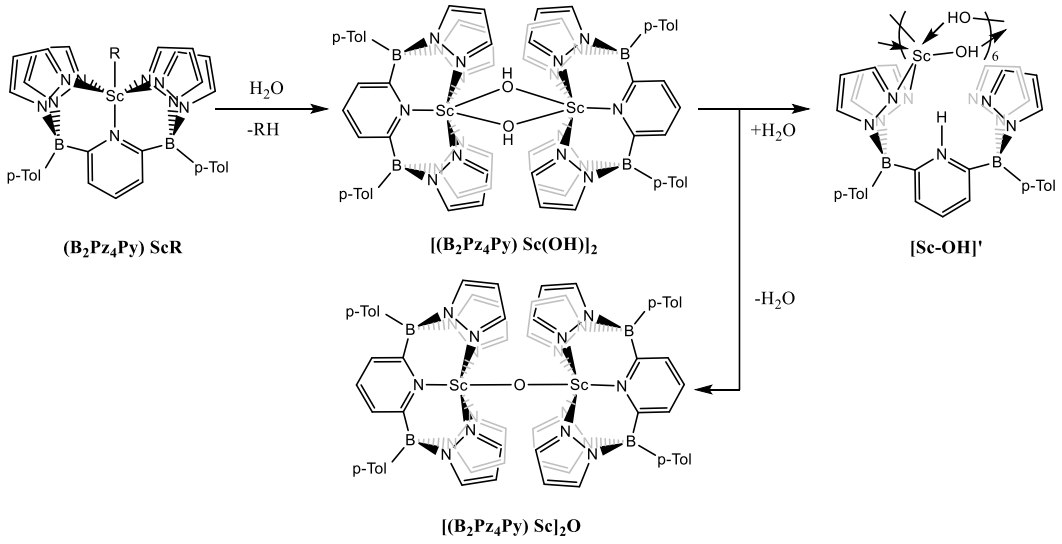

Scheme 3.1 Reaction with water and (*B_2Pz_4Py*)Sc-CH_3 to generate hydroxo bridged complexes and oxo bridged complexes

III.1.1.2. The formation of the Sc=E bond by scandium complexes supported by the monoanionic pentadentate ligand BPz_2Py_3.

The reaction between d-block metal complexes and main group elements to form M=E (E=O, NR, PR, CR) compounds has always been an area worth studying. For the dianion (*B_2Pz_4Py*)Sc, it is very difficult to generate the Sc=E double bond. This is because the dianion feature of the ligand leads to the high basicity of Sc=E[11]. Therefore, Professor Piers used a modified new ligand to remove one B atom, and the two pyrazoles in the ligand were replaced by pyridine. This new ligand *BPz_2Py_3* possesses monoanionic properties.

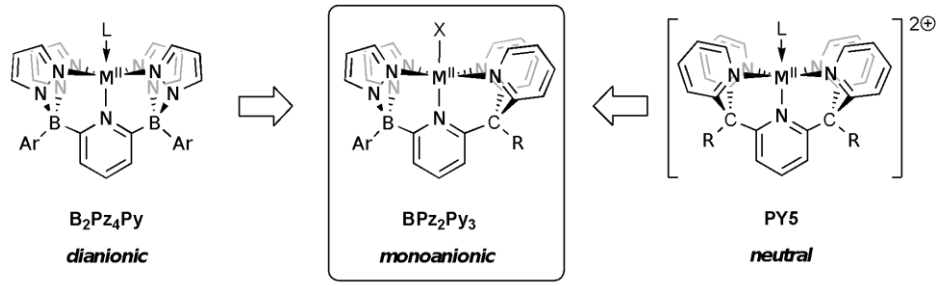

Scheme 3.2 The dianionic, monoanionic, neutral form of the pentadentate ligand

Professor Piers and his colleagues have been working on the preparation of (*BPz_2Py_3*)Sc=O and (*BPz_2Py_3*)Fe=O, and recently discovered a three-step excellent synthesis pathway. The protonated free ligand *BPz_2Py_3*-H reacts with ScR_3•THF_2 (R=CH_2SiMe_2Ph), and one RH is removed to form (*BPz_2Py_3*)ScR_2. After adding hydrated $B(C_6F_5)_3$, the remaining two equivalents of RH are removed, thereby obtaining a Sc-O-B connection. We will study the mechanism of this process.

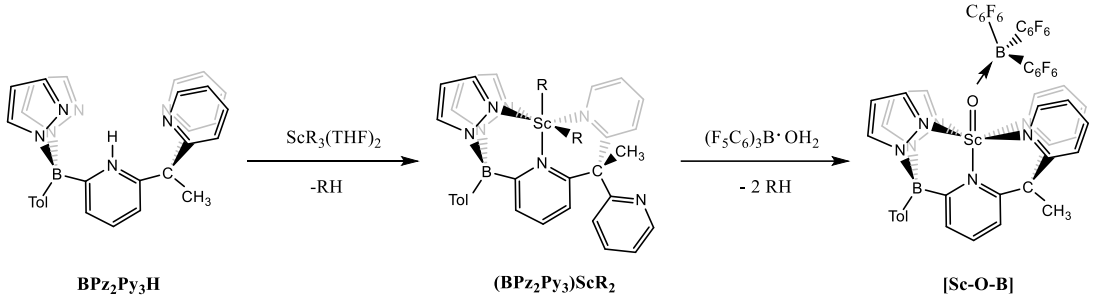

Scheme 3.3 The formation of Sc=O, where R=CH_2SiMe_2Ph

The application of the double bond is not limited to the synthesis of Sc=O.

Professor Piers [12] also found that when (*BPz$_2$Py$_3$*)ScR$_2$ is generated and then 2,6-di-iso-propylaniline is added, it still undergoes two equivalents of RH removal, and finally gets the terminal scandium imido complex. Using the same preparation route, 2,6-di-iso-propylphenyl phosphine can be added to the Sc terminal. At this time, however, unexpected changes occurred in the product. Through experimental characterization, it was found that in the phosphoalkyl complex, the characteristic of double bond of scandium phosphorus was lost, and the pyridyl group was transferred to the P group through the C-C bond cleavage, thereby forming a new tetradentate ligand. We will calculate the mechanism of this path.

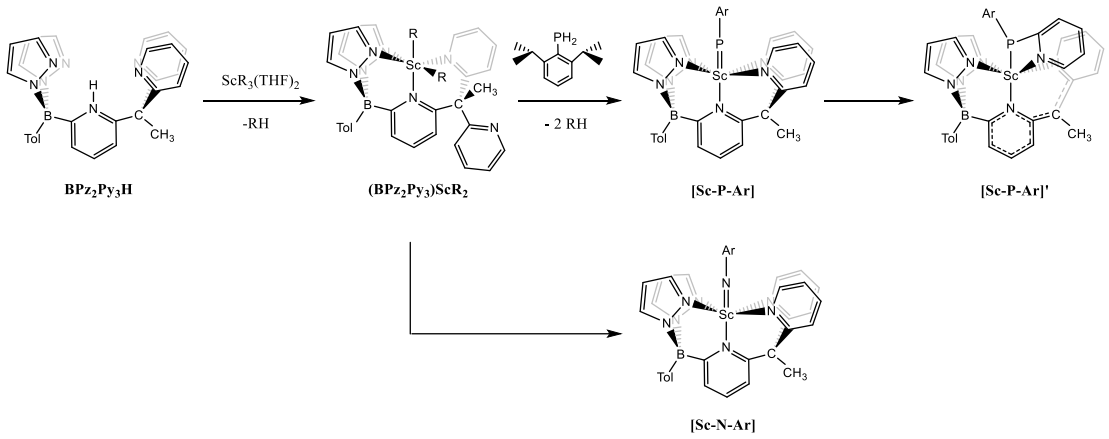

Scheme 3.4 The formation of [Sc-P-Ar], [Sc-N-Ar] and [Sc-P-Ar]', where R=CH_2SiMe_2Ph, Ar=2,6-phenylpropyl

III.1.1.3. Dianionic pentadentate ligand B$_2$Pz$_4$Py supported iron complex derivatives to activate ammonia and hydrazine

As a typical air pollutant, NH_3 is a widely used intermediate in the chemical industry. And in recent years NH_3 has the potential to become a carbon-free fuel. And NH_3 has a high N-H bond dissociation energy of 107.6kcal/mol[13]. The process of oxidizing NH_3 to N_2 is not easy. So activation of ammonia has always been an interesting challenge. However Coordination of NH_3 in the metal center can reduce the energy of nitrogen-hydrogen bond cleavage in NH_3. So Doctor Nurdin and Professor Piers [14] used the dianionic pentadentate ligand *B$_2$Pz$_4$Py* coordinated to iron atom as the catalyst to active the ammonia. The electron-rich *B$_2$Pz$_4$Py* is easier to obtain higher-form oxides. First, ammonia oxidation requires the loss of a hydrogen atom from NH_3.

Therefore, 2,4,6-tri-tert-butylphenoxy radical (ArO) was selected to treat the (*B_2Pz_4Py*) Fe-NH_3 obtained through a series of preparations. After ArO takes a H from NH_3 to form Fe(III)–NH_2, excessive ArO will cause itself to lose a ^{t}Bu group to form product C. After a series of experimental testing and characterization, Doctor Nurdin found that the NH_2 group was connected to the ortho-position ^{t}Bu group, and the N-C_{ortho} coupling and the cleavage of the C-C bond in the aromatic group occurred. We will calculate the reaction mechanism for this step.

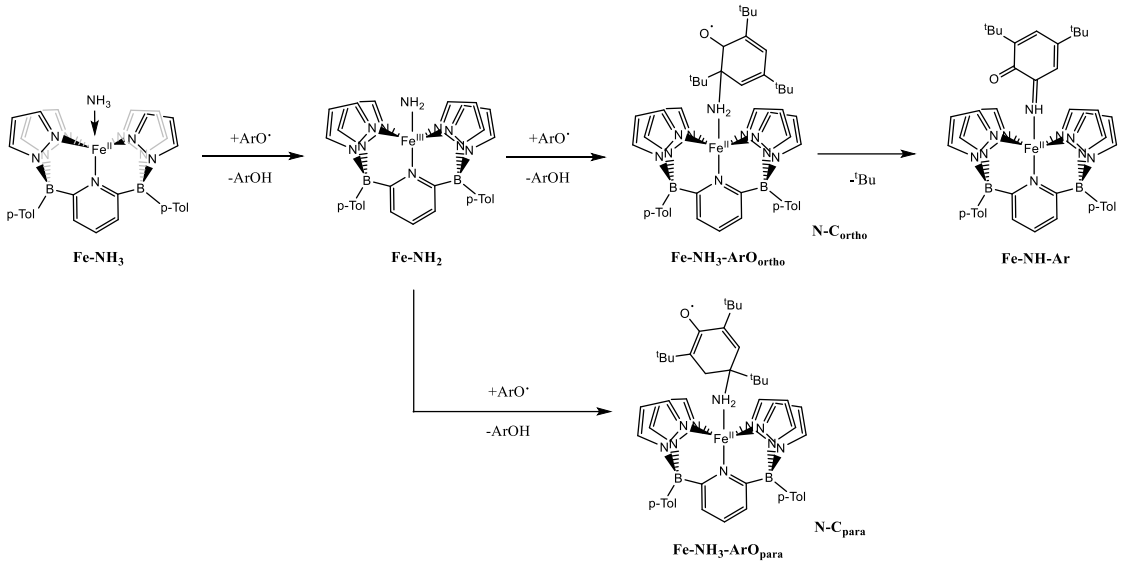

Scheme 3.5 Activation of ammonia by dianionic iron complex

Due to the dianionic nature of the *B_2Pz_4Py* ligand, the divalent iron compound may be a strong reducing agent that can induce the cleavage of the nitrogen-nitrogen bond in hydrazine. Therefore, when H_2N-NH_2 is added to (*B_2Pz_4Py*) Fe, two products will be obtained, trans diazene dimer [(*B_2Pz_4Py*)Fe(NH_2)]$_2$ and (*B_2Pz_4Py*)Fe-NH_3. In this section, mechanism calculations will be made on this basis.

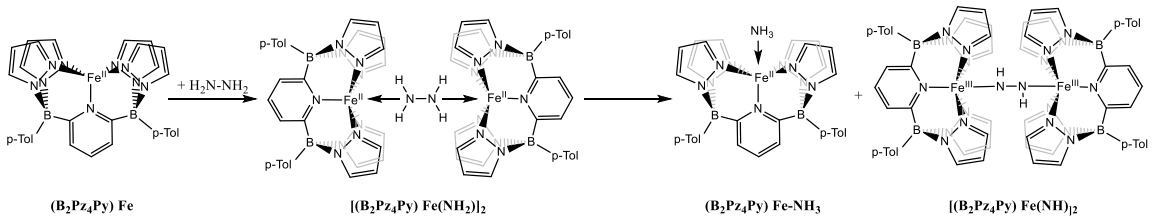

Scheme 3.6 Activation of hydrazine by dianionic iron complex

III.1.2. Computational details

The geometries were fully optimized and the total energies were calculated using the Becke's three-parameter hybrid method with the Perdew and Wang PW91 correlation functional (B3PW91)[15, 16]. The Sc,Fe,P atoms participating in the reaction use SDDall basis set, and the 6-31G(d,p) basis set is used for remaining atoms (C, H, O, N, B)[17, 18]. Intrinsic reaction coordinates (IRC) are used to calculate the transition states obtained by connecting with their respective intermediates[19, 20]. Use NBO to analyze the natural bond orbital of the optimized structure in order to study the bonding.

III.1.3. Results and discussion

III.1.3.1. Interconversion of hydroxo and oxo using scandium complexes supported by the dianionic pentadentate ligand B_2Pz_4Py

In the experiment, the scandium hydroxo compounds were verified to be bound in a dimeric manner by a nuclear overhauser effect spectroscopy (NOESY) method. The crystal structures of the experimentally obtained dimeric hydroxo-bridged compound [(*B_2Pz_4Py*)Sc(OH)]$_2$ and oxo-bridged compound [(*B_2Pz_4Py*)Sc]$_2$O were optimised to give figures (a) and (b) (figure 3.1). In the scandium hydroxo compound, the bond length of Sc-O is in the range of 2.103-2.116 Å, which is comparable to that of other scandium μ-OH dimers [21]. and the bond lengths obtained by calculation are consistent with the 2.118 Å and 2.196 Å bond lengths obtained experimentally, thus demonstrating the experimental dimerisation nature of hydroxo. Based on the calculated bond lengths obtained for the Sc=O double bond in the monomeric (*B_2Pz_4Py*)Sc=O (1.732 Å), it is clear that in the scandium oxo compound The bond length of Sc-O (1.892 Å) is intermediate between the single and double bond.

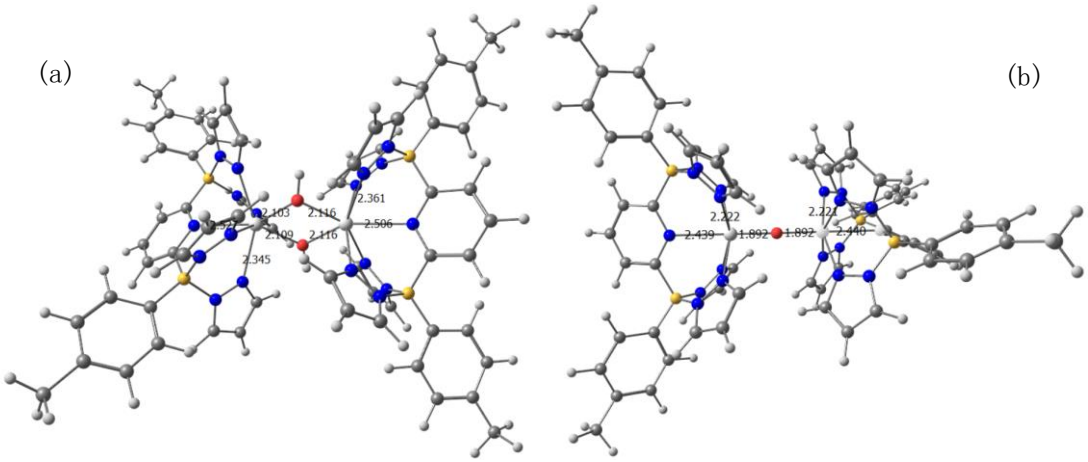

Figure 3.1 3D representation of (a) [(*B*$_2$*Pz*$_4$*Py*)Sc(OH)]$_2$ and (b) [(*B*$_2$*Pz*$_4$*Py*)Sc]$_2$O. Red for oxygen atoms, blue for nitrogen atoms, yellow for boron atoms and white for scandium atoms.

Based on the experimentally observed hydrolysis reactions of the scandium alkyl complex, we found that the hydroxyl bridging dimer [(*B*$_2$*Pz*$_4$*Py*)Sc(OH)]$_2$ can be dehydrated to form the oxo bridging complex [(*B*$_2$*Pz*$_4$*Py*)Sc]$_2$O. conversely when [(*B*$_2$*Pz*$_4$*Py*)Sc]$_2$O is reacted with an equivalent amount of water to form a mixture of the hydroxo dimer In contrast, when [(*B*$_2$*Pz*$_4$*Py*)Sc]$_2$O is reacted with an equivalent amount of water, a mixture of a hydroxyl dimer, an oxo dimer and a further hydrolysis product [Sc-OH]' is formed.

According to the mechanism obtained from the theoretical calculations (Figure3.2), we can see that the loss of water from the scandium hydroxy to scandium oxo is a heat-absorbing process with a reaction enthalpy ΔH = 13.2kcal/mol. One OH in the hydroxyo Hydrogen is transferred from the oxygen atom to the hydroxyo group through this structure, resulting in an adduct of scandium complexes with water bridged by the oxygen atom. This process requires overcoming the not so high energy barrier of 14.7 kcal/mol. The adduct of scandium oxo complexes with water, [(*B*$_2$*Pz*$_4$*Py*)Sc]$_2$O▪H$_2$O, then has a lower energy and shows relatively stable properties compared to [(*B*$_2$*Pz*$_4$*Py*)Sc]$_2$O. Therefore the final pure oxo product still needs to overcome an energy barrier of 11.0 kcal/mol.

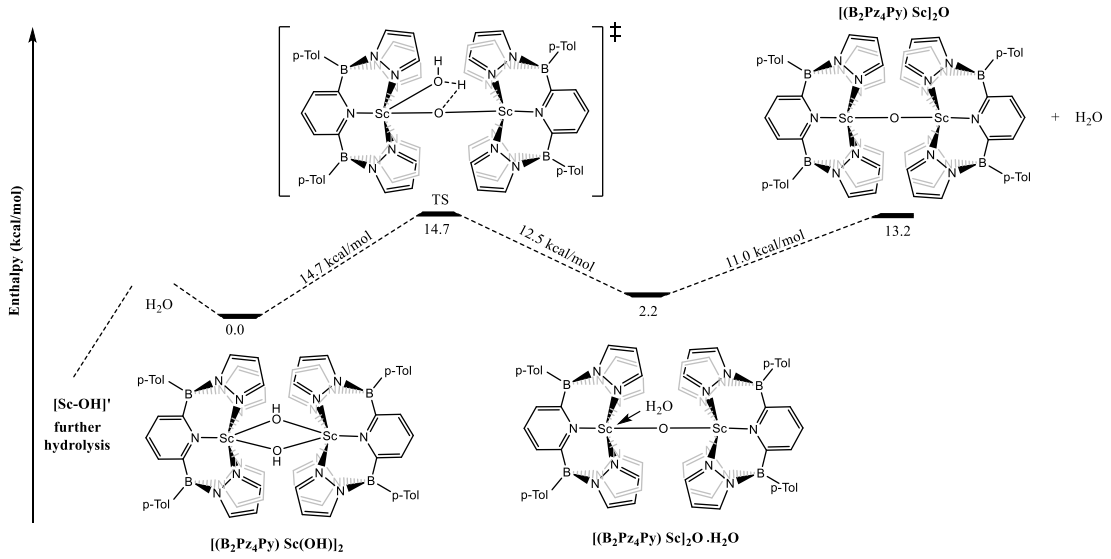

Figure 3.2 Computed enthalpy profile for the interconversion of hydroxo and oxo

Conversely, the reaction of the oxo-bridging complex with water is exothermic. The reaction only requires overcoming the transition state from the water adduct [(*B*$_2$*Pz*$_4$*Py*)Sc]$_2$O▪H$_2$O to 12.5 kcal/mol. However, it has been shown that the oxo complex is more readily observed in the reaction products. This is because the eventual removal of water from the hydroxyl group will allow further hydrolysis of the hydroxyl group, a step that renders the otherwise relatively stable [(*B*$_2$*Pz*$_4$*Py*)Sc(OH)]$_2$ kinetically unstable. Although the inverse reaction is thermodynamically more favourable, the presence of the racemization reaction and the fact that the energy barrier is also not high in the positive reaction leads to the hydroxo complex, although more stable, still being readily interconvertible with the oxo complex.

III.1.3.2. The formation of the Sc=E bond by scandium complexes supported by the monoanionic pentadentate ligand BPz$_2$Py$_3$.

We have obtained oxo derivatives from the hydrolysis of scandium alkyl complexes possessing a dianionic ligand. This section will explore the generation of the Sc=O oxide complexes as a monomer, as well as the properties of similar Sc=N imido complexes, and Sc=P phosphorylidene complexes. To obtain neutral Sc=E(O, NR, PR) complex, the monoanionic ligand *BPz$_2$Py$_3$* is used here.

The protonated proligand reacts with ScR$_3$ (R=CH$_2$SiMe$_2$Ph) and one equivalent

of HR is eliminated to give what we believe to be a complex of bis(BPz_2Py_3)ScR_2; it is subsequently reacted with hydrated $B(C_6F_5)_3$ and two equivalents of RH are eliminated. Proton NMR showed that the monoanion ligand was coordinated to the Sc centre in a pentadentate fashion in the product. The ^{11}B and ^{19}F NMR spectroscopy also show that $B(C_6F_5)_3$ has been incorporated into the product, which is the Sc-O-B compound shown.

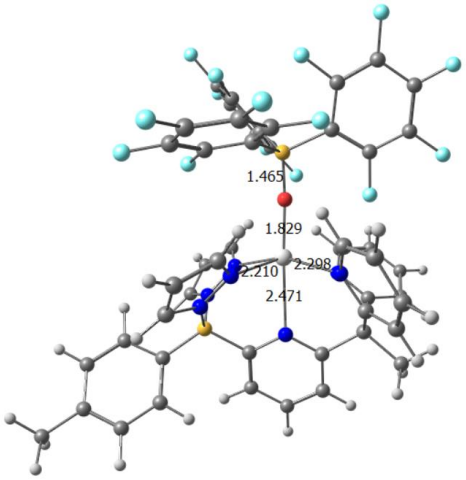

Figure 3.3 3D representation of [Sc-O-B] compound. Red for oxygen atoms, blue for nitrogen atoms, yellow for boron atoms and white for scandium atoms, green for fluorine atoms.

We have designed the reaction mechanism based on this structure and the enthalpy profiles are shown below. When the protonated proligand is added to ScR_3, it is immediately exothermic by 62.8kcal/mol, after which 24.6kcal/mol is used to pass through the first transition state. At this point the bis-alkyl intermediate is obtained as shown in figure, but the isolation in experiments of this intermediate is not successful, so we have attempted to simulate the structure of the bis-alkyl scandium complex (BPz_2Py_3)ScR_2 using a computational model. The exotherm of 104.0 kcal/mol was calculated to produce this structure, indicating that the bis-alkyl group is highly stable. This intermediate is the basis for the subsequent Sc=E double bond.

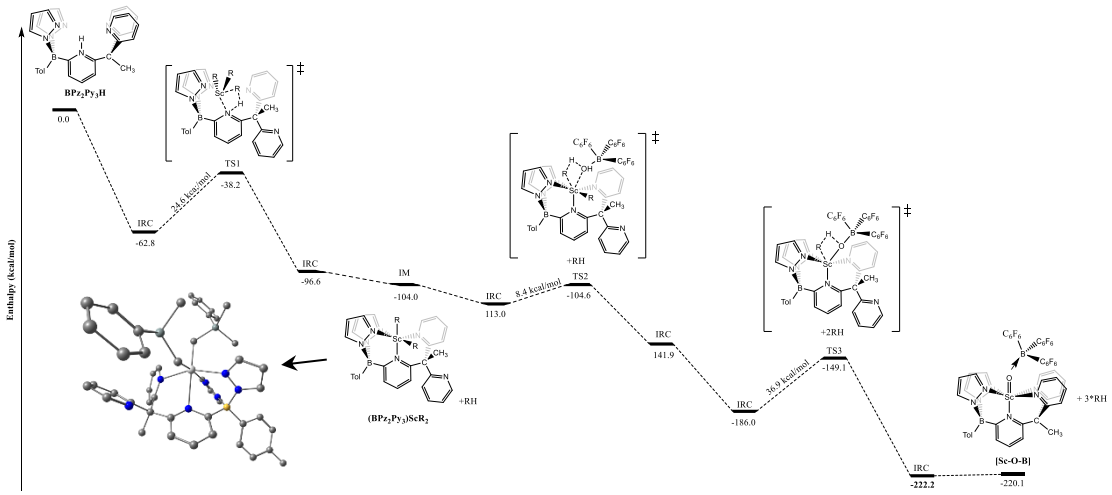

Figure 3.4 Computed enthalpy profile for the formation of scandium-oxygen double bond

When we add the hydrated fluoropentane ($B(C_6F_6)_3 \cdot H_2O$) to bring a proton to the R group, after the RH elimination of the transition state TS2, $B(C_6F_6)_3$ is linked to Sc via a hydroxyl group. The energy barrier of TS2 is only 8.4 kcal/mol. when the last H is taken away by R, the final product is produced, in the Sc-O-B mode. This final step of the hydrogen transfer transition state is clearly the rate-determining step of the reaction, as its energy barrier is 36.9 kcal/mol. Although this step has a relatively high energy barrier, the overall reaction to produce [Sc-O-B] is thermodynamically very powerful through an exothermic process by 220.1 kcal/mol.

This mechanism reveals that this mode of reaction readily yields terminal Sc=E, which is an excellent synthetic pathway. This mechanism can therefore be used to extend the diversity of double bonds, such as Sc=N imido complexes, and Sc=P phosphorylidene complexes.

For example, on the basis of the dialkyl scandium complex obtained, the reaction with 2,6-di-iso-propylaniline gave [Sc-N-Ar] after the elimination of two RH. After structural optimization of [Sc-N-Ar], we obtained a bond length of 1.848 Å for Sc-N, which is consistent with the properties of a double bond. Moreover, the bond angle of Sc-N-Ar is almost close to 180° linear. According to the calculated Wiberg bond index, Sc-N is 1.298 Å, possessing the characteristics of a double bond. And the NBO orbital analysis of [Sc-N-Ar] revealed a clear π-bonding feature between Sc-N in HOMO and HOMO-1.

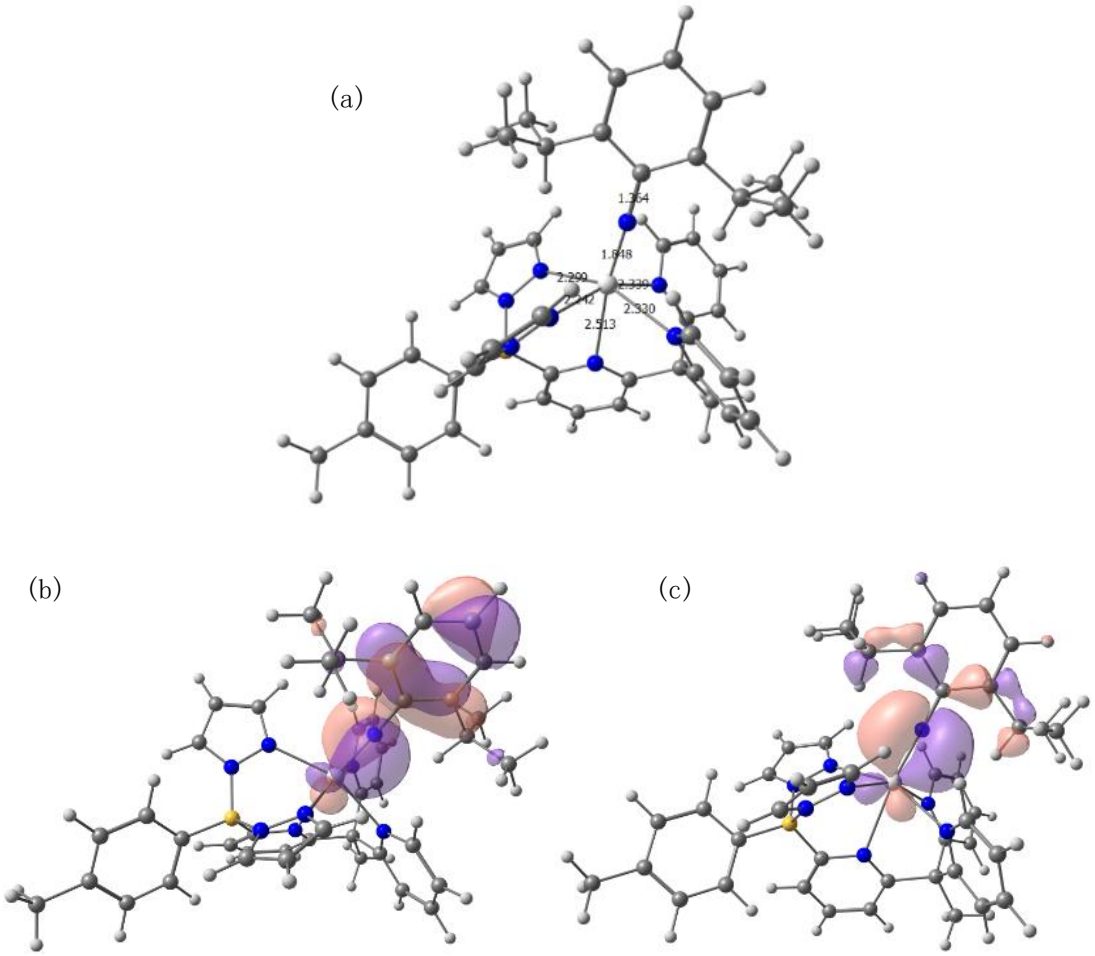

Figure 3.5 3D representation of (a) [Sc-N-Ar] and (b) HOMO of [Sc-N-Ar], (c) HOMO-1 of [Sc-N-Ar]. Blue for nitrogen atoms, yellow for boron atoms and white for scandium atoms.

When dialkyl scandium (*BPz*$_2$*Py*$_3$)ScR$_2$ was reacted with 2,6-di-iso-propylphenyl phosphine to prepare phosphinidene analog [Sc-P-Ar], yet another new product was found [Sc-P-Ar]'. Experimental characterisation illustrated that in this product, no Sc=P was found and the symmetry was significantly lower than in the structure of [Sc-P-Ar]. The structure of the product [Sc-P-Ar]' obtained by optimisation shows that one of the equatorial pyridine groups in the ligand has undergone a C-C bond cleavage, generating a new tetradentate ligand. We have carried out a mechanistic study on the formation of this new tetradentate ligand.

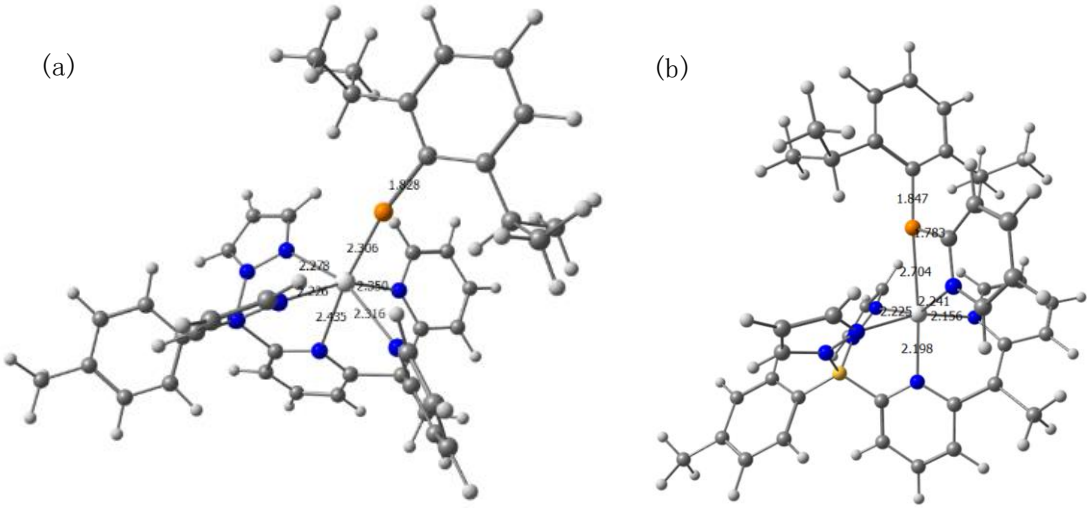

Figure 3.6 3D representation of (a) reactant [Sc-P-Ar] and (b) product [Sc-P-Ar]'. Orange for phosphorus atoms, blue for nitrogen atoms, yellow for boron atoms and white for scandium atoms.

Firstly we consider that the production of [Sc-P-Ar]' is based on [Sc-P-Ar]. Figure 3.6 are the structures of the reactant [Sc-P-Ar] and the product [Sc-P-Ar]'. Comparing [Sc-N-Ar] and [Sc-P-Ar] ', we can see that the angular bending of Sc-P-Ar is greater (169°). The bond length of Sc-P in the product reaches 2.704 Å, which is much higher than the 2.306 Å in the reactants, indicating that the Sc-P distance in the product is already greater than that of the double bond. This is also verified by the Wiberg bond index, which is 1.978 in the reactants (pointing to the bond level of a double bond), compared to 0.95 in the products (pointing to the bond level of a single bond).

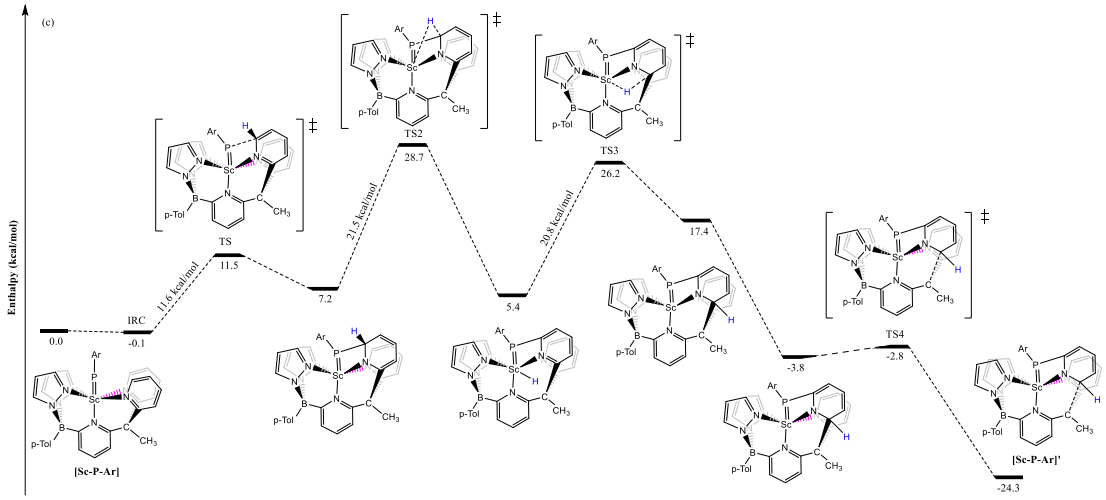

Figure 3.7 Computed enthalpy profile for the formation of a new product [Sc-P-Ar]' from phosphinidene [Sc-P-Ar]

We first propose a reaction pathway for the transfer of H from the ortho carbon

position of pyridine to secondary ortho carbon involving the Sc centre. The phosphorylidene group nucleophilically attacks the ortho-C on the pyridine, which results in the transfer of H from the ortho-C to the Sc centre. The Sc centre, in turn, undergoes a second H-transfer to the other end of the pyridine, ortho-C. This results in the final product [Sc-P-Ar]'. The total exotherm of the reaction is 24.3 kcal/mol. However, four transition states are required to move from the product to the reactant and the high energy barrier of 28.7 kcal/mol from the reactant to the first hydrogen transfer transition state needs to be overcome. and it is clear that the H transfer transition states in which Sc is involved all show a high energy barrier. The mechanism that does not require H-transfer is thus of greater interest.

We propose an alternative reaction mechanism in which phosphinidene phosphorus directly nucleophilically attacks secondary ortho carbon. The formation of a bond between P and secondary ortho carbon is accompanied by the breaking of the bond between secondary ortho carbon and C. The transition state in this step is 25.6 kcal/mol and the exotherm is 24.3 kcal/mol. In contrast to the first reaction mechanism, it is clearly easier to achieve kinetically. We also performed the same calculation for the imido complex, but in this transition state the energy barrier was as high as 44.8 kcal/mol. It was therefore demonstrated that similar products could not be observed for reactions involving the imido complex in the experiment.

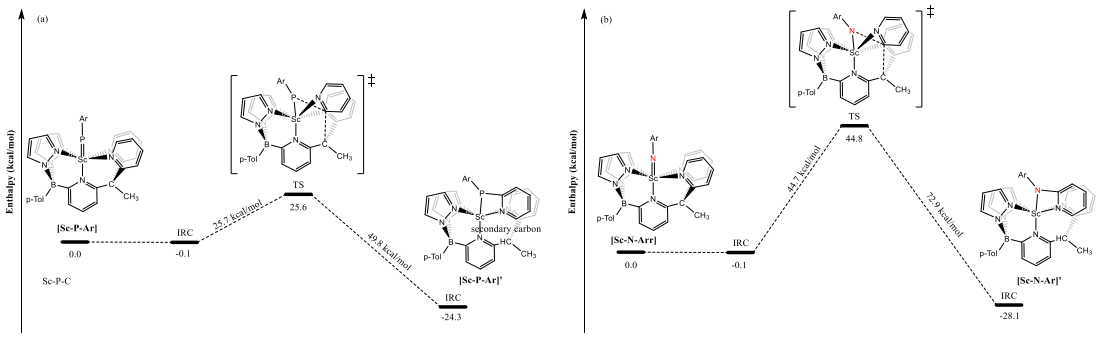

Figure 3.8 Computed enthalpy profile of another pathway for the formation of a new product [Sc-P-Ar]' from phosphinidene [Sc-P-Ar]

In the transition state of Figure (a), the Sc-P bond length becomes 2.555Å (reactant 2.306Å) and the Sc-P-Ar bond angle becomes 114° (reactant 169°). This indicates that the pai bond between Sc=P is absent and the lone pair of electrons on P interacts with the pai* orbital on the equatorial pyridine group.

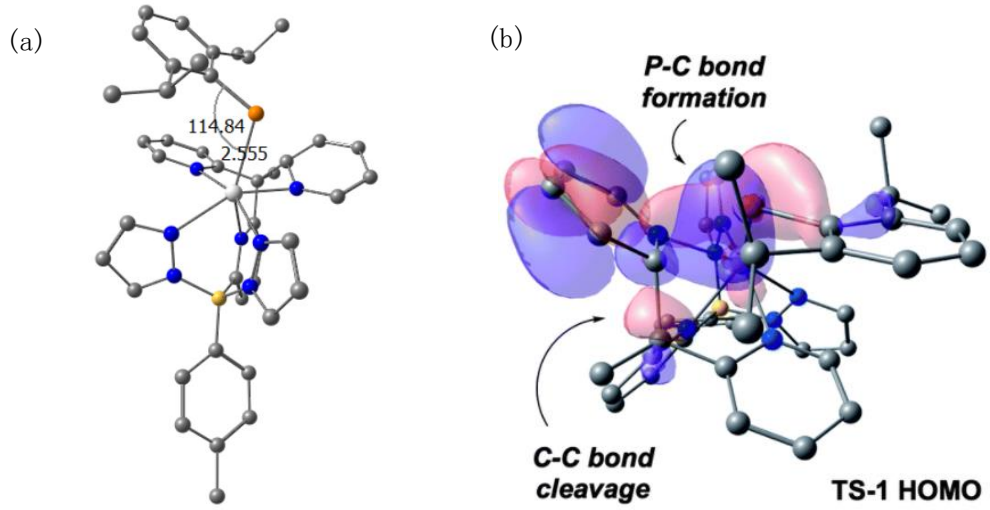

Figure 3.9 3D representation of (a) [Sc-P-Ar] and (b) HOMO of [Sc-P-Ar]. Blue for nitrogen atoms, yellow for boron atoms and white for scandium atoms, orange for phosphorus atoms.

III.1.3.3. Dianionic pentadentate ligand B_2Pz_4Py supported iron complex derivatives to activate ammonia and hydrazine

The activation mechanisms of ammonia and hydrazine are discussed in this sub-section. The ligand used was still the double anion *B_2Pz_4Py* with Fe at the metal centre. ammonia adduct (*B_2Pz_4Py*)Fe-NH_3 was first activated using 2,4,6-tri-tert-butylphenoxy radical (ArO) as a hydrogen ion extractant. Two different C-N heterocoupling products, para coupling and ortho coupling, were obtained. A prerequisite for a mechanistic study of this reaction is to first clarify the spin state of (*B_2Pz_4Py*)Fe-NH_3. By calculating the energies of ammonia adducts with different spin multiplicities, the anti-magnetic low-spin (LS) Fe is finally determined to be the ground state. The optimised structure of the low spin (*B_2Pz_4Py*)Fe-NH_3 system is shown below and we can see that the iron is close to the five N on the ligand *B_2Pz_4Py* and the N on the NH_3.

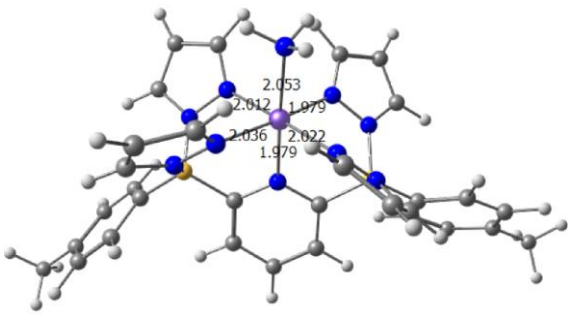

Figure 3.10 3D representation of (B_2Pz_4Py)Fe-NH_3. Blue for nitrogen atoms, yellow for boron atoms and purple for iron atoms.

First, we calculated several intermediates involved in the activation of NH_3 and N_2H_2. For example, the spin density of Fe(III)-NH_2 is mostly concentrated in the trivalent iron centre (78%) as well as in NH_2 (22%), indicating that the NH_2 fraction gives rise to a radical nature. And from a thermodynamic point of view, the bond dissociation energy of N-H in Fe(III)-NH_2 is very high (97.1 kcal/mol), whereas the energy required to dissociate the NH_2 group is only 46.5 kcal/mol. Thus it can be demonstrated that it is not easy to further break N-H bond in the Fe-NH_2 system.

Table 3.1 Bond dissociation energy involving Fe(III)-NH_2 and Fe(II)-NH_3

	BDE(kcal/mol)	
	Fe-NH_n bond	**N-H bond**
Fe(II)-NH_3	**20.3**	**75.5**
Fe(III)-NH_2	**46.5**	**97.1**

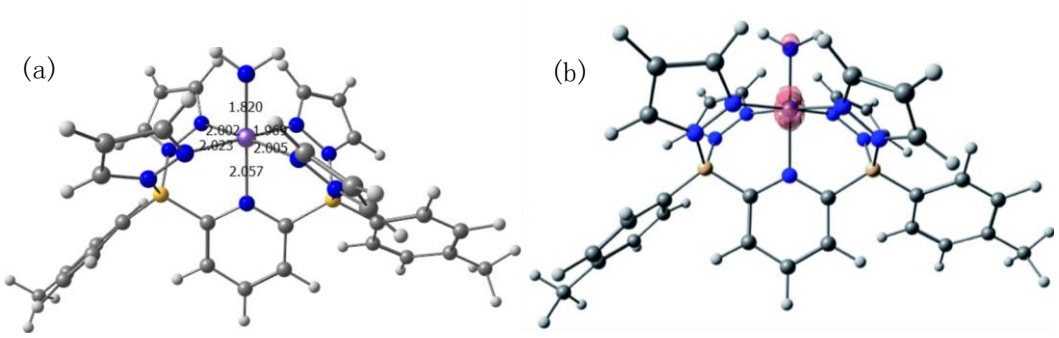

Figure 3.11 (a) 3D representation of Fe(III)-NH_2, and (b) the spin density of Fe(III)-NH_2. Red for oxygen atoms, blue for nitrogen atoms, yellow for boron atoms and white for scandium atoms. 78% of the unpaired electron density is distributed on Fe and 22% on N.

Next we calculated the bond dissociation energy of the ArO-H bond (81.6kcal/mol) after protonation of the hydrogen ion extractant ArO radical. This is higher than the bond dissociation energy of the N-H bond in Fe(II)-NH_3 (75.5kcal/mol). Thus the effectiveness of ArO radical as a hydrogen ion extractant can be demonstrated.

As can be seen in the enthalpy profile of the reaction, the ArO radical extracts the

first hydrogen atom only through a very small energy barrier (5.1kcal/mol), giving a NH_2 group (Fe(III)-NH_2 mentioned above) that possesses some radical properties. On this basis an excess of ArO will no longer undergo extraction of the H atom (because of the BDE of the large N-H bond), but instead takes a kind of heterocoupling of C and N. Here the heterocoupling involves two different positions, namely the carbon of ortho and para in the aromatic ring. We calculated these two reaction pathways separately. The transition states of N-C_{ortho} and N-C_{para} were obtained.

It can be seen that the transition state energy barriers for the N-C_{ortho} and N-C_{para} heterocouplings are the same, but the energy of the ortho product is 10.0kcal/mol lower than that of the para product. this suggests that the Fe-NH_3-ArO_{ortho} structure is more stable and that the transition from the initial Fe(II)-NH_3 to the ortho product is thermodynamically favoured: ΔH = -4.2kcal/mol. whereas the para product generation is endothermic, therefore in agreement with the experimentally observed Fe-NH_3-ArO_{ortho} complex.

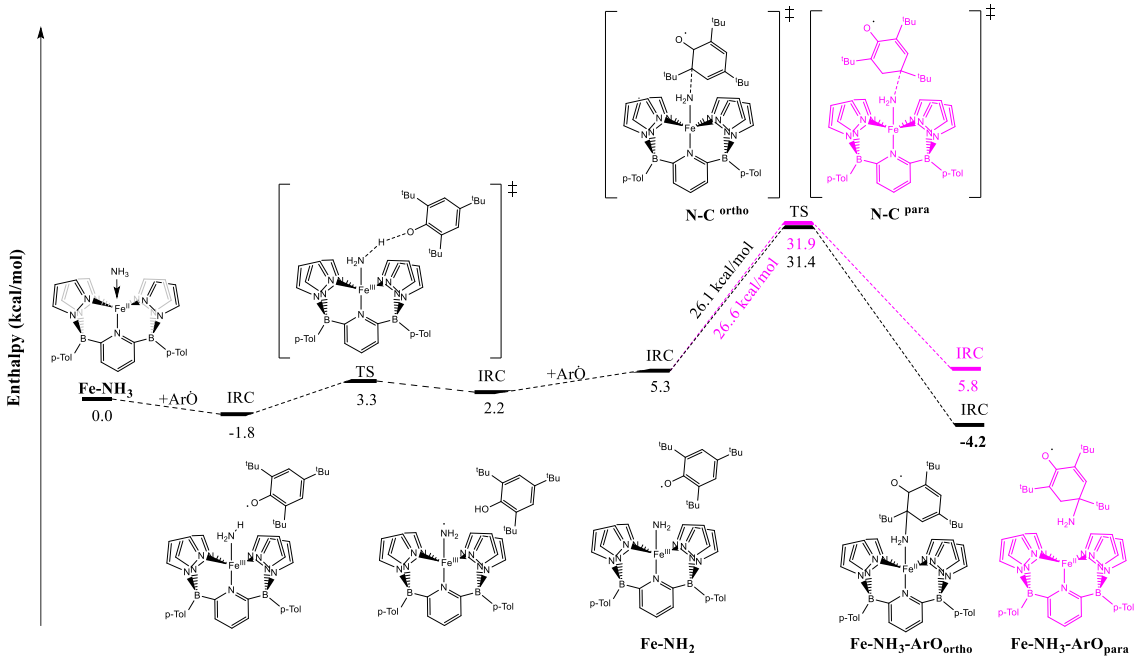

Figure 3.12 Computed enthalpy profile for the activation of ammonia

Subsequently, a mechanistic study of iron complexes with hydrazine N_2H_2 was carried out in order to verify the reactivity of the double anion-supported iron complexes towards the breakage of N-N. ^{1}H NMR spectra indicated the presence of two different products, Fe(II)-NH_3 complexes and diazene dimer Fe(II)-NHNH-Fe(II). The product Fe(II)-NHNH-Fe(II) and the intermediate diazene adduct Fe(II)-NH_2NH_2-

Fe(II) involved in the reaction were also shown to be low-spin and diamagnetic. The bond length of N-N in Fe(II)-NHNH-Fe(II) is calculated to be 1.263Å , which is consistent with the bond length of a double bond. And the Fe-N-N bond angle is 135°, which is consistent with the sp^2 hybridisation of the N atom.

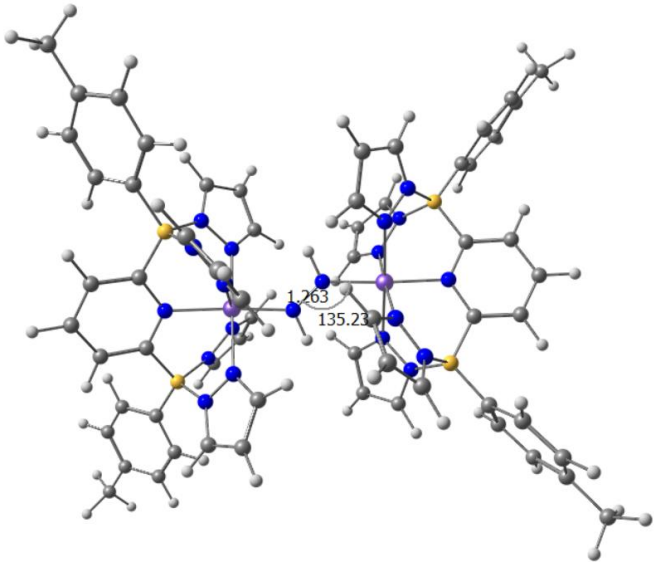

Figure 3.13 3D representation of Fe(II)-NH_2NH_2-Fe(II) Red for oxygen atoms, blue for nitrogen atoms, yellow for boron atoms and white for scandium atoms.

The first (*B_2Pz_4Py*)Fe complex reacts with N_2H_2 to become a dimeric hydrazine adduct with an exothermic heat of 40.0 kcal/mol. The reaction pathways are derived using the dimeric hydrazine adduct Fe-NH_2NH_2-Fe as an important intermediate. The pathway undergoes mainly a proton transfer on both nitrogen of the hydrazine. The transition state energy barrier for this step is 28.9 kcal/mol. The activation of the N-H bond can be seen in the structure of the transition state, where the distance between the original nitrogen atom and the H gradually elongates to 1.370 Å. This step produces the target product Fe-NH_3, as well as the Fe-NH intermediate used for dimerisation. However this step is unstable, resulting in an energy requirement of 6.6kcal/mol. And the energy barrier of 31.5kcal/mol needs to be overcome to go from the lowest energy Fe-NH_2NH_2-Fe to the highest energy Fe-NH.

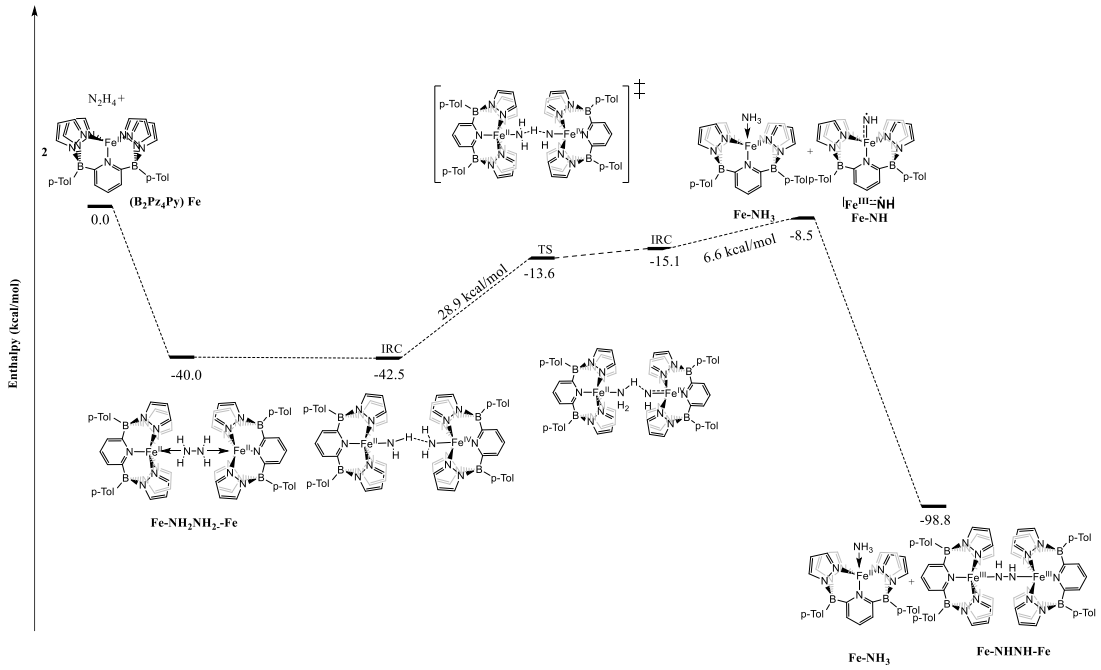

Figure 3.14 Computed enthalpy profile for the activation of hydrazine

However the Fe-NH generated is pleasing. This is because the spin density distribution shows that a higher proportion of unpaired electrons are distributed on N than on Fe-NH_2, which can reach 54%. This makes the dimerisation of monomeric Fe-NH highly reactive and generates a very stable Fe-NHNH-Fe dimer.

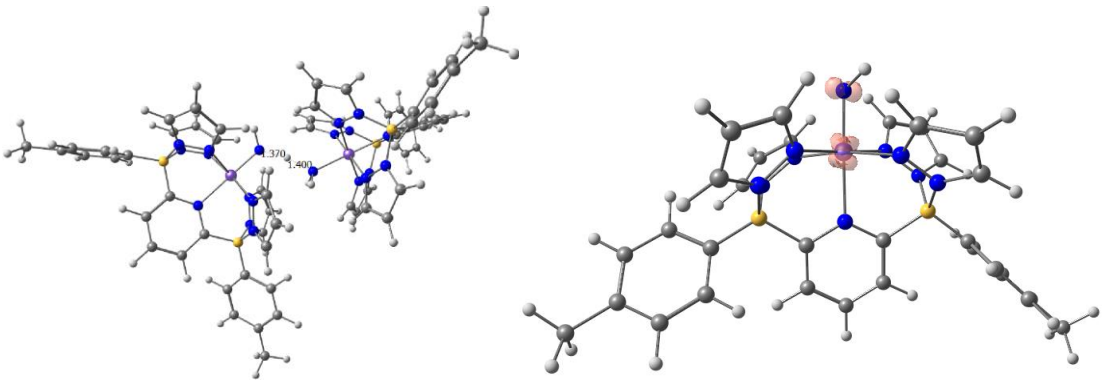

Figure 3.15 (a) 3D representation of transition state of the activation of hydrazine. (b) the spin density of Fe-NH. Red for oxygen atoms, blue for nitrogen atoms, yellow for boron atoms and white for scandium atoms. 46% of the unpaired electron density is distributed on Fe and 54% on N.

III.1.4. Conclusion

This chapter focuses on the mechanism of small molecule activation reactions involving d-block metals (iron and scandium) using double and single anionic pentadentate ligands. The main division is into the interconversion of scandium

hydroxo and oxo bridging complexes supported by the double anion B_2Pz_4Py via water addition and dehydration. DFT calculations demonstrate the thermodynamic stability of the dimeric hydroxyl scandium and that its hydrolytic conversion to oxo complexes only requires overcoming a low energy barrier of 13.2 kcal/mol. As water is generated during the conversion process, it causes further hydrolysis of the dimeric hydroxy-scandium to produce other products. The formation of hydroxo from oxo with water is therefore hindered by the further hydrolysis of the dimeric hydroxy-scandium.

A mechanistic study has also been done for the synthesis process of scandium forming a double bond with a main group element at the terminal of a coordination metal. Here a new ligand BPz_2Py_3 with monoanion is proposed to reduce the high basicity that the double anion imparts to the Sc=E complex. The perfect synthetic pathway found in the experiments is corroborated by the fact that there are no high-energy barriers to be overcome throughout the exothermic reaction for the formation of the double bond. And on this basis, the Sc=O double bond is extended to the Sc=P and Sc=N double bonds. The reaction products of the Sc=P double bond were found to show a distinctive change. It was demonstrated computationally that the Sc=P double bond can induce the breakage of the C-C bond in the ligand to produce the phosphido-pyridyl complex.

Finally we calculated the activation of ammonia and hydrazine through the Fe complexes supported by the double anionic ligand B_2Pz_4Py. Where the activation pathway for ammonia requires the presence of the hydrogen atom extractant ArO, the ortho carbon in ArO will be coupled to the nitrogen in NH_2 after the H atom in Fe-NH_3 has been extracted. The calculations verify the validity of this step and explain why the coupling of the para-C to NH_2 could not be observed experimentally. And the oxidation process of hydrazine was also investigated by DFT. When Fe-NH_2NH_2-Fe undergoes hydrogen transfer between the internal hydrazines to give the imido species, this Fe-NH very quickly polymerises into a dimer.

This quadrupedal pentadentate ligand is so robust that it can support the earth-abundant transition metals exhibiting variety oxidation states. And these complexes and their derivatives will exhibit better catalytic properties, offering richer possibilities for the activation of small molecules.

III.2. Reaction of di-iron imidophosphorane complexes with nitrous oxide

III.2.1. Introduction

Professeur La Pierre HS 's group has been trying to use monodentate weak-field ligands to construct metal-metal bonding compounds. And they have extended this tris(dialkylamido)-imidophosphoranes ligand to the redox chemistry of lanthanide and actinide metal complexes[21-25]. The dialkylamido backbone in this ligand architecture better supports the zwitterionic character in the P–N moiety of imidophosphoranes, favoring a P^{+}–N^{2-} configuration. The steric profile and donor properties of this ligand framework support low-coordinate iron and give rise to clusters with metal–metal bonds. They then investigated the reaction of tris(dialkyl)imidophosphorane-supported Fe(II) complexes with dinitrogen oxide, which was used to examine the reactivity of this bimetallic complex. Nitrous oxide is a greenhouse gas and its potential utilization as a green oxidant has become an important technological target. So far, few iron compounds have been reported to bind or activate with nitrous oxide under mild conditions.

And Professeur La Pierre HS [26]used this weak-field ligand-supported bimetallic complex to study the reactivity of nitrous oxide. A solution of the Fe complex [$Fe_2(\mu^2$-$NP(pip)_3)_2(NP(pip)_3)_2$] , (1-Fe) in diethyl ether was exposed to an atmosphere of nitrous oxide and reacted within 10 min to produce the product [$Fe_2(\mu^2$-$O)(\mu_2$-$NP(pip)_3)_2(NP(pip)_3)_2$] , (2-Fe) .

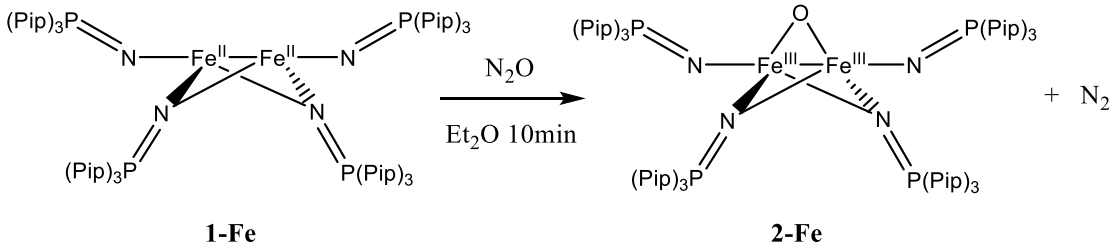

1-Fe **2-Fe**

Scheme 3.7 Reaction of [$Fe_2(\mu^2$-$NP(pip)_3)_2(NP(pip)_3)_2$] with N_2O

III.2.2. Computational details

In this section, the density functional theory (DFT/B3PW91) method is used to carry out theoretical calculations on the lanthanum-mediated aldehyde addition reaction[27-29]. 6 For Fe, the relativistic energy-consistent pseudopotential of the Stuttgart-Köln ECP library was used in combination with its adapted segmented basis. The split basis set 6-31G (d, p) is used for atoms such as C, H, O, and N[17]. The structural optimization and energy correction calculations are carried out for each stagnation point in the reaction, and it is confirmed that the transition state has unique negative frequency and negative eigenvalues. In addition, the intrinsic reaction coordinate calculation (IRC) was performed on the transition state to confirm that the transition state is on the reaction path of the reactants and products[30, 31]. All calculations use the Gaussian09 computing software package and are completed on the high-performance computing platform. Reactant $[Fe_2(\mu^2\text{-}NP(pip)_3)_2(NP\ (pip)_3)_2]$, intermediate and transition state are calculated using the singlet spin state, and product $[Fe_2(\mu^2\text{-}O)(\mu_2\text{-}NP(pip)_3)_2(NP(pip)_3)_2]$ is calculated using a triplet spin state(ground state).

III.2.3. Results and discussion

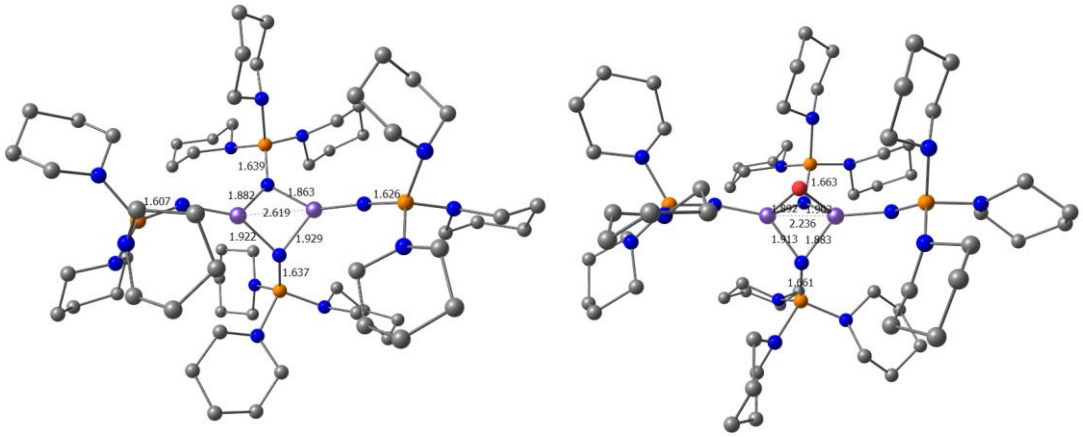

Figure 3.16 3D representation of (a) reactant [1-Fe] and (b) product [2-Fe]. Yellow represents phosphorus atoms, blue represents nitrogen atoms, and purple represents iron atoms. In [2-Fe], the distances of Fe and O are 1.794 Å and 1.782 Å, respectively.

The distance between the two Fe and N does not vary much in the reactants and products, while the N-P distance in the products is a little longer than that in the products. And it can be seen that the Fe-Fe distance in the products is very short, only 2.236 Å. This is consistent with experiment.

In order to gain insight into the observed reactivity, the reaction of 1-Fe with N_2O was calculated under DFT (B3PW91). Energy profiles reveal that N_2O is first bound by an oxygen atom to one of the Fe centers when added to the system. This asymmetric coordination exotherm of 2.1 kcal/mol. After this intermediate, O binds to the other Fe and the distance between O and N is gradually elongated. The energy barrier in this transition state is 4.1 kcal/mol. This energy barrier is low because the nucleophilic assistance of the second iron in the transition state facilitates the breaking of the N-O bond. The distances between the two irons and O are 1.99 Å and 2.53 Å, respectively, both longer than the Fe-O bond length in the product.

Following the intrinsic reaction coordinates, the complex 2-Fe is formed in a thermodynamically favorable manner and releases N_2 gas. This energy profile indicates that the metal-metal bonding complex 1-Fe is able to participate synergistically in the two-electron reduction of N_2O by single-electron oxidation at each metal center.

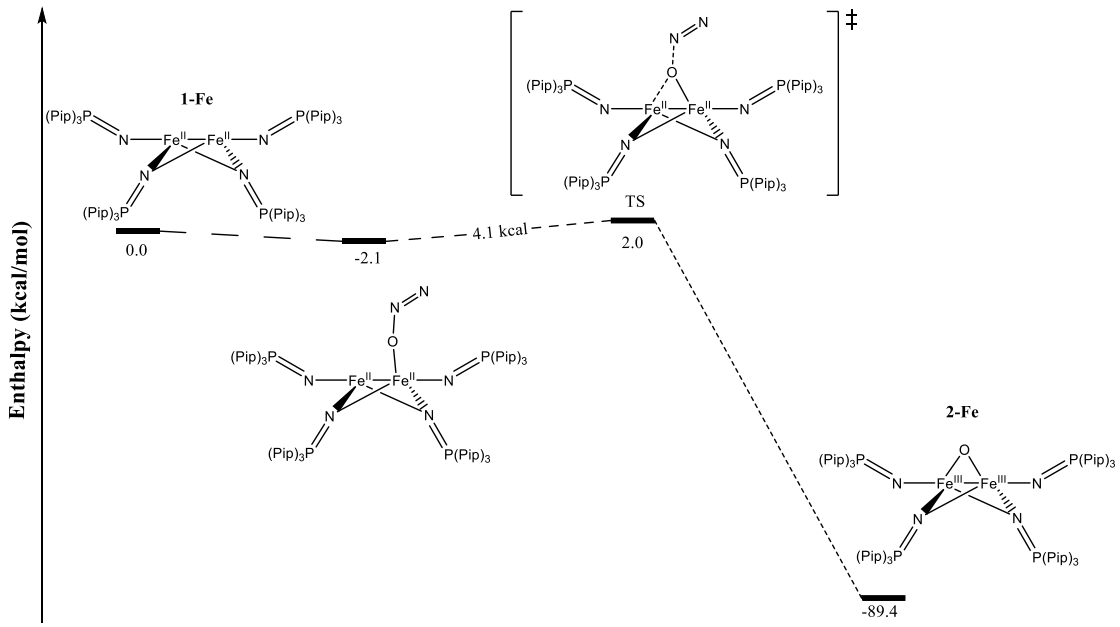

Figure 3.17 Computed enthalpy profile for the reaction of [1-Fe] with N_2O

III.2.4. Conclusion

We calculated the reaction mechanism of [$Fe_2(\mu^2$-NP (pip)$_3)_2$(NP (pip)$_3)_2$] catalyzing the reduction of N_2O to N_2. A thermodynamically very favorable pathway and stable μ^2-O product were obtained. And in this product [$Fe_2(\mu^2$-O)(μ_2-

$NP(pip)_3)_2(NP(pip)_3)_2]$ was shown to posses the shortest Fe-Fe distance comparing with other reports[32, 33].

III.3. Conclusion

Firstly, a pentadentate ligand is proposed that can adjust the charge of the ligand by adding or subtracting boron atoms, namely B_2Pz_4Py and BPz_2Py_3. The reactions of interconversion of scandium hydroxo bridged complexes and oxo bridged complexes supported by the dianionic ligand B_2Pz_4Py by adding or subtracting water are firstly calculated DFT calculations demonstrate the thermodynamic stability of the dimeric hydroxyl scandium and that its hydrolytic conversion to oxo complexes only requires overcoming a low energy barrier of 13.2 kcal/mol. Thus the two can be easily transformed into each other. Next, the catalytic activation of ammonia and hydrazine by iron complexes supported by the same double anionic ligands was calculated. The calculations verify the validity of t activation of ammonia and explain why the coupling of the para-C to NH_2 could not be observed experimentally. And in the activation of hydrazine, a reaction mechanism in which hydrogen transfer occurs within hydrazine was proposed. A mechanistic study has also been done for the synthesis process of scandium forming a double bond with a main group element at the terminal of a coordination metal. A perfect mechanism for the generation of Sc=O double bond from a scandium complex with a monoanion BPz_2Py_3 coordination found in the experiment is verified and explained by calculations. This leads to the study of the properties of Sc=P and Sc=N double bonds. It was demonstrated computationally that the Sc=P double bond can induce the breakage of the C-C bond in the ligand to produce the phosphido-pyridyl complex. At the same time we also calculated the reaction mechanism of $[Fe_2(\mu^2\text{-NP (pip)}_3)_2(\text{NP (pip)}_3)_2]$ catalyzing the reduction of N_2O to N_2. A thermodynamically very favorable pathway and stable μ^2-O product were obtained. And in this product $[Fe_2(\mu^2\text{-O})(\mu_2\text{-NP(pip)}_3)_2(\text{NP(pip)}_3)_2]$ was shown to possess the shortest Fe-Fe distance comparing with other reports.

References:

1. Beh, D.W., et al., *Tandem deoxygenative hydrosilation of carbon dioxide with a cationic scandium hydridoborate and B (C 6 F 5) 3.* Dalton Transactions, 2020. 49(1): p. 95-101.
2. Spasyuk, D.M., et al., *Facile hydrogen atom transfer to iron (III) imido radical complexes supported by a dianionic pentadentate ligand.* Chemical science, 2016. 7(9): p. 5939-5944.
3. Beh, D.W., et al., *Scandium alkyl and hydride complexes supported by a pentadentate diborate ligand: reactions with CO 2 and N 2 O.* Dalton Transactions, 2018. 47(38): p. 13680-13688.
4. Nurdin, L., et al., *Oxygen–oxygen bond cleavage and formation in Co (II)-mediated stoichiometric O2 reduction via the potential intermediacy of a Co (IV) oxyl radical.* Journal of the American Chemical Society, 2018. 140(47): p. 16094-16105.
5. Nurdin, L., et al., *Reactions of Neutral Cobalt (II) Complexes of a Dianionic Tetrapodal Pentadentate Ligand: Cobalt (III) Amides from Imido Radicals.* Inorganic chemistry, 2017. 56(7): p. 4157-4168.
6. Thompson, M.E., et al., . *sigma.-Bond metathesis for carbon-hydrogen bonds of hydrocarbons and Sc-R (R= H, alkyl, aryl) bonds of permethylscandocene derivatives. Evidence for noninvolvement of the. pi. system in electrophilic activation of aromatic and vinylic CH bonds.* Journal of the American Chemical Society, 1987. 109(1): p. 203-219.
7. Bochmann, M., et al., *Synthesis of cationic alkyl bis (cyclopentadienyl) titanium complexes by one-electron oxidation of titanium (III) alkyls. The structure of [Cp2* TiMe (THF)] BPh4 and [Cp2* Ti (OH)(H2O)] BPh4· 2THF.* Polyhedron, 1989. 8(13-14): p. 1838-1843.
8. Kessler, M., et al., *Synthesis and Structures of ansa-Titanocene Complexes with Diatomic Bridging Units for Overall Water Splitting.* Chemistry–A European Journal, 2013. 19(20): p. 6350-6357.
9. Horáček, M., et al., *Synthesis and crystal structure of decamethyltitanocene hydroxide.* Inorganic Chemistry Communications, 2004. 7(2): p. 155-159.
10. Beh, D.W., et al., *Hydrolysis of scandium alkyl derivatives supported by a pentadentate diborate ligand: Interconversion of hydroxo and oxo complexes.* Polyhedron, 2020. 179: p. 114410.
11. Lu, E., J. Chu, and Y. Chen, *Scandium terminal imido chemistry.* Accounts of chemical research, 2018. 51(2): p. 557-566.
12. Patrick, E.A., et al., *A monoanionic pentadentate ligand platform for scandium–pnictogen multiple bonds.* Chemical Communications, 2021. 57(69): p. 8640-8643.
13. Warren, J.J., T.A. Tronic, and J.M. Mayer, *Thermochemistry of proton-coupled electron transfer reagents and its implications.* Chemical reviews, 2010. 110(12): p. 6961-7001.
14. Nurdin, L., et al., *Activation of ammonia and hydrazine by electron rich Fe (ii) complexes supported by a dianionic pentadentate ligand platform through a common terminal Fe (iii) amido intermediate.* Chemical Science, 2021. 12(6): p. 2231-2241.
15. Dobson, J.F., G. Vignale, and M.P. Das, *Electronic density functional theory: recent progress and new directions.* 2013.

16. Becke, A.D., *Density-functional thermochemistry. I. The effect of the exchange-only gradient correction.* The Journal of chemical physics, 1992. 96(3): p. 2155-2160.
17. Hariharan, P.C. and J.A. Pople, *The influence of polarization functions on molecular orbital hydrogenation energies.* Theoretica chimica acta, 1973. 28(3): p. 213-222.
18. Ditchfield, R., D. Miller, and J. Pople, *Self-consistent molecular orbital methods. xi. molecular orbital theory of nmr chemical shifts.* The Journal of Chemical Physics, 1971. 54(10): p. 4186-4193.
19. Dolg, M., et al., *Energy-adjusted abinitio pseudopotentials for the first row transition elements.* The Journal of chemical physics, 1987. 86(2): p. 866-872.
20. Martin, J.M. and A. Sundermann, *Correlation consistent valence basis sets for use with the Stuttgart–Dresden–Bonn relativistic effective core potentials: The atoms Ga–Kr and In–Xe.* The Journal of Chemical Physics, 2001. 114(8): p. 3408-3420.
21. Rice, N.T., et al., *Homoleptic imidophosphorane stabilization of tetravalent cerium.* Inorganic chemistry, 2019. 58(8): p. 5289-5304.
22. Rice, N.T., et al., *Two-Electron Oxidative Atom Transfer at a Homoleptic, Tetravalent Uranium Complex.* Journal of the American Chemical Society, 2020. 142(16): p. 7368-7373.
23. Gompa, T.P., et al., *The chemical and physical properties of tetravalent lanthanides: Pr, Nd, Tb, and Dy.* Dalton Transactions, 2020. 49(45): p. 15945-15987.
24. Rice, N.T., et al., *Design, isolation, and spectroscopic analysis of a tetravalent terbium complex.* Journal of the American Chemical Society, 2019. 141(33): p. 13222-13233.
25. Rice, N.T., et al., *Comparison of tetravalent cerium and terbium ions in a conserved, homoleptic imidophosphorane ligand field.* Chemical science, 2020. 11(24): p. 6149-6159.
26. Quintana, L.M.A., et al., *Chalcogen-Atom Abstraction Reactions of a Di-Iron Imidophosphorane Complex.* Chemical Communications, 2021.
27. Perdew, J.P. and Y. Wang, *Erratum: Accurate and simple analytic representation of the electron-gas correlation energy [Phys. Rev. B 45, 13244 (1992)]*. Physical Review B, 2018. 98(7): p. 079904.
28. Becke, A.D., *Density-functional thermochemistry. V. Systematic optimization of exchange-correlation functionals.* The Journal of chemical physics, 1997. 107(20): p. 8554-8560.
29. Becke, A.D., *Density-functional thermochemistry. IV. A new dynamical correlation functional and implications for exact-exchange mixing.* The Journal of chemical physics, 1996. 104(3): p. 1040-1046.
30. Fukui, K., *The path of chemical reactions-the IRC approach.* Accounts of chemical research, 1981. 14(12): p. 363-368.
31. Fukui, K., *Formulation of the reaction coordinate.* The Journal of Physical Chemistry, 1970. 74(23): p. 4161-4163.
32. Delabie, A., et al., *Evaluating the activation barriers for transition metal N2O reactions.* The Journal of Physical Chemistry A, 2001. 105(22): p. 5479-5485.
33. Zhao, L., et al., *Theoretical investigation of the Fe+-catalyzed oxidation of acetylene by N2O.* The Journal of Physical Chemistry A, 2008. 112(25): p. 5676-5683.

Chapter IV

f-block metal complexes

The f-block elements are also known as inner transition elements, referring to the lanthanides and actinides in the periodic table. There is very little difference in properties between elements of the same period in this region, which is evident in the lanthanide elements.

In the past 60 years, there have been important developments in the chemistry of rare earth metals complexes. The auxiliary ligands have evolved from cyclopentadienyl, pentamethylcyclopentadienyl, indenyl to various non metallocene ligands such as β-diimine. The application of non-metallocene ligands not only expand the structural variety of rare earth metal organocomplexes, but also greatly promote the application in organic synthesis. Rare earth metal organocomplexes can effectively catalyze important organic reactions such as selective addition of aldehydes, ketones and olefins.

However, lanthanide/actinide complexes are computationally difficult to SCF converge due to the near-simplification of f-orbitals than transition metal complexes, unless the lanthanide/actinide atoms use large nuclear pseudopotentials, at which point there is no need to describe the f electrons.

In this chapter we will use a computational approach to mechanistically investigate the activation of organic and inorganic small molecules catalyzed by several f-block metal complexes.

IV.1. Lanthanum-assisted selective addition of aldehydes

Organic fluorine compounds have a very wide range of uses, such as Freon, fluorine-containing liquid crystal, optical fibers, polytetrafluoroethylene, pharmaceuticals and agricultural chemicals, etc.[1]. However, its unique properties different from other organic compounds make it attract more and more attention in various fields. Therefore, it is highly desirable to selectively prepare fluorine-containing compounds under atomic economy and mild conditions. Because fluorine is the most electronegative element in the periodic table of elements, and the C(sp^3)-F bond has a high dissociation energy[2], the activation research of C-F bond has attracted attention in recent years, especially metal-catalyzed C-F bond activation of aryl and vinyl fluorides. At present, the use of trifluoromethyl-containing compounds for defluorination functionalization has become one of the most direct strategies for the

preparation of organic fluorine compounds [3]. In these reactions, the control of regioselectivity and chemoselectivity is crucial.

Professor Jaroschik's group discovered a metal-difluoropentadienyl complex in the C-F activation of CF_3-benzofulvene, and this complex can undergo highly regioselective and diastereoselective addition reactions with aldehydes[4]. Existing reports have documented that metal-pentadienyl complexes as nucleophiles can undergo regioselective transformation with electrophiles and their diverse structures [5-11]. However, no examples of ϵ, ϵ-metal difluoride-difluoropentadienyl derivatives have been reported before。In order to obtain this conjugated nucleophilic species, zero-valent lanthanide metals with strong reduction potential are used, and trifluoromethylated benzofulvene derivatives are used as substrates. However, when only zero-valent metals act on benzofulvenes, the reaction cannot proceed.

However, according to the reports of Professor Joosten [12] and Professor Umeda [13], lanthanide metals can catalyze the formation of C-C in the presence of I_2 or $AlCl_3$. So they tested different lanthanide metals (La, Ce, Nd, Sm, Gd, Dy, Yb, Y), and different Lewis acids ($AlCl_3$, $ZrCl_4$, $Sc(OTf)_3$, TMSOTf, BF_3-OEt_2, $ZnCl_3$)) selectively produce branched product and its yield. It is found that when the metal is Dy, it will only produce branched products when it is added to most aromatic aldehydes, f aliphatic aldehydes and other aldehydes. Unless it is aldehydes with very large steric effrct(such as mesitaldehyde and tert-butylaldehyde), mixed linear products and branched products will be generated. And the reaction of 1.3 equiv of benzofulvene with p-Br-benzaldehyd can produce branched products with a yield of up to 93%, by using the system with Dy metal and 3 equiv of $AlCl_3$. This is the best condition for the reaction. It is worth noting that when only excess La and I_2 are added to the system, only linear product is formed. But when $AlCl_3$ was added, the branched product appeared at the same time.

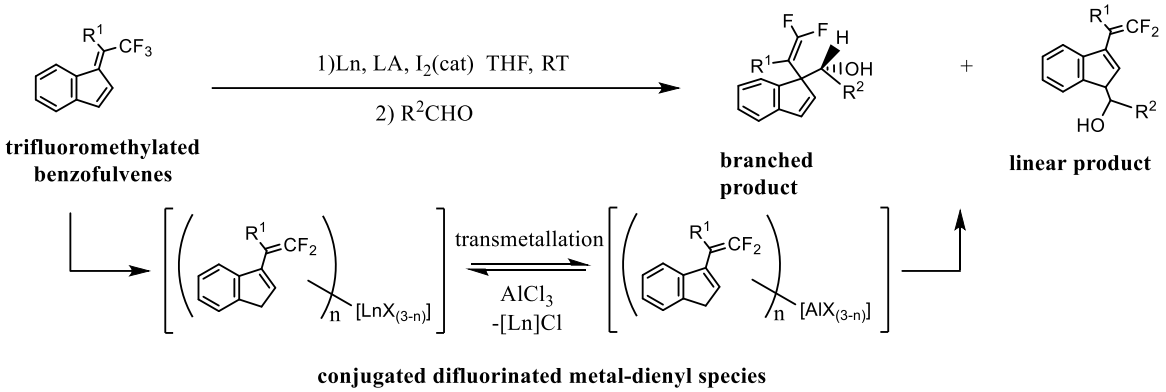

Scheme 4.1 Selective addition reaction after C-F activation. Among them, R1 and R2 are groups on benzofulvene and groups on aromatic aldehyde or aliphatic aldehyde, respectively.

In order to further study the reaction conditions of the linear product, Professor Jaroschik's group tested different Lewis acids, such as $AlCl_3$, $EtAlCl_2$, Et_2AlCl, $^{i}Bu_2AlCl$, as well as $LaI_3(THF)_x$ which contains no aluminum source at all[14]. According to literature reports[15-18], the reaction of allyl-lanthanide-halide species with aldehydes or ketones selectively produces linear homoallyl alcohols, while allyl-aluminum species tend to be branched products. It is indeed found in the experiment that in the most basic La/$AlCl_3$ system, when the $AlCl_3$ equivalent drops to 1, the overall yield of all products decreases, but the proportion of linear products is higher than that of branched products.

The bulky Lewis acids, such as Et_2AlCl and $^{i}Bu_2AlCl$, will increase the yield of linear products, but cannot completely avoid the formation of branched products.。

However, in the system completely free of aluminum source, $LaI_3(THF)_x$ is completely used as the Lewis acid, and the formation of branched products is indeed no longer observed. However, the presence of Al can increase the overall product yield and make purification easier. Therefore, 0.2 equivalent of Al source is added to the system after the reduction step and before the addition of aldehydes, linear products are still unique products. Interestingly, when the aromatic ring on the aldehyde has a strong electron withdrawing group, such as p-NO_2, an unexpected ipso product is observed. We will use DFT calculations to study the selective addition reaction mechanism of aldehydes with lanthanum metal as a catalyst, explore the production pathways to generate three different products, and make reasonable explanations for the experimental phenomena.

IV.1.1. Computational details

In this section, the density functional theory (DFT/B3PW91) method is used to carry out theoretical calculations on the lanthanum-mediated aldehyde addition reaction[19-21]. Among them, the Stuttgart-Dresden-Bonn relativistic small or large effective core potential (RECP) is used as the pseudopotential basis set for the f-block metal La atom and the f-polarization function is added[22-24]. For F and I, the large core RECP is used and combined a set of d functions enhance the basis set[25]. The split basis set 6-31G (d, p) is used for atoms such as C, H, 0, and N[26]. The structural optimization and energy correction calculations are carried out for each stagnation point in the reaction, and it is confirmed that the transition state has unique negative frequency and negative eigenvalues. In addition, the intrinsic reaction coordinate calculation (IRC) was performed on the transition state to confirm that the transition state is on the reaction path of the reactants and products[27, 28]. All calculations use the Gaussian09 computing software package and are completed on the high-performance computing platform.

IV.1.2. Computational models

First, we choose La metal as the catalytic metal for the mechanism study, trifluoromethylated benzofulvene as the reaction substrate, and benzaldehyde as the electrophile. When the system does not contain aluminum source, only linear products are formed。 But when $AlCl_3$ participates in the catalytic system, a mixture of branched products and linear products is observed. When p-NO_2-benzaldehyde which with a strong electron withdrawing group was used as the reactant, the special ipso product appeared with a small amount in a large number of linear products. Therefore, we can divide the reaction into three routes, through different α-, γ-, and ε-additions, respectively pointing to linear product, branched product and ipso product.

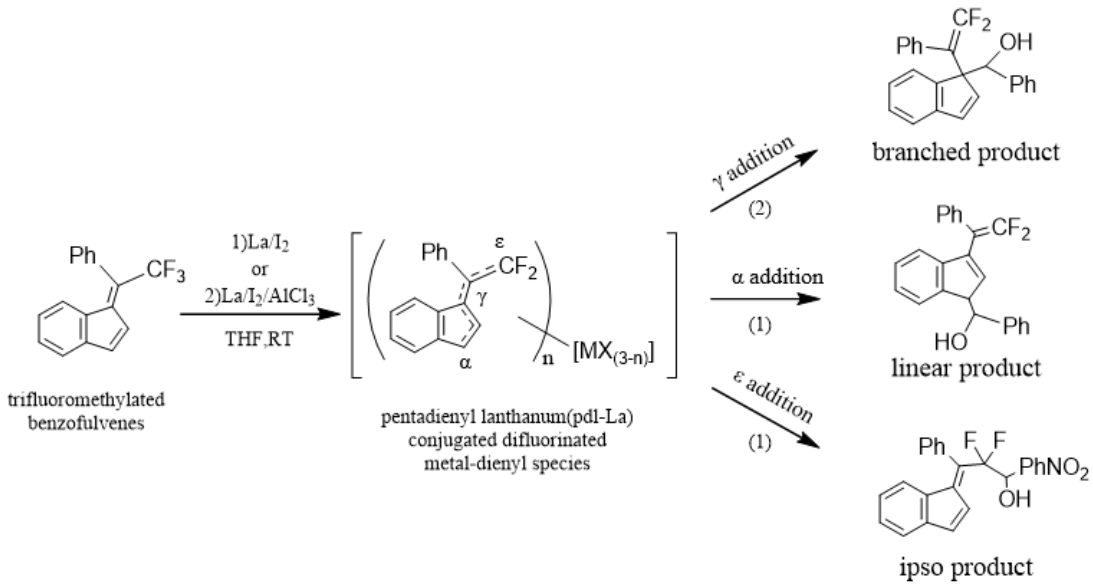

Scheme 4.2 Three kinds of product formation methods

The ^{19}F spectrum proved that in the $La/I_2/AlCl_3$ system, there are two different metal dienyl complexes as intermediates. When $AlCl_3$ was added to the La/I_2 system, a peak corresponding to Al-dienyl substances gradually appeared in the ^{19}F spectrum, which proved the metal transfer of lanthanum to aluminum. High resolution mass spectrometry (HRMS) gave the structure of a possible pentadienyl aluminum (pdl-Al) intermediate complex produced by the C-F activation process, the structure are $[(pdl)AlCl_2]$ and $[(pdl)_2AlCl]$, but the La-pentadienyl intermediate could not be observed[4]. Based on this structure, we propose two different models for this intermediate. In this model, when n=1, two iodine atoms and one pentadienyl are coordinated on the metal; when n=2, one iodine atom and two pentadienyl are coordinated on the metal.

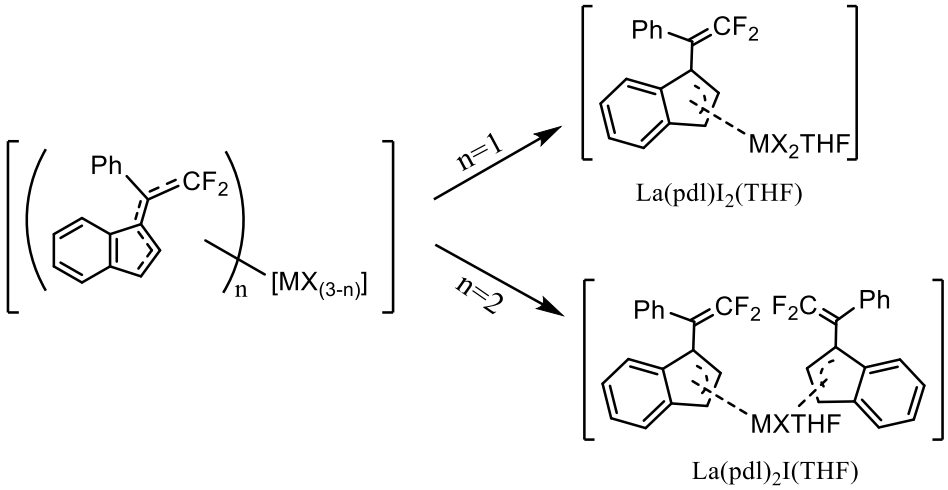

Scheme 4.3 Three kinds of product formation methods

Therefore, for La and Al, we optimized the structures of the following four intermediates as the basis for mechanism calculations. It can be seen from the optimized structure of the pentadienyl-La intermediate that the metal and the indenyl moiety belong to the η^5 coordination. However, when Al coordinates an indenyl group as the metal center, the bond length between it and the α carbon of the indenyl group is 2.00 Å. However the distance between Al and the ortho-C on the both sides of the α carbon is 2.87 Å and 2.91 Å, respectively. It can be seen that for Al, the coordination mode is no longer η^5. Instead, it belongs to the η^1 coordination mode, linked to a C in the indene group.. And in [$(pdl)_2$AlCl(THF)], the coordination mode is also the same, the distance between Al metal and non-α carbon C atoms is almost all higher than 2.80 Å.

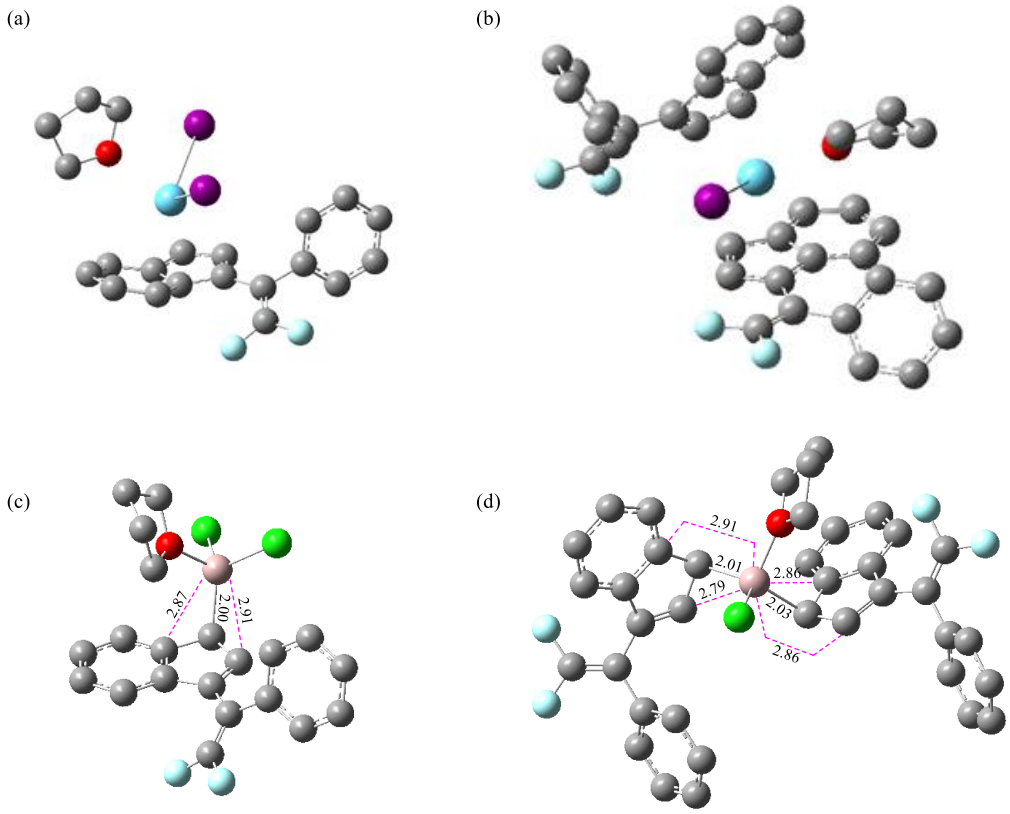

Figure 4.1 3D representation of (a)[(pdl)LaI_2(THF)], (b)[$(pdl)_2$LaI(THF)], (c)[(pdl)$AlCl_2$(THF)] and (d)[$(pdl)_2$AlCl(THF)], The gray represents the C atom, the red represents the O atom, the green represents the I atom, and the light blue represents the F atom. The color of metal La is dark blue, and Al is pink.

VI.1.3. Results and discussion

Figure 4.2 shows the aldehyde addition reaction of difluoromethylated benzofulvene on [(pdl)LaI_2(THF)] and [$(pdl)_2$LaI(THF)] based on the experimental analysis of the Professor Jaroschik's group. Three addition pathway to generate different products for the intermediate with ligand pentadienyl was calculated. The black color is the the addition of benzaldehyde at the indenyl α site to generate linear product promoted by LaI_2THF. The blue color is γ addition to generate branched product, and the pink color is ε addition to generate the ipso product.

First, a single pentadienyl group [(pdl)LaI_2(THF)] was used for mechanism research. It can be seen that the energy of the branched product is higher than that of the reactant in the γ addition pathway(blue line), the reaction entropy ΔH of the branched product is 4.2kcal/mol. So this reaction is thermodynamically unfavorable. This can well explain why the corresponding branched products cannot be observed when there is no $AlCl_3$ aldehyde addition reaction. The energy barriers of the α addition

transition state (black) and the ε addition transition state (pink) are 17.6kcal/mol and 12.8kcal/mol, respectively. The energy difference of 5.0kcal/mol is within an acceptable range. And the linear products and ipso products are both exothermic processes and thermodynamically favorable, and their ΔH is -3.5kcal/mol and -4kcal/mol, respectively. The energy of the two products based on the [(pdl)LaI_2(THF)] system is similar. Therefore, it can be said that in the calculation model with [(pdl)LaI_2(THF)] as the intermediate, there is still a competitive relationship between the paths of α addition and ε addition. From the calculation results, the product seems to be a mixture of black linear products and pink ipso products. However, according to experiments, if the aldehyde involved in the addition reaction is benzaldehyde without a strong electron-withdrawing group on the aromatic ring, only linear products will be observed without ipso products.

Therefore, it seems that the bis(indenyl) lanthanide complexes must be considered in the study of the reaction mechanism of the α addition and ε addition, as shown in the Figure4.2(b). The two transition states have close energy barriers, however, the energy of the linear product is thermodynamically superior to the ipso product by 7.4kcal/mol, that is to say, the structure of the linear product is more stable. Comparing the reaction enthalpies of the two addition modes, which are -3.6kcal/mol and -12.5kcal/mol, respectively, it can be seen that the exothermic process of α addition is more intense than that of ε addition. Therefore, the transition state mechanism study using [(pdl)$_2$LaI(THF)] as an intermediate proves the experimental phenomenon that linear products are more likely to be generated in the La/I_2 system. It also proved that the lanthanum complex with bis-indenyl ligand seems to be a reasonable intermediate in the C-F activation process of trifluoromethylated benzofulvene.

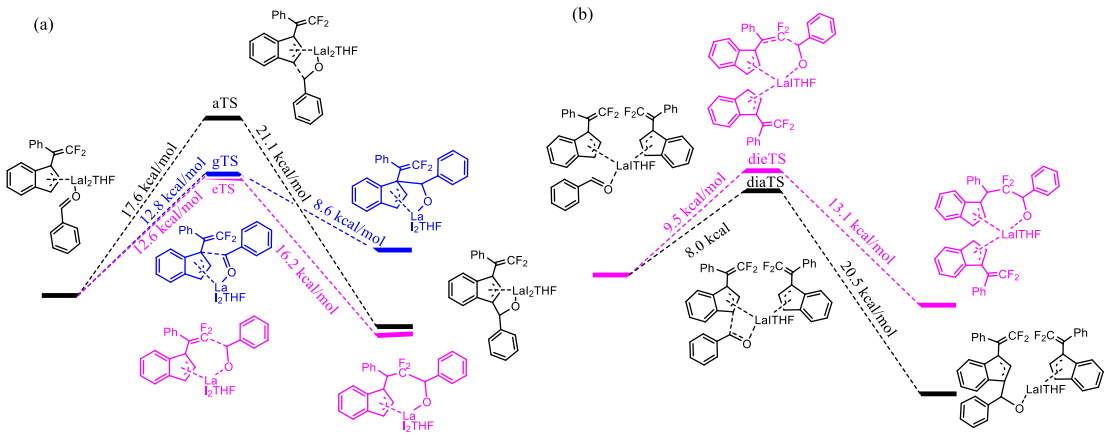

Figure 4.2 Reaction mechanism of benzaldehyde addition with (a)[(pdl)LaI_2(THF)], (b)[$(pdl)_2$LaI(THF)].

When we introduce the electron withdrawing group -NO_2, it is same as the phenomenon observed in the experiment, the calculated reaction mechanism reveals that the electron withdrawing group can well reduce the energy barrier of ε addition. The energy barrier is almost reduced by half. Whether it is the mono-indenyl on the left or the bis-indenyl on the right, it is shown that the ipso product is easier to obtain in this case.

When we are using p-NO_2-benzaldehyde for nucleophilic addition with [(pdl)LaI_2(THF)] or [$(pdl)_2$LaI(THF)], the energy barrier of the ε addition transition state is only that of α addition half. And the reaction process is an exothermic reaction with favorable thermodynamics. In the [(pdl)LaI_2(THF)] catalytic system, the energy barrier difference between the two transition states is 7.0kcal/mol; while in the [$(pdl)_2$LaI(THF)] catalytic system, the energy barrier difference is 8.7kcal/mol. This shows that ε addition is more dynamic favorable than α addition.

In a more reasonable bis-indenyl lanthanum model, the linear product of α addition still has a great advantage in thermodynamics. The α reaction exotherm is 16.1kcal/mol, while the ε addition exotherm is 6.3kcal/mol. Therefore, combining the viewpoints of kinetics and thermodynamics, the benzaldehyde with strong electron-withdrawing group can better access to the ipso product, and at the same time there is still a considerable part of the linear product.

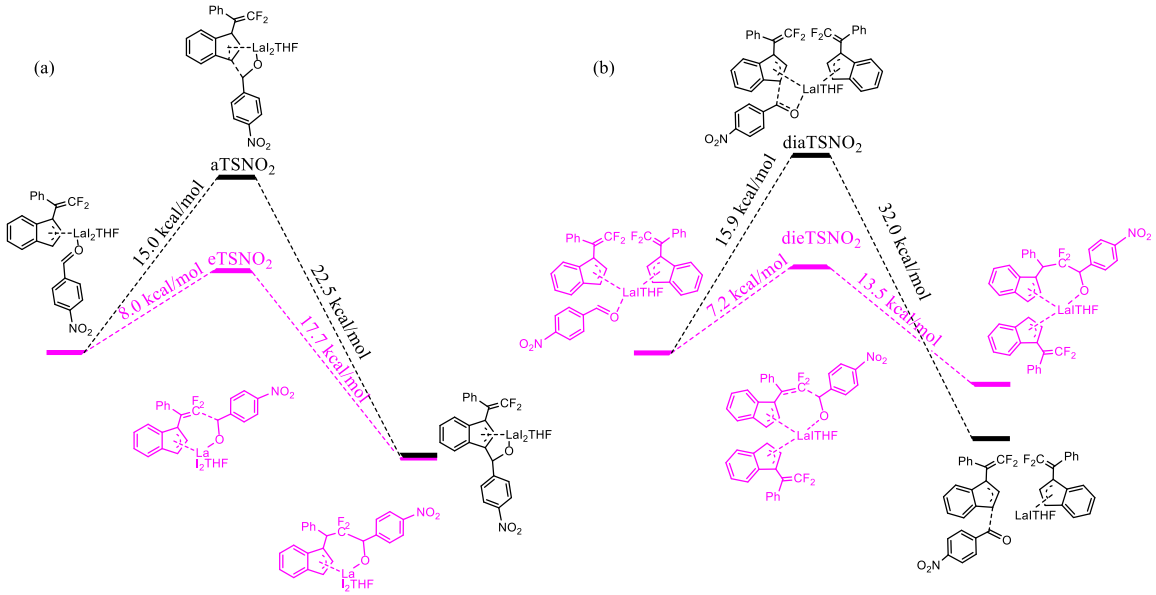

Figure 4.3 Reaction mechanism of p-NO_2-benzaldehyde addition with (a)[(pdl)LaI_2(THF)], (b)[$(pdl)_2$LaI(THF)].

In the experiment, it was found that the addition of aluminum source can produce branched products that never existed in the La/I_2 system. In the study of Dy, the content of $AlCl_3$ can also influence the yield of branched products. Therefore, it is believed that the selective formation of branched products in the addition reaction is mainly due to the transmentallation from La to Al. Therefore, by calculating the reaction enthalpy of the conversion process from [$(pdl)_2$LaI(THF)] to [(pdl)$AlCl_2$(THF)], the reaction exotherm is 9.1kcal/mol. This illustrates the good transmetallation between La and Al.

$$(pdl)_2LaI(THF) + AlCl_3(THF) = (pdl)LaICl(THF) + (pdl)AlCl_2(THF) \qquad \text{Eq 4.1}$$

$$\Delta H = -9.1 \text{ kcal/mol}$$

We used two aluminum catalysis models [(pdl)$AlCl_2$(THF)] and [$(pdl)_2$AlCl(THF)] to study the transition states of γ addition. For both models, the energies of the transition state and the reactant and product calculated in the internal coordinate calculation are similar. And compared with the lanthanum complex system, the energy barrier of the γ addition transition state on the Al center is very low, and the branched products produced are also very stable. At the La center, the transition state energy barriers of the three addition reactions are much higher than 3.4kcal/mol. Therefore, this can also explain that the presence of Al in the experiment has a decisive influence on the branched products.

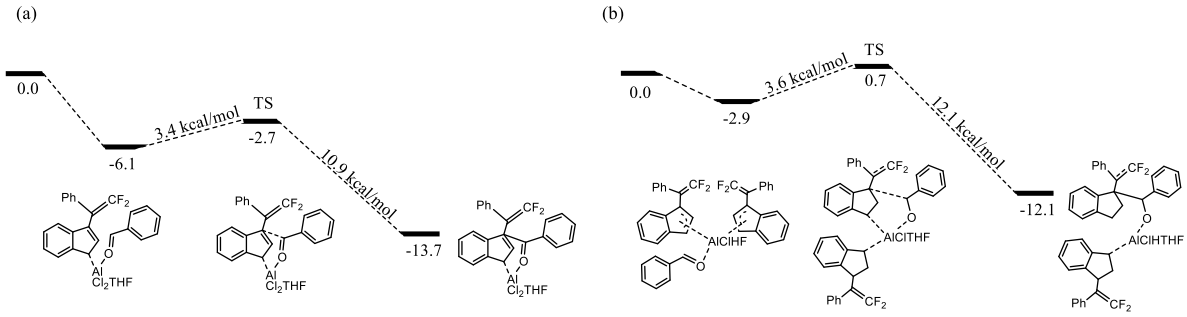

Figure 4.4 γ addition mechanism of benzaldehyde with (a)[(pdl)$AlCl_2$(THF)] and (b)[$(pdl)_2$AlCl(THF)].

VI.1.4 Conclusion

In this section, the density functional theory method is used to carry out the mechanism of the regioselective addition reaction of benzaldehyde and pentadienyl

lanthanum metal complex. Several phenomena in the experiment were explained one by one. For example: (1) In the La/I_2 system, the addition of benzaldehyde only produces linear products. [(pdl)LaI_2(THF)] is calculated to confirm the three addition methods. Since the formation of branched products on [(pdl)LaI_2(THF)] is thermodynamically unfavorable, it is a reversible reaction. (2) In the La/I2 system, the addition of p-EWG-benzaldehyde can generate linear products and unexpected ipso products. This is confirmed in the mechanism study of [$(pdl)_2$LaI(THF)] on the transition state of α addition. The introduction of electron-withdrawing p-NO_2-benzaldehyde lowers the energy barrier of epsilon attack, and the ε addition transition state is more favorable from a kinetic point of view. (3) In the $La/I_2/AlCl_3$ system, the addition of benzaldehyde can generate branched products. By calculating the γ addition that occurs on [(pdl)$AlCl_2$(THF)] and [$(pdl)_2$AlCl(THF)], it is found that it has a lower reaction energy barrier. From the perspective of kinetics and thermodynamics, γ addition is more likely to occur in the aluminum metal center.

IV.2. Samarium-assisted coupling of ketones and N-heterocyclic aromatics

The formation of the C-C bond is the foundation of organic synthesis, and it is also the basis for the construction of colorful organic compounds[29]. Since the French chemist Kagan[30] first introduced samarium diiodide into organic synthesis in 1977, samarium diiodide has played an important role in the synthesis of carbon-carbon bonds as an excellent single electron transfer reagent[31]. Following Kagan's pioneering work, Inanaga, Professor Molander and others have achieved further fruitful research results in this research field, making samarium diiodide rapidly developed into a widely used single electron transfer coupling agent and reducing agent[32, 33]. It not only promotes many types of organic reactions and functional group conversions, but also is widely used in the synthesis of natural products[34, 35]. It is also one of the most effective and important methods for forming new bonds.

Samarium diiodide is often used to promote the coupling of aldehydes or ketones. For example, Professor Weitgenantet et al.[36, 37] used pyridine, bipyridine,

phenanthroline and other N heterocyclic aromatic compounds to react with aldehydes or ketones to produce hydroxyl substituent at the α position. The substituent can be further functionalized under the presence of SmI_2. Because multiple N atoms can be used as coordination sites for multidentate chelates, a variety of substituted nitrogen heterocyclic aromatic compounds can enrich the library of organic ligands. Professor Weitgenantet et al studied the coupling reaction of benzophenone and N-heterocyclic aromatics on this basis[38].

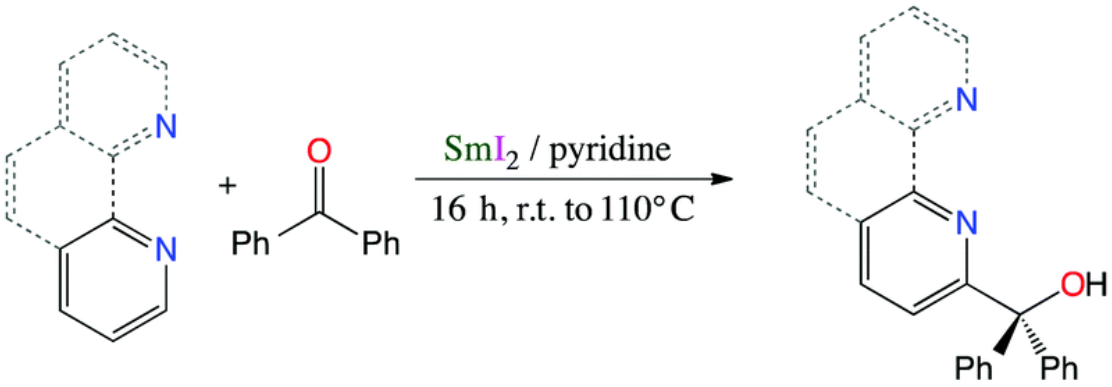

Scheme 4.4 Coupling reaction of benzophenone and N-heterocyclic aromatics (pyridine, bipyridine and phenanthroline) in the presence of SmI_2/pyridine

The reaction of SmI_2 and benzophenone in THF forms a pinacol-like structure in which each samarium ion coordinates two iodide ions and three THF or pyridine ions. The configuration of this coordination compound shows a twisted square pyramid. When the pyridine solvent was added, the solution immediately showed a deep purple color, and the characteristic peaks in the visible spectrum indicated the generation of the charge-separated ketyl radical I. When the temperature rises to 100°C, a new characteristic peak appears in the visible spectrum. According to the literature, SmI_2 can reduce pyridine, so we obtained compound II after electron transfer.

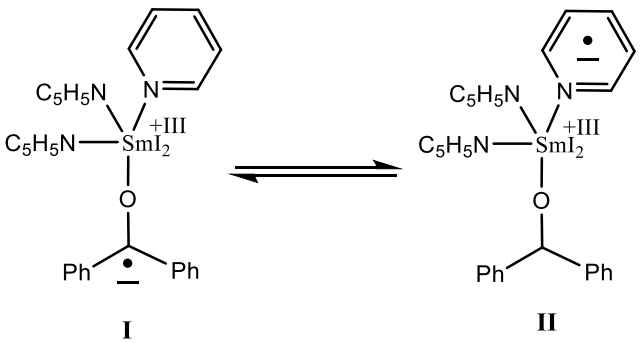

Scheme 4.5 Electron transfer from the benzophenone to the pyridine

When bipyridine and phenanthroline, which have a higher reduction potential than pyridine, are added to the purple compound I, the solution gradually changes color to the final yellow color at room temperature, and the alcohol after benzophenone reduction can be obtained by cooling and crystallizing. However, if the I compound solution is heated directly at 110°C for 16 hours, it will also turn yellow. Therefore, in order to understand the mechanism of this change, we will perform theoretical calculations.

IV.2.1. Computational details

In Gaussian 09, the B3PW91 hybrid functional is used to optimize the geometric configuration of the reactants, intermediates and products[19-21, 27, 28]. For trivalent samarium atoms, the large core effective core potential extended by the f polarization function(α=1.0) is used, while the basis set of the iodine atom uses the Stuttgart-Dresden effective core potential extended by the d polarization function(α=0.730) [22-24]. The remaining C, N, O and H atoms use 6-31G(d, p) basis set.

IV.2.2. Computational models

When the purple compound I is heated at 110° C. for 16 hours, a yellow solution is obtained. After crystallization, crystals of product G were obtained. The same is that when phenanthroline is added to compound I, the solution obtained at room temperature can be crystallized to obtain light yellow crystals of product B. According to the crystal structure data obtained in the experiment, we established the calculation model of the products G and D. In the G product, Sm is connected to two I atoms and three pyridine ligands, and a coupling reaction of benzophenone occurs at the α substitution position of the fourth pyridine. Two pyridine molecules in product D are connected to Sm, and two N in phenanthroline are connected to Sm as bidentate coordinatio, and a coupling reaction occurs at the α position.

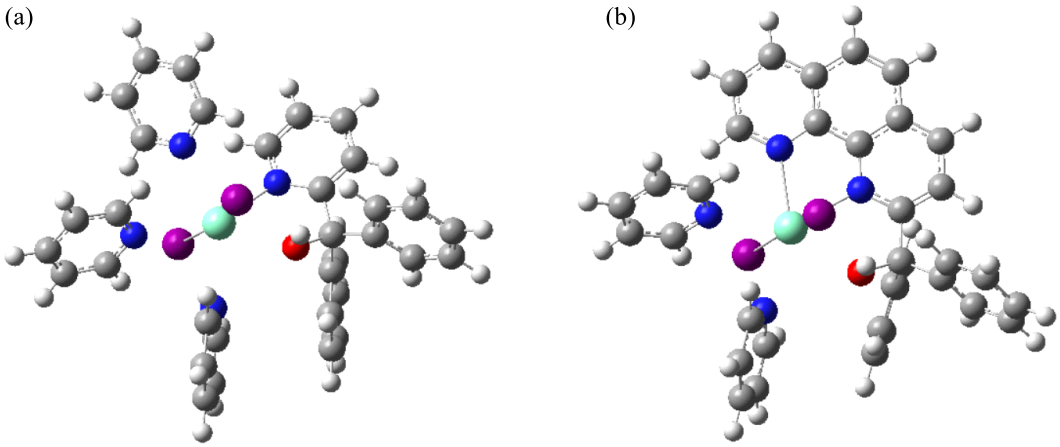

Figure 4.5 3D representation of (a)[$SmI_2(pyr)_3$(pyr-alcoholate)], (b) [$SmI_2(pyr)_2$(phen-alcoholate)], The gray represents the C atom, the red represents the O atom, the green represents the I atom, and the blue represents the N atom. The color of metal Sm is green.

Through structural optimization, we have obtained the distance between the main atoms, as shown in the following table:

Table 4.1 The distance between the main atoms in calculations and experiments. The bond length unit is Å.

	Calculation		Experiment	
	G(pyridine)	D(phenanthroline)	G(pyridine)	D(phenanthroline)
Sm-I	3.13	3.11	3.12	3.24
Sm-N(Pyridine)	2.60	2.68	2.63	2.67
Sm-N(L)	2.41	2.49/2.44	2.57	2.56
Sm-O	2.51	2.50	2.13	2.15
O-C(Ph_2)	1.47	1.46	1.4	1.4
C-C(Ph_2)	1.52	1.53	1.55	1.54

The distance of Sm-I is 3.13Å and 3.11Å in G and D respectively, which is more in line with the existence of trivalent samarium. The calculated data of the distance

between Sm and N (pyridine) are in good agreement with the experimental data, and they are slightly larger than the distance between Sm and the N on the pyridine or phenanthroline involved in the reaction. The distance between O-C (Ph_2) and C-C (Ph_2) is about 1.47Å and 1.52Å respectively, which is consistent with the formation of alcoholate and proves that the C-C bond is a single bond.

VI.2.3. Results and discussion

First, the energy of the electrons transfer equilibrium of [$SmI_2(pyr)_4$(benzophenone)] and [$SmI_2(pyr)_2$(phen)(benzophenone)] in Scheme 4.4 is calculated. The energy difference between the different electron arrangement structures in pyridine and phenanthroline is 12.7kcal/mol and 7.8kcal/mol, respectively. This shows that both tend to generate ketyl radicals. And because pyridine has a higher π* energy, the energy difference is lower than phenanthroline. The spin density diagram shows that in the original [$SmI_2(pyr)_4$(benzophenone)], unpaired electrons are basically distributed on the O and benzene rings of the ketyl group.

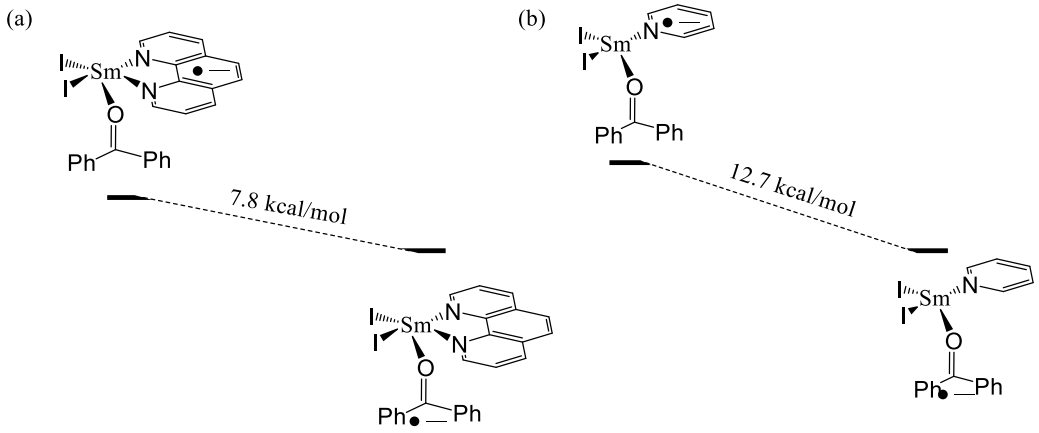

Figure 4.6 Computed enthalpy for the equilibrium of (a) ketyl-phenanthroline and (b) ketyl-pyridine. Because of the convenience of drawing, the pyridine that is not involved in the reaction is hidden, but it needs to be clear that the calculation uses the complete structure.

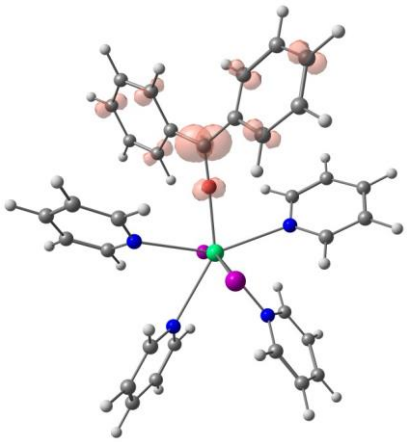

Figure 4.7 The spin density of [$SmI_2(pyr)_4$(benzophenone)].

First, after phenanthroline is added to compound A, -7.6kcal/mol heat is released to generate reactant B in which Sm coordinated phenanthroline and ketyl radical. Then the C-C bond is gradually formed between the α carbon on the benzophenone and the phenanthroline. The transition state undergoes a radical coupling reaction between the unpaired electron of the ketyl radical and the π electron of the α carbon, resulting in the intermediate C. The transition state energy barrier of this step is 18.5kcal/mol, while the transition state of [$SmI_2(pyr)_4$(benzophenone)] is slightly higher at 21.9kcal/mol. Intermediate C calculated by IRC requires reactant B to endothermic 8.8kcal/mol, and F relative to E also needs to endothermic 10.6kcal/mol. This is because the formation of the C-C bond causes the loss of aromaticity to pyridine or phenanthroline.

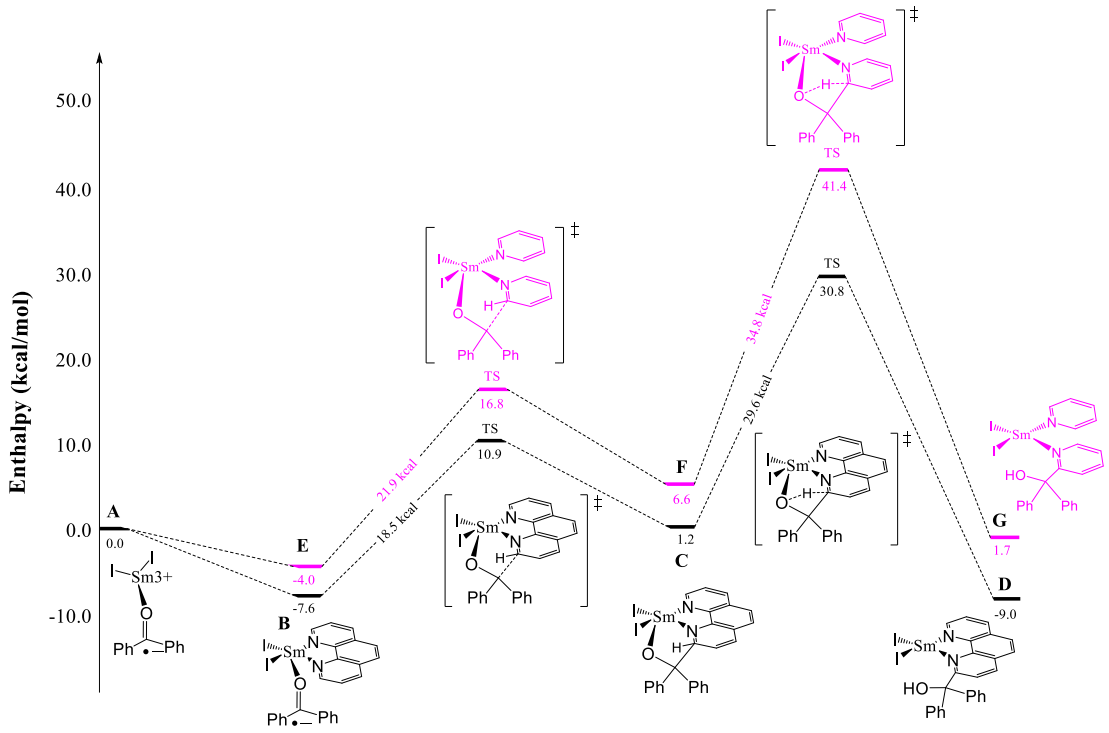

Figure 4.8 Computed enthalpy profile for the formation of D (black) and G (pink).

In order to make up for this loss of aromaticity, a 4-ring structure is formed in the second transition state. The distance between α-C and H gradually increases, and the hydroxyl group gradually forms, obtaining the final product [$SmI_2(pyr)_3$(pyr-alcoholate)] and [$SmI_2(pyr)_2$(phen-alcoholate)]. The energy barrier of this step is obviously high which is enough to be the speed determining step of the entire reaction pathway. In phenanthroline, the energy barrier is 29.6kcal/mol, and in pyridine, it reaches 34.8kcal/mol. The reason for this high value is that Sm does not participate in the transfer process of hydrogen atoms, but the stable oxygen coordinated atom will gradually move away from the metal center. The formation of the final product [$SmI_2(pyr)_2$(phen-alcoholate)] is thermodynamically favorable, and the reaction is exothermic 9.0kcal/mol. However, the formation of [$SmI_2(pyr)_3$(pyr-alcoholate)] thermodynamically endothermics 1.7kcal/mol. And in terms of kinetics, the energy barrier of the speed-determining step is higher than that of the coupling reaction involving phenanthroline. This can well explain the phenomenon observed in the experiment. When phenanthroline is not added, a higher temperature (110°C) is required to drive the reaction.

VI.2.4. Conclusion

We have studied the mechanism of direct coupling of benzophenone and N-heterocycle (such as pyridine and phenanthroline) to form methanol by DFT. In this reaction, there is no other coupling agent participated except SmI_2. The electron arrangement of the ketyl radical is verified by spin density analysis. Using ketyl radical as the starting point of the mechanism calculation, the reaction mechanism is divided into two parts. The first step is the formation of C-C bond, and the second step is the transfer of H atoms as the speed determining step. Finally, compared with pyridine, it was verified that the addition of phenanthroline in the experiment can make the coupling reaction occur under mild conditions.

IV.3. Samarium/ytterbium-mediated reductive coupling of CO_2 and CS_2

Due to the extensive use of fossil fuels in human activities, the concentration of carbon dioxide in the earth's atmosphere continues to increase. The resulting air pollution and greenhouse effect are seriously threatening the living environment of human beings[39-42]. At present, a large amount of carbon dioxide has become the most abundant C1 resource in nature[43, 44]. Therefore, the recovery, fixation, utilization and recycling of the emitted carbon dioxide has become an issue of great concern to countries all over the world. The activation and utilization of carbon dioxide has become a problem due to the chemical inertness of carbon dioxide. Carbon disulfide, which is similar to carbon dioxide, is considered a waste gas and a harmful air pollutant. The oxidation reaction of CS_2 in nature will lead to the formation of acid rain. The functionalization of organic substrates using carbon dioxide and carbon disulfide is currently a major research direction.

Lots of research shows that d&f block metal complexes have high catalytic performance. dπ orbital of metal can be well transferred to the π* antibonding orbital of CO_2, this form a backdonation effect which makes the combination of metal and CO_2 stronger. For f block metal, the bimetallic complex of samarium or uranium reported in the past few years can be proved to convert carbon dioxide into oxos, oxalates (kinetic products), and carbonates (thermodynamic products)[45-52].

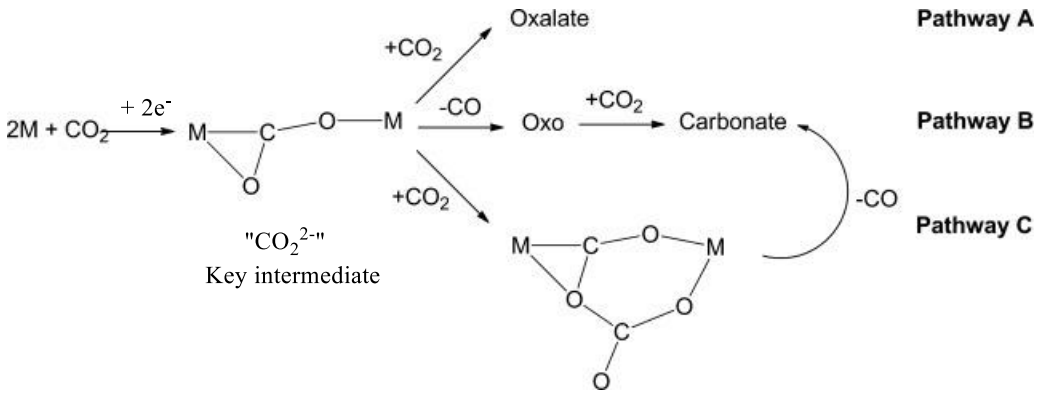

Scheme 4.6 The main modes of chemical reduction of carbon dioxide.

There is a basic pathways for the conversion of CO_2 by reduction at the bimetallic complex[52]. A two-electron reduction of one CO_2 molecule to generate a key intermediate M-$(CO_2)^{2-}$-M . And then a free CO_2 molecule adds into the system to form oxalate, or remove CO to generate carbonate.

Professor Mazzanti [53] reported a bimetallic coordination compound of a multidentate tris (tertbutoxy) siloxide ligand with samarium or ytterbium, which is $[Yb_2L_4]$ and $[Sm_2L_4]$ ($L=(O^tBu)_3SiO^-$), respectively. These two complexes react with carbon dioxide to produce oxalate and carbonate, and experiments have confirmed the species that exist as dimers in non-polar solutions are favorable to the formation of oxalate. Professor Mazzantiobtained an unprecedented acetylenedithiolate ($C_2S_2^{2-}$) product through the reductive coupling of $[Yb_2L_4]$ and CS_2[54]. We will study the mechanism of DFT based on these two reactions.

$$[Sm_2L_4] \xrightarrow{CO_2} [Sm_2L_4(C_2O_2)] + [Sm_2L_4(CO_3)]$$

$$[Yb_2L_4] \xrightarrow{CS_2} [Yb_2L_4(C_2S_2)] + [Yb_2L_4(CS_2)]$$

Scheme 4.7 Reduction of CO_2 and CS_2 on bimetal $[Yb_2L_4]$ and $[Sm_2L_4]$.

IV.3.1. Computational details

In this section, DFT (B3PW91) is still used for calculation. The basis sets of Sm and Yb are selected to use large-core relativistic effective core potential combined with f polarization function. The basis set of Si atom is selected the Stuttgart-Dresden

relativistic effective core potential SDD combined with d polarization function. The 6-31G(d) basis set is adopted by C, H, O atoms. Transition state calculations are verified using intrinsic coordinates. Use natural bond orbital (NBO) analysis to obtain atomic orbital population analysis[55]

IV.3.2. Computational models

First, we established the reactant model as shown in Figure 4.9. Two Sm/Yb ions are bridged asymmetrically by three oxygen atoms on three different silicon oxide ligands. The Sm-O bond length ranges from 2.15 Å to 2. 48Å. And the Yb-O bond length ranges from 2.27 Å to 2.57 Å.

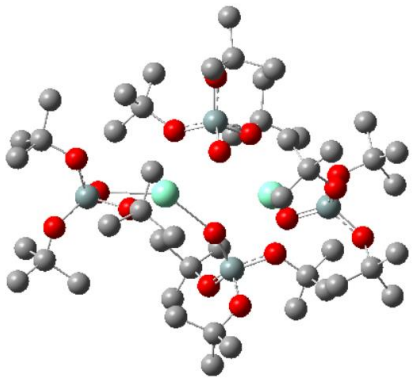

Figure 4.9 3D representation of $[Sm_2L_4]$ (L = $(O^tBu)_3SiO^-$). In order to make the structure clearer, the H atom is hidden in the figure.

According to the data obtained in the experiment, the model structures of the two key intermediates in the Sm-mediated reduction of carbon dioxide and Yb-mediated reduction of CS_2 were optimized. Among them, the key intermediate of samarium bimetallic ligand, the CO_2^{2-} part and the two Sm centers are the bonding mode of μ:μ:η(C-O). On the other hand, a dimer with a six-coordinate metal center appears on Yb, and the bonding mode of CS_2^{2-} moiety is μ-μ-η^2(CS): η^2(CS′). This coordination mode is different from that of most lanthanide metals coordinated with CS_2. We speculated the mechanism based on the crystal structures of the obtained products and intermediates.

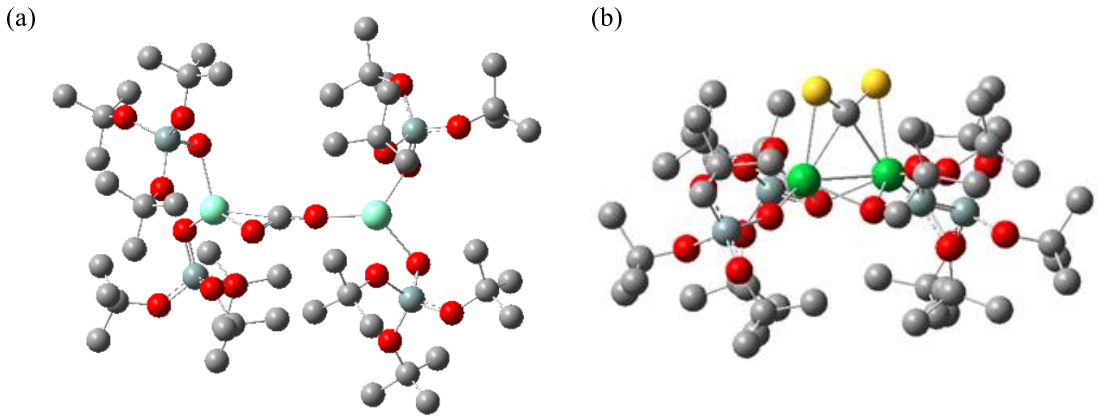

Figure 4.10 3D representation of Sm-$(CO_2)^{2-}$-Sm, Yb-$(CS_2)^{2-}$-Yb. In order to make the structure clearer, the H atom is hidden in the figure. Light green and dark green represent Sm and Yb respectively. And yellow represents S atom.

VI.3.3. Results and discussion

Therefore, we calculated the following reaction mechanism. The black profile is the carbonate formation pathway and the red profile is the oxalate formation pathway. For both pathways, the first step are always to form the key intermediate. This process is exothermic by 106.2kcal/mol. But after that, there occurs a energy difference of 12.8kcal/mol between structure of dioxocarbene intermediate in oxalate formation and the transition state structure in carbonate formation. This is because the two SmL_2 fragments in dioxocarbene intermediate is closer and it will increase the steric repulsion. Therefore, the energy of dioxocarbene as an intermediate is even higher than the transition state on the other reaction pathway. The energy barrier is 15.9kcal/mol from key intermediate to dioxocarbene. So this process is less favorable in kinetic compering with the small energy barrier of first transition state of carbonate formation. For the black pathway, the first transition state is another CO_2 electrophilic attack on the negative charged oxygen, and then form a five-membered ring structure.

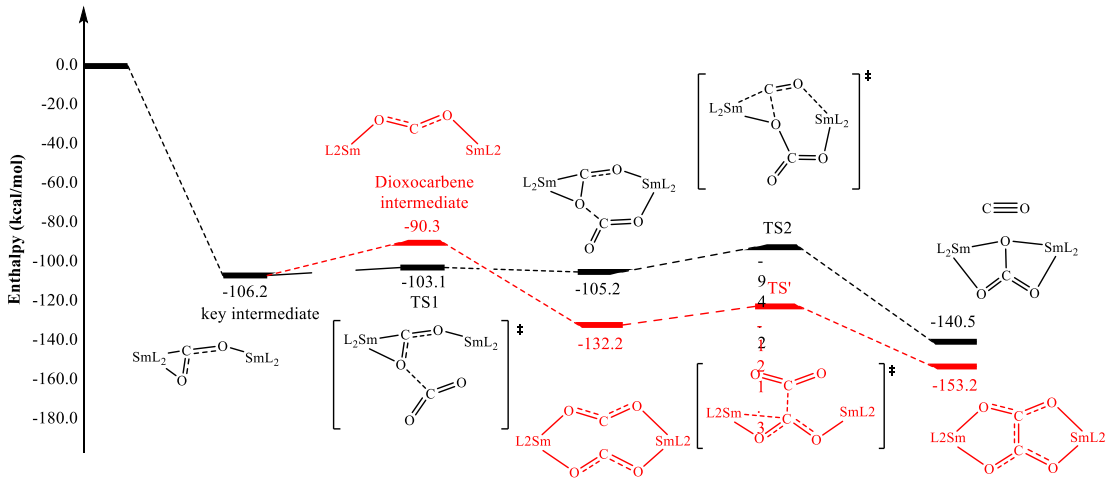

Figure 4.11 Computed enthalpy profile for the reaction of [Yb2L4] with CO2. The black profile is the carbonate formation pathway and the red profile is the oxalate formation pathway.

The formation reaction of carbonate will undergo a CO removal. The distance between C-O gradually elongates, and finally leaves the metal center and becomes CO escape. This energy barrier is only 11.0kcal/mol, and exothermic by 35.3kcal/mol. While for the red transition state, C-C coupling is required to generate oxalate. This energy barrier is almost the same as the second black transition state. The carbonate formation from key intermediate is endothermic by 34.3kcal/mol, but he oxalates formation is endothermic by 47.0kcal/mol. So, the formation of the oxalate is thermodynamic favorable. But considering the energy barrier of the first step (from key intermediates, dioxocarbene and the transition state of CO_2 addition are generated respectively), from the kinetic point of view, the reaction also allows the formation of carbonate.

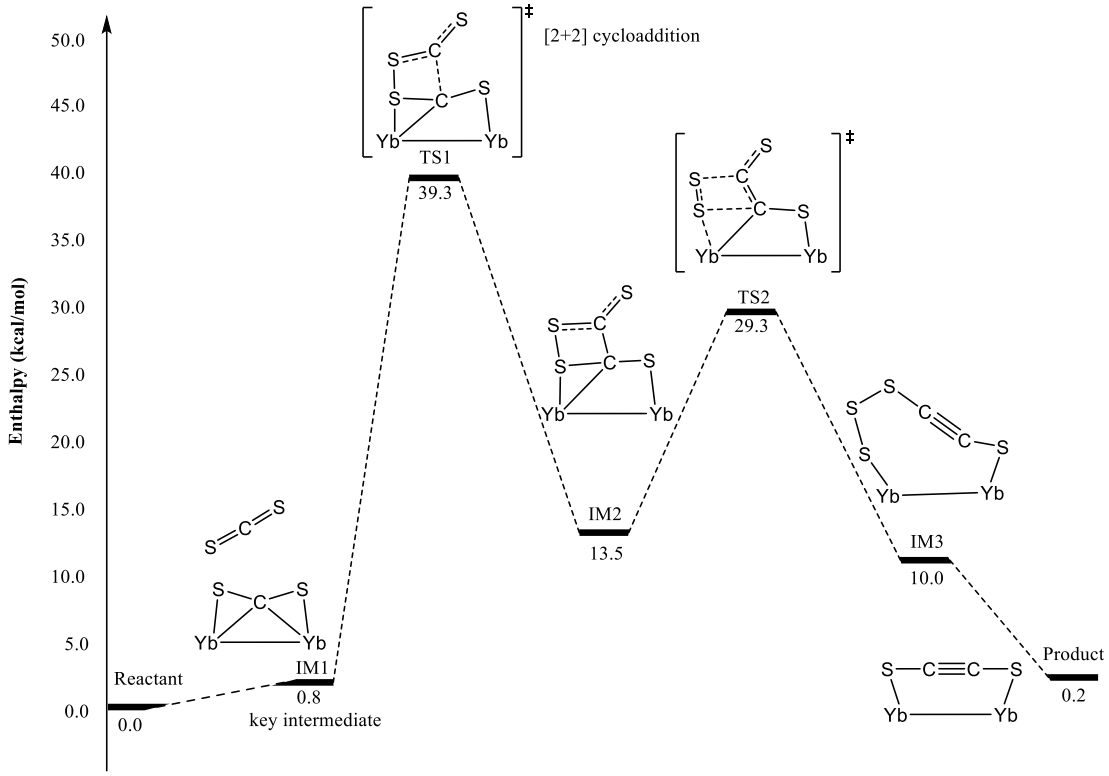

Figure 4.12 Computed enthalpy profile for the reaction of $[Yb_2L_4]$ with CS_2

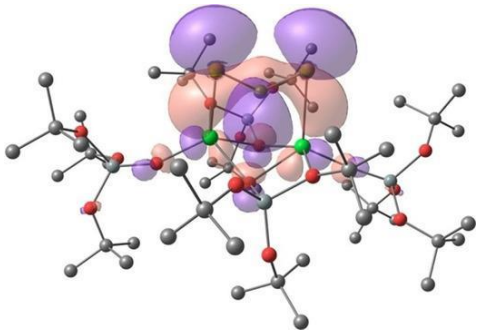

Figure 4.13 3D representation of the HOMO of key intermediate.

In the previously reported mechanism on Sm complex, the key intermediate is similar to the structure in CO_2 reduction. After forming a key intermediate, it is nucleophilic addition with another free CS_2. But we have a different mechanism because of the unique key intermediates found in the experiment. The first step is to generate the dinuclear key intermediate Yb-$(CS_2)^{2-}$-Yb. The key intermediate can then further react with another CS_2 molecule, but in a different way. The system is undergoing a [2+2] cycloaddition, rather than a nucleophilic addition. For this intermediate, we conducted an analysis of the NBO, and the shape of the HOMO orbital shows the interaction of the bond between the sulfur atom and Yb. By checking the

charge, it was found that there was a negative charge of -0.13 on S, which caused the polarity change seen on CS_2. Therefore, when excess CS_2 is added, the connection between S-S and C-C is more inclined. And finally formed an [2+2] cycloaddition transition state. It is precisely because of this different addition method that the energy barrier of the transition state is larger, 38.5kcal/mol, which becomes the speed determining step of the entire reaction. This step is slightly unfavorable in terms of kinetics. After the cycloaddition, S_2 will move out of the system to form the final special product. The process to generate product from key intermediate is endothermic by 0.2 kcal/mol.

VI.3.4. Conclusion

We used DFT to calculate the reduction mechanism of CO_2 and CS_2 on a bimetallic coordination compound of a multidentate tris (tertbutoxy) siloxide ligand with samarium or ytterbium. In $[Sm_2L_4]$, the calculation results support the bimetallic synergistic effect observed in the experiment, which is more conducive to the production of oxalate. And from the theoretical mechanism level, it is explained the reason that why the oxalate is a thermodynamic product, and the carbonate is a kinetic product. In $[Yb_2L_4]$, we verified the bonding mode of a new key intermediate found in the experiment, and because of this unique intermediate, the reaction experienced a different cycloaddition mechanism, causing the transition state to appear sulfur-to-sulfur , carbon to carbon four-membered ring. This will provide new ideas for future experimental directions.

IV.4. Conclusion

For f-block metal complexes, there are three main systems: The first one is the mechanism of the regioselective addition reaction of benzaldehyde and pentadienyl lanthanum metal complex. Several phenomena in the experiment were explained :(1) In the La/I_2 system, the addition of benzaldehyde only produces linear products. Since the formation of branched products on $[(pdl)LaI_2(THF)]$ is thermodynamically unfavorable, it is a reversible reaction. (2) In the La/I_2 system, the addition of p-EWG-benzaldehyde can generate linear products and unexpected ipso products. The introduction of electron-withdrawing p-NO_2-benzaldehyde lowers the energy barrier of epsilon attack, and the ε addition transition state is more favorable from a kinetic point

of view. (3) In the La/I_2/$AlCl_3$ system, the addition of benzaldehyde can generate branched products. That is because from the perspective of kinetics and thermodynamics, γ addition is more likely to occur in the aluminum metal center. The second system is the mechanism of direct coupling of benzophenone and N-heterocycle (such as pyridine and phenanthroline) to form methanol by DFT. The reaction mechanism is divided into two parts. The first step is the formation of C-C bond, and the second step is the transfer of H atoms as the speed determining step. Finally, compared with pyridine, it was verified that the addition of phenanthroline in the experiment can make the coupling reaction occur under mild conditions. The third system is the reduction mechanism of CO_2 and CS_2 on a bimetallic coordination compound of a multidentate tris(tertbutoxy)siloxide ligand with samarium or ytterbium. In [Sm_2L_4], the calculation results support the bimetallic synergistic effect observed in the experiment, which is more conducive to the production of oxalate. In [Yb_2L_4], we verified the bonding mode of a new key intermediate found in the experiment, and because of this unique intermediate, the reaction experienced a different cycloaddition mechanism, causing the transition state to appear sulfur-to-sulfur , carbon to carbon four-membered ring.

References:

1. Dewar, M.J., *Chemical implications of. sigma. conjugation.* Journal of the American Chemical Society, 1984. **106**(3): p. 669-682.
2. Schleyer, P.v.R., et al., *Nucleus-independent chemical shifts: a simple and efficient aromaticity probe.* Journal of the American Chemical Society, 1996. **118**(26): p. 6317-6318.
3. Fowler, P.W., et al., *Ring Currents in Tangentially p− p Bonded σ-Aromatic Systems.* The Journal of organic chemistry, 2006. **71**(17): p. 6459-6467.
4. Kumar, T., et al., *Generation of ε, ε-difluorinated metal-pentadienyl species through lanthanide-mediated CF activation.* Chem. Eur. J, 2017. **23**(65): p. 16460-16465.
5. Yasuda, H., et al., *Regioselective pentadienylation of carbonyl compounds by oligosilylated pentadienylmetals.* Organometallics, 1985. **4**(2): p. 359-367.
6. Seyferth, D. and J. Pornet, *(2, 4-Pentadienyl) trimethylsilane: a useful pentadienylation reagent.* The Journal of Organic Chemistry, 1980. **45**(9): p. 1721-1722.
7. Yasuda, H. and A. Nakamura, *Pentadienylmetal compounds. Structural analyses and applications in organic synthesis.* Journal of organometallic chemistry, 1985. **285**(1-3): p. 15-29.
8. Woo, S., N. Squires, and A.G. Fallis, *Indium-mediated γ-pentadienylation of aldehydes and ketones: cross-conjugated trienes for diene-transmissive cycloadditions.* Organic Letters, 1999. **1**(4): p. 573-576.
9. Wilson, S.R., K.M. Jernberg, and D.T. Mao, *Terpene synthesis via pentadienyl anions.* The Journal of Organic Chemistry, 1976. **41**(19): p. 3209-3210.
10. Fan, Q., et al., *Ligand conformations and spin states in open metallocenes of the first row transition metals having U-shaped 2, 4-dimethylpentadienyl ligands.* New Journal of Chemistry, 2016. **40**(10): p. 8511-8521.
11. Rahif, M., et al., *3-Bromopenta-2, 4-dienylsilane: a useful reagent for the preparation of [3] dendralenes and polycyclic compounds.* Molecular diversity, 2013. **17**(1): p. 49-53.
12. Joosten, A., et al., *Multimetallic zirconocene-based catalysis: Alkyne dimerization and cyclotrimerization reactions.* Organometallics, 2008. **27**(16): p. 4152-4157.
13. Umeda, R., et al., *A novel lanthanum metal-assisted reaction of diaryl ketones and electrophiles.* Tetrahedron, 2015. **71**(8): p. 1287-1291.
14. Kumar, T., et al., *Tuning the Regioselective Functionalization of Trifluoromethylated Dienes via Lanthanum-Mediated Single C− F Bond Activation.* Chemistry-A European Journal, 2021. **27**(12): p. 4016-4021.
15. Joseph, J., et al., *Titanium-catalyzed hydroalumination of conjugated dienes: Access to fulvene-derived allylaluminium reagents and their diastereoselective reactions with carbonyl compounds.* Chemistry–A European Journal, 2014. **20**(18): p. 5433-5438.
16. Shen, Z.-L., et al., *Highly Diastereoselective Preparation of Aldol Products Using New Functionalized Allylic Aluminum Reagents.* Organic letters, 2014. **16**(3): p. 956-959.
17. Peng, Z., et al., *Diastereoselective synthesis of homoallylic alcohols with adjacent tertiary and quaternary centers by using functionalized allylic aluminum reagents.* Angewandte Chemie International Edition, 2010. **49**(45):

p. 8516-8519.
18. Yamamoto, Y. and N. Asao, *Selective reactions using allylic metals.* Chemical reviews, 1993. **93**(6): p. 2207-2293.
19. Perdew, J.P. and Y. Wang, *Erratum: Accurate and simple analytic representation of the electron-gas correlation energy [Phys. Rev. B 45, 13244 (1992)]*. Physical Review B, 2018. **98**(7): p. 079904.
20. Becke, A.D., *Density-functional thermochemistry. V. Systematic optimization of exchange-correlation functionals.* The Journal of chemical physics, 1997. **107**(20): p. 8554-8560.
21. Becke, A.D., *Density-functional thermochemistry. IV. A new dynamical correlation functional and implications for exact-exchange mixing.* The Journal of chemical physics, 1996. **104**(3): p. 1040-1046.
22. Maron, L. and O. Eisenstein, *Do f Electrons Play a Role in the Lanthanide− Ligand Bonds? A DFT Study of Ln (NR2) 3; R= H, SiH3.* The Journal of Physical Chemistry A, 2000. **104**(30): p. 7140-7143.
23. Dolg, M., H. Stoll, and H. Preuss, *A combination of quasirelativistic pseudopotential and ligand field calculations for lanthanoid compounds.* Theoretica chimica acta, 1993. **85**(6): p. 441-450.
24. Dolg, M., et al., *Energy-adjusted pseudopotentials for the rare earth elements.* Theoretica chimica acta, 1989. **75**(3): p. 173-194.
25. Bergner, A., et al., *Ab initio energy-adjusted pseudopotentials for elements of groups 13–17.* Molecular Physics, 1993. **80**(6): p. 1431-1441.
26. Hariharan, P.C. and J.A. Pople, *The influence of polarization functions on molecular orbital hydrogenation energies.* Theoretica chimica acta, 1973. **28**(3): p. 213-222.
27. Fukui, K., *The path of chemical reactions-the IRC approach.* Accounts of chemical research, 1981. **14**(12): p. 363-368.
28. Fukui, K., *Formulation of the reaction coordinate.* The Journal of Physical Chemistry, 1970. **74**(23): p. 4161-4163.
29. Li, C.-J., *Organic reactions in aqueous media with a focus on carbon− carbon bond formations: a decade update.* Chemical Reviews, 2005. **105**(8): p. 3095-3166.
30. Girard, P., J. Namy, and H. Kagan, *Divalent lanthanide derivatives in organic synthesis. 1. Mild preparation of samarium iodide and ytterbium iodide and their use as reducing or coupling agents.* Journal of the American Chemical Society, 1980. **102**(8): p. 2693-2698.
31. Price, K., *Reductive Cyclisation Cascades of Lactones Using SmI 2-H 2 O*. 2011: The University of Manchester (United Kingdom).
32. Inanaga, J., M. Ishikawa, and M. Yamaguchi, *A mild and convenient method for the reduction of organic halides by using a SmI2-THF solution in the presence of hexamethylphosphoric triamide (HMPA).* Chemistry Letters, 1987. **16**(7): p. 1485-1486.
33. Molander, G.A., *Application of lanthanide reagents in organic synthesis.* Chemical reviews, 1992. **92**(1): p. 29-68.
34. Hasegawa, E. and D.P. Curran, *Additive and solvent effects on samarium diiodide reductions: the effects of water and DMPU.* The Journal of Organic Chemistry, 1993. **58**(18): p. 5008-5010.
35. Kan, T., et al., *Total synthesis of (-)-grayanotoxin III.* The Journal of Organic Chemistry, 1994. **59**(19): p. 5532-5534.
36. Weitgenant, J.A., J.D. Mortison, and P. Helquist, *Samarium-promoted coupling*

of pyridine-based heteroaryl analogues of benzylic acetates with carbonyl compounds. Organic letters, 2005. **7**(17): p. 3609-3612.
37. Weitgenant, J.A., et al., *Samarium-promoted coupling of 1, 10-phenanthroline with carbonyl compounds for synthesis of new ligands.* The Journal of organic chemistry, 2004. **69**(8): p. 2809-2815.
38. Jaoul, A., et al., *Atom economical coupling of benzophenone and N-heterocyclic aromatics with SmI 2.* Chemical Communications, 2020. **56**(79): p. 11875-11878.
39. Arakawa, H., et al., *Catalysis research of relevance to carbon management: progress, challenges, and opportunities.* Chemical reviews, 2001. **101**(4): p. 953-996.
40. Meehl, G.A. and W.M. Washington, *El Niño-like climate change in a model with increased atmospheric CO 2 concentrations.* Nature, 1996. **382**(6586): p. 56-60.
41. Broecker, W.S., *Thermohaline circulation, the Achilles heel of our climate system: Will man-made CO2 upset the current balance?* Science, 1997. **278**(5343): p. 1582-1588.
42. Khoo, H.H. and R.B. Tan, *Life cycle investigation of CO2 recovery and sequestration.* Environmental science & technology, 2006. **40**(12): p. 4016-4024.
43. Grice, K.A., *Carbon dioxide reduction with homogenous early transition metal complexes: Opportunities and challenges for developing CO2 catalysis.* Coordination Chemistry Reviews, 2017. **336**: p. 78-95.
44. Frey, A.S., et al., *Facile conversion of CO/H2 into methoxide at a uranium (iii) center.* Angewandte Chemie, 2011. **123**(30): p. 7013-7015.
45. Summerscales, O.T., et al., *Anti-bimetallic complexes of divalent lanthanides with silylated pentalene and cyclooctatetraenyl bridging ligands as molecular models for lanthanide-based polymers.* Organometallics, 2009. **28**(20): p. 5896-5908.
46. Castro-Rodriguez, I. and K. Meyer, *Carbon dioxide reduction and carbon monoxide activation employing a reactive uranium (III) complex.* Journal of the American Chemical Society, 2005. **127**(32): p. 11242-11243.
47. Lam, O.P., et al., *Insights into the mechanism of carbonate formation through reductive cleavage of carbon dioxide with low-valent uranium centers.* Chemical communications, 2010. **46**(18): p. 3137-3139.
48. Berthet, J.-C., et al., *Synthesis and crystal structure of the oxo-bridged bimetallic organouranium complex [(Me3SiC5H4) 3U] 2 [μ-O].* Journal of organometallic chemistry, 1991. **408**(3): p. 335-341.
49. Davies, N.W., et al., *Reductive disproportionation of carbon dioxide by a Sm (II) complex: Unprecedented f-block element reactivity giving a carbonate complex.* Chemical communications, 2006(46): p. 4853-4855.
50. Evans, W.J., et al., *Tethered olefin studies of alkene versus tetraphenylborate coordination and lanthanide olefin interactions in metallocenes.* Journal of the American Chemical Society, 2003. **125**(17): p. 5204-5212.
51. Evans, W.J., C.A. Seibel, and J.W. Ziller, *Organosamarium-Mediated Transformations of CO2 and COS: Monoinsertion and Disproportionation Reactions and the Reductive Coupling of CO2 to [O2CCO2] 2.* Inorganic Chemistry, 1998. **37**(4): p. 770-776.
52. Castro, L., et al., *Insights into the Mechanism of Reaction of [(C5Me5) 2SmII (thf) 2] with CO2 and COS by DFT Studies.* Chemistry–A European Journal,

2012. **18**(25): p. 7886-7895.
53. Willauer, A.R., et al., *Carbon dioxide reduction by dinuclear Yb (ii) and Sm (ii) complexes supported by siloxide ligands.* Dalton Transactions, 2019. **48**(18): p. 6100-6110.
54. Mazzanti, M., et al., *CS2 Reductive Coupling to Acetylenedithiolate by a Dinuclear Ytterbium (II) Complex*. 2019.
55. Reed, A.E., L.A. Curtiss, and F. Weinhold, *Intermolecular interactions from a natural bond orbital, donor-acceptor viewpoint.* Chemical Reviews, 1988. **88**(6): p. 899-926.

Chapter V

s-block metal complexes

V.1. Introduction

Activation of organic or inorganic small molecules catalysed by compounds of main group elements has been extensively studied in the last decade. However, main group metal catalysts for functionalisation are still underdeveloped compared to systems based on transition metals and lanthanides. Some experimental and computational studies have however been carried out for main group metals in catalytic reactions of small molecules supported by multi-dentate N heterocyclic ligands.

Molecular hydride calcium contains a variety of co-ligands and has shown activity in many relevant catalytic reactions such as olefin hydrogenation and CO reduction[1-8]. As an example of a mononuclear calcium hydride with a terminal Ca-H bond, [($Tp^{Ad,iPr}$)Ca(H)(thp)] ($Tp^{Ad,iPr}$=hydrotris(3-adamantyl-5-isopropyl-pyrazolyl)borate) has been reported more recently to catalyze olefin hydrogenation[9]. Such reactive mononuclear calcium hydrides can generally be conceived as the active species in catalytic reactions involving olefinic substrates.

Professor Hill and Professor Mahon[10] have collaborated with our group in a mechanistic study of the reactions of β-diketiminato magnesium and calcium hydrides with CO. The reactions of β-diketiminato-supported heavier alkaline earth (Ca, Sr, Ba) with CO to form cis-ethenediolate derivatives have been verified by DFT.

Cationic calcium hydride supported by 12-membered macrocyclic and 15-membered macrocyclic ligands has been studied by Professor Okuda group[11, 12]. The former refers to a NNNN-type macrocycle $[(Me_4TACD)_2Ca_2(\mu\text{-}H)_2]^{2+}$ (Me_4TACD=1,4,7,10-tetramethyl-1,4,7,10-tetraazacyclododecane); and the latter refers to a NNNNN-type macrocycle $[(Me_5PACP)_2Ca_2(\mu\text{-}H)_2]^{2+}$ (Me_5PACP=1,4,7,10,13-pentamethyl-1,4,7,10,13-pentaazacyclopentadecane). The reactivity pattern of a cationic calcium hydride supported by an NNNN macrocycle has been probed with CO. The calcium hydrides underwent a reaction with CO in THF for 5 min and culminated in a colourless cis-ethenediolate complex $[(Me_4TACD)_2Ca_2(\mu\text{-}OCH{=}CHO)]^{2+}$. The single crystal structure demonstrates that the cis-ethenediolate complex is a nonsymmetrical dimer, and the calcium centre is seven-coordinated. This reactivity of macrocyclic calcium hydride with CO warrants a computational mechanism study.

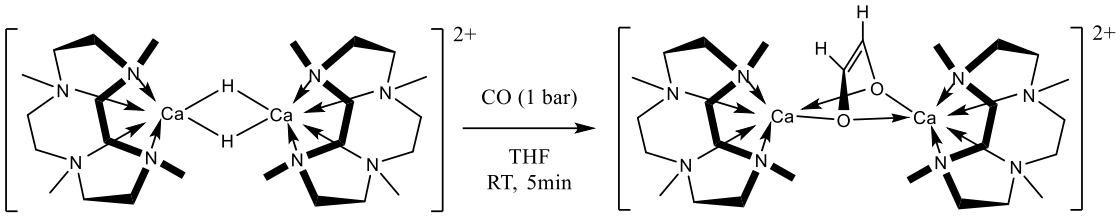

Scheme 5.1 The reaction of hydride calcium and CO to form cis-enediolato complex

On the other hand , molecular hydrides of Mg(II),Al(III),Ge(II) and Sn(II) catalyzing the reduction of aldehydes and ketones with pinacol borane has been reported[13-21]. These reports have spurred research into the main group of compounds as promising catalysts. Professor Venugopal's group investigated the hydroboration of benzophenone by the butylmagnesium complex $[(Me_6Tren)MgOCHPh_2]^+$ (Me_6Tren=tris[2-(dimethylamino)-ethyl]amine) and found a six-membered transition state involving Mg-$OCHPh_2$, H-Bpin and O=CR_2[22]. Their report provides a new idea for the recent study of the hydroboration of ketones without the involvement of metal hydrides. Afterwards, they performed the equimolar amount reaction of PhMeCO and HBpin in toluene and observed the products $[(Me_6Tren)MgOCHMePh]^+$ and $Ph_2C(H)OBpin$. we can see that in this reaction, the dumb acetophenone PhCOMe is reduced to the alkoxy group PhMeC(H)O, while at the same time the alkoxy group of the metal complex terminal is substitution to pinacol.

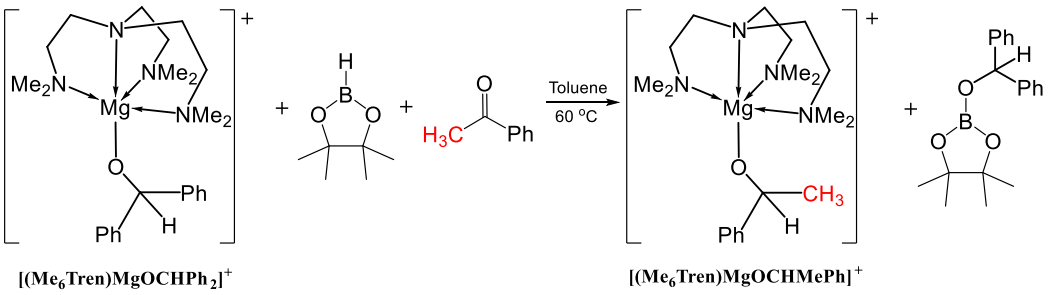

Scheme 5.2 The ketone hydroboration catalyzed by magnesium alkoxide

Here $Ph_2C(H)O$ is considered as a sacrificial ligand. In their experiments, they extended the aldehydes to generate hydroboration product (R_1R_2) CHO-Bpin, such as dibenzaldehyde and 2-pentanone. For the alkyl-substituted ketone 2-pentanone, 95% yields could be achieved within half an hour. But for benzophenone, the reaction takes 14 hours and the yield is only 65%. Therefore, we will investigate this mechanistically.

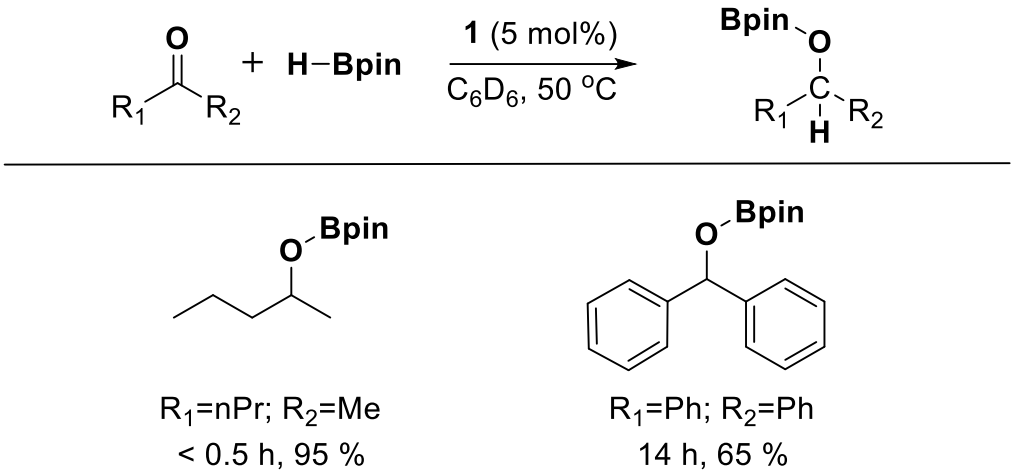

Scheme 5.3 Hydroboration of 2-pentanone and benzophenone.

V.2. Computational details

Calculations were carried out at the DFT level using the hybrid functional B3PW91[23, 24] with the Gaussian 09 suite of programs. Polarized all-electron triple-ζ 6-311G(d,p)[25] basis sets were used for Ca, Mg, C, H, O, B and N. Geometry optimization was carried out without any symmetry restriction. The nature of the extrema (minimum or transition state) was verified with analytical frequency calculations.

V.3. Results and discussion

V.3.1. Reduction of CO catalyzed by NNNN-type macrocyclic-supported hydride calcium

The reaction of the calcium hydride complex with CO gave the product cis-ethenediolate complex $[(Me_4TACD)_2Ca_2(\mu\text{-}OCH{=}CHO)]^{2+}$. The structures of the products were characterized by NMR spectroscopy and single-crystal X-ray diffraction. Using this as a basis for calculation, we optimized the $[(Me_4TACD)_2Ca_2(\mu\text{-}OCH{=}CHO)]^{2+}$ model and obtained the results of Figure 5.1. It can be seen that the distance of the Ca-O bond is between 2.358-2.381 Å, which is close to the experimentally obtained results (2.347-2.371 Å). The four close bond lengths prove the structure of bridging between two calcium via oxygen atoms. And in agreement with what was observed

experimentally, there is an additional C=C double bond formed between the two oxygens in the structure. It has a bond length of 1.377 Å, which is consistent with the bond length of a double bond (1.369 Å in the experiment).

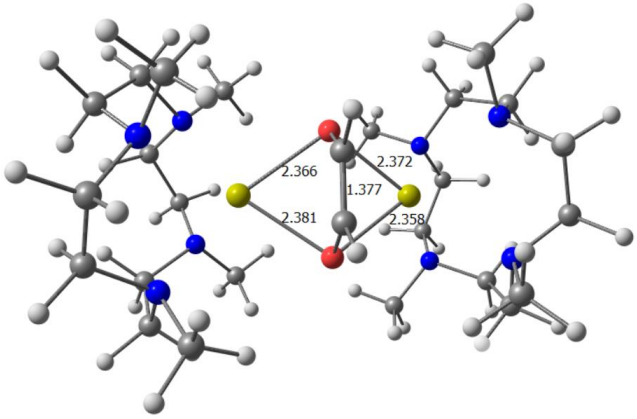

Figure 5.1 3D representation of computed product cis-ethenediolate complex. Red for oxygen atoms, blue for nitrogen atoms, yellow for calcium atoms.

The energy profiles obtained from the calculations show that the reaction to generate the cis-ethenediolate product is exothermic by 100.0 kcal/mol. Dimeric hydride calcium first undergoes dissociation to the mononuclear cyanide [Ca]-H. The energy barrier of the reaction in this step is only 5.4 kcal/mol. Afterwards CO is inserted into the metal-hydrogen bond through the transition state TS1 to produce mononuclear formyl or oxymethylene intermediate, $[(Me_4TACD)Ca(OCH)]^+$. Through the structure of TS1, it can be seen that the distance of Ca-H bond is gradually elongating, while the distance of C-H bond is gradually decreasing, accompanied by the approach of C to the metal center.

Subsequent dimerization of the mononuclear intermediate requires overcoming an energy barrier of 20.2 kcal/mol, which becomes the rate-determining step of the overall reaction. This transient dimer immediately undergoes the transition state step of C=C formation. The final cis-ethenediolate product is produced. It can be seen from the structure of the TS2 that the Ca-O distances (2.468-2.513 Å) are both longer than the Ca-O distances (2.358-2.381 Å) in the products at this time. And the distance between C and C is 2.905 Å, which shows the interaction between C and C.

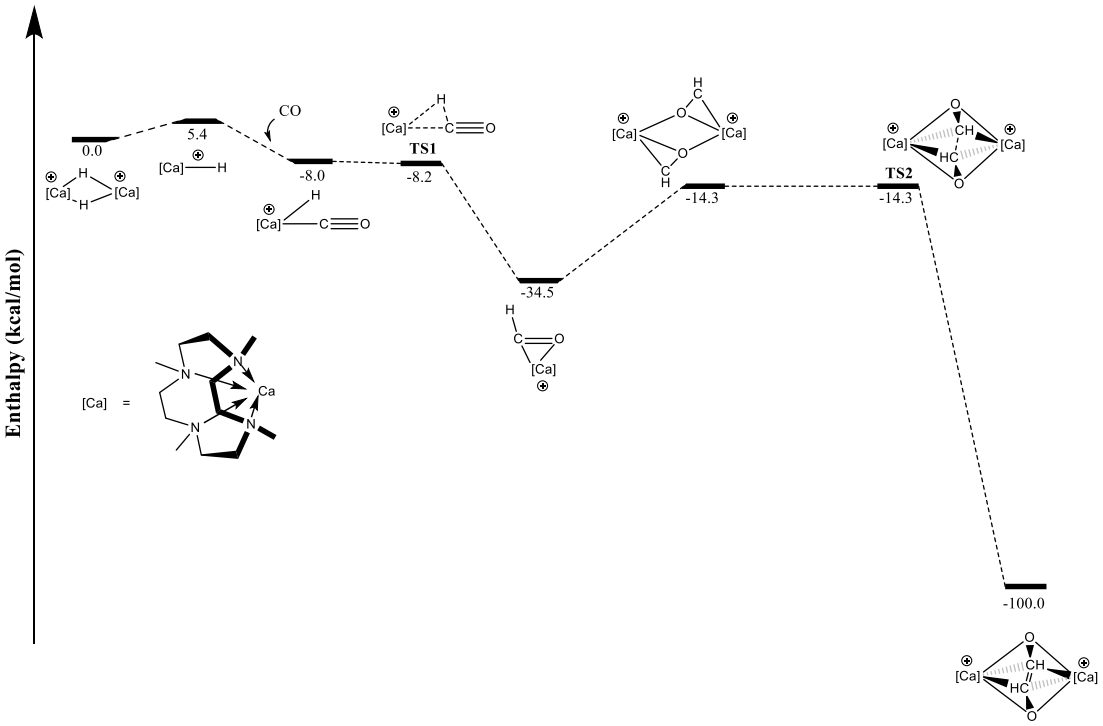

Figure 5.2 Computed enthalpy profile for the formation of calcium cis-ethenediolate complex

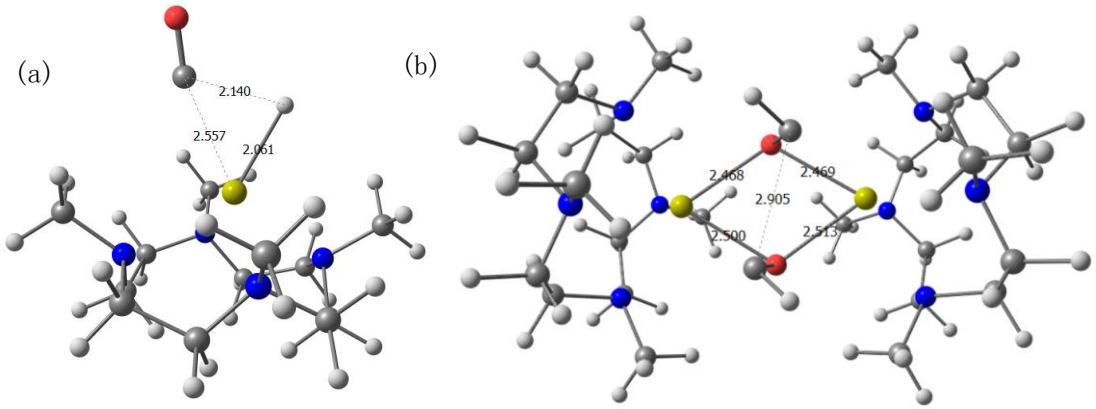

Figure 5.3 3D representation of (a) computed transition state TS1 and (b) computed transition state TS2. Red for oxygen atoms, blue for nitrogen atoms, yellow for calcium atoms.

In previous mechanistic studies of the reaction of the central complex $[(DIPPBDI)_2Ca_2(\mu\text{-}H)]$ with CO, the whole process does not excite the mechanism of calcium dimerization. However, we newly propose the idea that dimeric calcium hydride is dissociated into mononuclear $[CaH]^+$ prior to the reduction of CO The intermediate product $[(Me_4TACD)Ca(OCH)]^+$ is formed and then dimerizes into the product[10]. Therefore the key point of this mechanism is the mononuclear $[CaH]^+$.

This can be verified in a similar calcium catalyst $[(Me_5PCAP)_2Ca_2(\mu\text{-}H)_2]^{2+}$ containing a 15-membered NNNNN macrocycle. This catalyst was experimentally

shown to be more reactive for olefin hydrofunctionalization. Calculations confirmed the significant exothermicity of dimer-monomer dissociation in the presence of THF (-34.1 kcal/mol). Thus the improved catalytic performance may be due to the easier dissociation of the dinuclear hydride into the more reactive monomeric calcium hydride cation in solution.

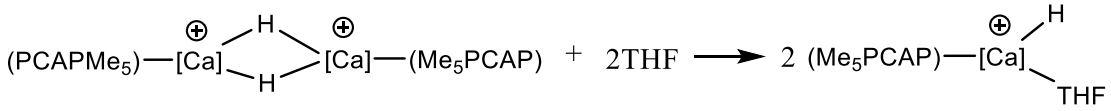

ΔH = -34.1kcal/mol Eq 5.1

V.3.2. Magnesium alkoxide catalyzed ketone hydroboration

We used two different alkyl-substituted ketones for the mechanism calculation of the hydroboration reaction based on the experimentally obtained data. Firstly, according to the experiments, the reaction of 2-pentanone is easier than benzophenone in the presence of alkoxy-coordinated Mg complexes and pinacol. Therefore, we designed two pathways to obtain the hydroboration product (R_1R_2)CHO-Bpin using alkoxylated magnesium $[(Me_6Tren)MgOCHPh_2]^+$ as well as HBpin as reactants. For example, Me^nPrCHO-Bpin generated by reaction with 2-pentanone and Ph_2CHO-Bpin generated with benzophenone.

First, when benzophenone is added to the system, an adduct is formed in which the ketone binds to the magnesium center and HBpin interacts with the alkoxy group in the catalyst-magnesium complex. This step is endothermic by 9.2 kcal/mol, after which a six-ring transition state (TS) is formed, and the process from adduct to TS requires overcoming an energy barrier of 10.8 kcal/mol. In this transition state the distance between Mg and O (alkoxy) grows and at the same time shortens the B-O distance, demonstrating the interaction between B-O.

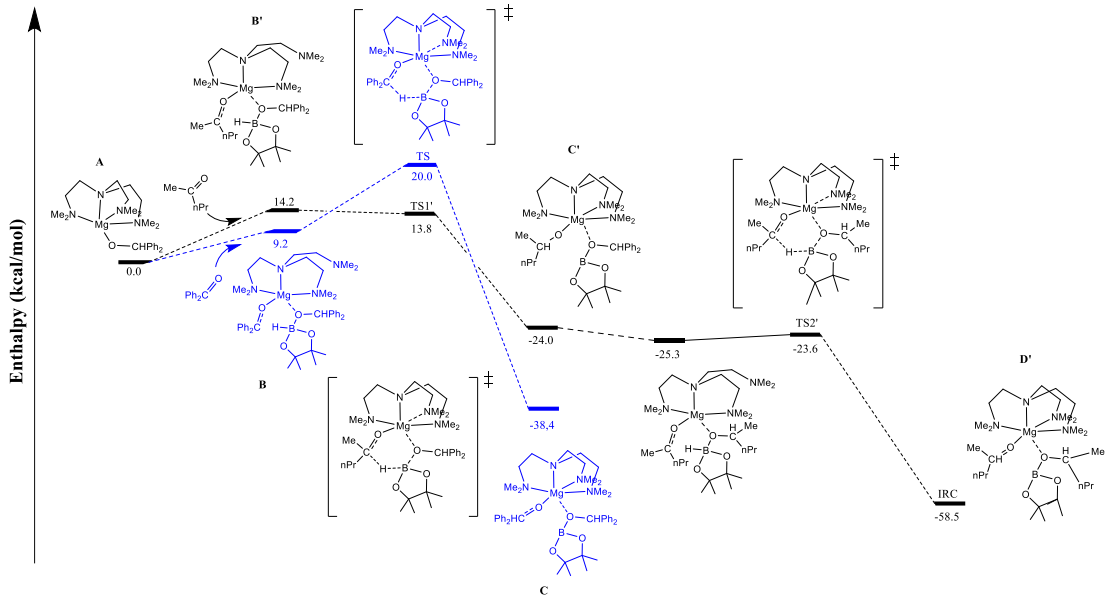

Figure 5.4 Computed enthalpy profile for the hydroboration of benzophenone catalysed by (Me_6Tren)MgOCHMePh. Where blue line represents the reaction of benzophenone and black line represents the reaction of 2-pentanone.

And the distance of B-H has been significantly extended. And C-H interactions were observed on the carbonyl carbon of Ph_2C=O and the hydrogen of HBpin. the carbonyl distance in Ph_2C=O was slightly extended (1.28 Å vs. 1.22 Å for free benzophenone), while the new Mg-O (ketone) was almost formed (1.93 Å vs. 1.87 Å). The energy barrier from the reactants to the transition state (20.0 kcal/mol) is acceptable. Through an exothermic process, the reaction produces a stable complex C from TS. The release of borate ester will result in the coordination of a second ketone to HBpin, which remains endothermic by 9.2 kcal/mol.

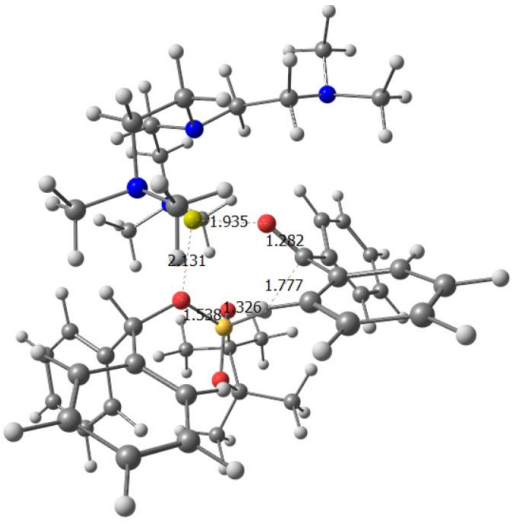

Figure 5.5 3D representation of computed transition state TS. Red for oxygen atoms, blue for

nitrogen atoms, yellow-green color represents the dollar self and the bright yellow color represents the boron atom.

Based on the reaction pathway of benzophenone, we proposed the reaction mechanism of 2-pentanone. It can be found that in the reaction firstly the formation of adduct causes an energy barrier of 14.2kcal/mol, after which the transition state TS1' similar to TS which produced by benzophenone. At this point the intermediate C' is generated, and while $OCHMe^nPr$ and Mg remain attached, the boron ester with two Ph substituents is also attached to Mg. The release of the boron ester requires the another 2-pentanone. At this point the pentanone continues to react with the new alkyl magnesium Mg-$OCHMe^nPr$ obtained after experiencing TS1' with HBpin, which eventually brings out the sacrificial ligand $OCHMe^nPr$ in the form of boron ester. The energy barrier of TS2' is only 1.7kcal/mol and the product is stable (-58.5kcal/mol). Therefore, the borohydride of 2-pentanone is more favorable from both kinetic and thermodynamic points of view, which is consistent with the experiment.

The mechanism of magnesium-catalyzed synergistic ketone borohydride supported by N-polydentate ligands induced us to investigate the catalytic activity of the simple Homoleptic magnesium alkoxides $Mg(OR)_2$. For example, $Mg(OCHPh_2)_2$ acts as a catalyst for the reaction with benzophenone and HBpin to produce boron esters in solvent-free conditions. And the yield was up to 90%. This easily available catalyst was shown to possess highly efficient catalytic performance.

Initially, the coordination of HBpin to $Mg(OR)_2$ produced intermediate I. Two of the HBpins were connected to the Mg center via O, while the other two HBpins interacted with O in the alkoxy group via B. This process exotherms 24.3 kcal/mol. The reaction continued exothermally after the addition of benzophenone, thus producing a stable Intermediate II, in which the benzophenone substitutes the two HBpin ligands on Mg. The boron center hydride then interacts with the carbonyl carbon in Ph_2CO to form the six-membered transition state III, which has a very low energy barrier of 3.1 kcal/mol. Intermediate IV is produced after transition state III, where the reduced benzophenone and the boronic acid ester remain bound to the Mg center. the process exotherms 27.6 kcal/mol. The second H-transfer on HBpin occurs on IV, with an energy barrier of 9.6 kcal/mol for the six-membered transition state V. This further leads to a stable intermediate, in which the two boronic esters bind to Mg.

We have computed this process using DFT. Initially, the coordination of HBpin to $Mg(OR)_2$ produced intermediate I. This process exotherms 24.3 kcal/mol. The reaction continued exothermally after the addition of benzophenone, thus producing a stable Intermediate II, in which the benzophenone substitutes the two HBpin ligands on Mg. The boron center hydride then interacts with the carbonyl carbon in Ph_2CO to form the six-membered transition state III, which has a very low energy barrier of 3.1 kcal/mol. Intermediate IV is produced after transition state III, where the reduced benzophenone and the boronic acid ester remain bound to the Mg center. the process exotherms 27.6 kcal/mol. The second H-transfer on HBpin occurs on IV, with an energy barrier of 9.6 kcal/mol for the six-membered transition state V. This further leads to a stable intermediate, in which the two boronic esters bind to Mg.

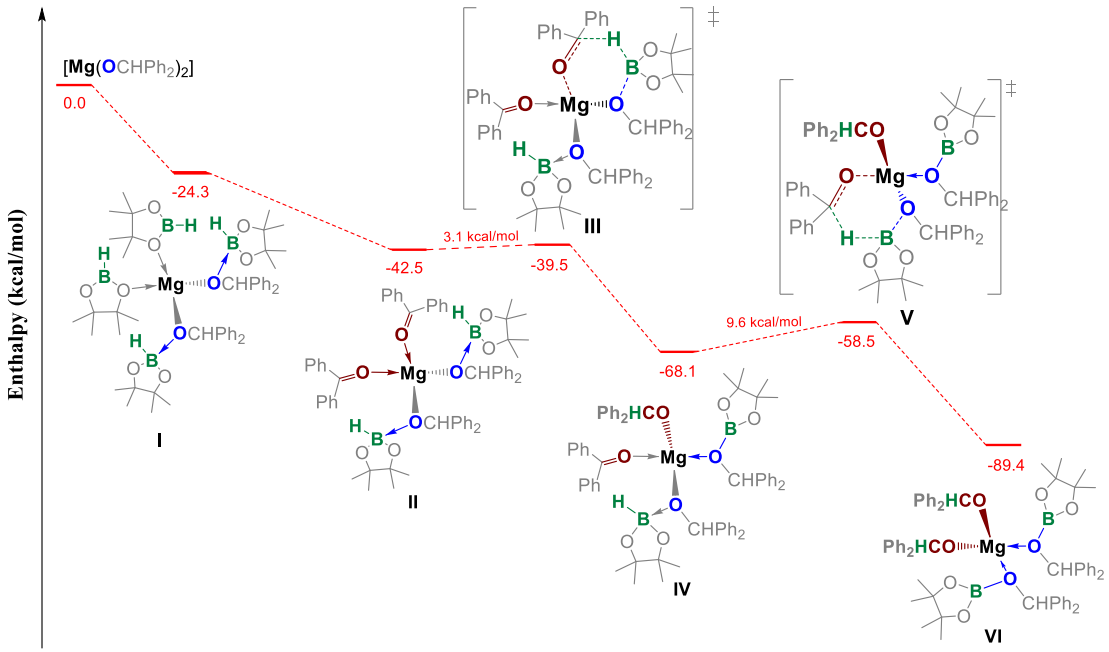

Figure 5.6 Computed enthalpy profile for the hydroboration of benzophenone catalysed by $Mg(OCHPh_2)_2$

Computer theory demonstrated that the reaction using simple $Mg(OCHPh_2)_2$ catalyzed hydroboration was kinetically and thermodynamically more favorable compared to $[(Me_6Tren)MgOCHPh_2]^+$, with a final reaction exotherm of 89.4 kcal/mol.

V.4. Conclusion

This chapter focuses on the small-molecule activation reactions of s-block metals

Mg and Ca supported by N heterocyclic polydentate ligands.

Firstly, for the calcium hydride catalyzed CO reduction reaction, we propose a new reaction pathway in which the dimeric calcium hydride under NNNN-type macrocyclic ligands first dissociates into the monomer $[CaH]^+$ possessing high reactivity. CO can be inserted between the metal-hydrogen to generate a monomeric intermediate, which dimerizes via a C=C double bond into the final cis- ethenediolate product. This new reaction pathway is mainly based on the generation of monomers, thus the thermodynamically favorable dissociation of the 15-membered macrocyclic dimeric calcium hydroxide possessing more N to monomers in THF leads to a higher catalytic activity of this macrocyclic ligand-supported calcium.

And by investigating the magnesium alkoxide catalyzed ketone hydroboration, we propose an addition mechanism that does not involve metal hydrides. Firstly, the hydroboration of benzophenone and 2-pentanone was investigated still using the N heterocyclic ligand-supported alkylmagnesium complex $[(Me_6Tren)MgOCHPh_2]^+$ as a catalyst. The results demonstrate that the process of Ph_2CHO-Bpin generation from benzophenone has a higher energy barrier, while MenPrCHO-Bpin generation from 2-pentanone is more stable. Thus the reaction of 2-pentanone is thermodynamically and kinetically more favorable than that of benzophenone. This is consistent with the experiment. At the same time we also proposed a simple catalyst $Mg(OCHPh_2)_2$, which proved to be more favorable for the reduction of benzophenone.

References:

1. Causero, A., et al., *Stabilization of calcium hydride complexes by fine tuning of amidinate ligands.* Organometallics, 2016. **35**(19): p. 3350-3360.
2. Jochmann, P., et al., *A Cationic Calcium Hydride Cluster Stabilized by Cyclen-Derived Macrocyclic N, N, N, N Ligands.* Angewandte Chemie International Edition, 2012. **51**(18): p. 4452-4455.
3. Harder, S. and J. Brettar, *Rational Design of a Well-Defined Soluble Calcium Hydride Complex.* Angewandte Chemie, 2006. **118**(21): p. 3554-3558.
4. Leich, V., et al., *Molecular Calcium Hydride: Dicalcium Trihydride Cation Stabilized by a Neutral NNNN-Type Macrocyclic Ligand.* Angewandte Chemie International Edition, 2016. **55**(15): p. 4794-4797.
5. Shi, X., et al., *Super-Bulky Penta-arylcyclopentadienyl Ligands: Isolation of the Full Range of Half-Sandwich Heavy Alkaline-Earth Metal Hydrides.* Angewandte Chemie, 2019. **131**(13): p. 4400-4404.
6. Mukherjee, D., D. Schuhknecht, and J. Okuda, *Hydrido Complexes of Calcium: A New Family of Molecular Alkaline-Earth-Metal Compounds.* Angewandte Chemie International Edition, 2018. **57**(31): p. 9590-9602.
7. Hill, M.S., D.J. Liptrot, and C. Weetman, *Alkaline earths as main group reagents in molecular catalysis.* Chemical Society Reviews, 2016. **45**(4): p. 972-988.
8. Harder, S., *From limestone to catalysis: application of calcium compounds as homogeneous catalysts.* Chemical reviews, 2010. **110**(7): p. 3852-3876.
9. Shi, X., et al., *Mononuclear calcium complex as effective catalyst for alkenes hydrogenation.* Chemical Communications, 2020. **56**(38): p. 5162-5165.
10. Anker, M.D., et al., *Alkaline earth-centered CO homologation, reduction, and amine carbonylation.* Journal of the American Chemical Society, 2017. **139**(29): p. 10036-10054.
11. Schuhknecht, D., et al., *Reactivity of a Molecular Calcium Hydride Cation ([CaH]+) Supported by an NNNN Macrocycle.* Inorganic Chemistry, 2020. **59**(13): p. 9406-9415.
12. Höllerhage, T., et al., *Calcium Hydride Catalysts for Olefin Hydrofunctionalization: Ring-Size Effect of Macrocyclic Ligands on Activity.* Chemistry (Weinheim an der Bergstrasse, Germany), 2021. **27**(9): p. 3002.
13. Hadlington, T.J., et al., *Low coordinate germanium (II) and tin (II) hydride complexes: efficient catalysts for the hydroboration of carbonyl compounds.* Journal of the American Chemical Society, 2014. **136**(8): p. 3028-3031.
14. Yang, Z., et al., *An Aluminum Hydride That Functions like a Transition-Metal Catalyst.* Angewandte Chemie, 2015. **127**(35): p. 10363-10367.
15. Arrowsmith, M., et al., *Magnesium-catalysed hydroboration of aldehydes and ketones.* Chemical Communications, 2012. **48**(38): p. 4567-4569.
16. Harinath, A., et al., *Alkali metal complexes as efficient catalysts for hydroboration and cyanosilylation of carbonyl compounds.* Dalton Transactions, 2018. **47**(36): p. 12613-12622.
17. Luo, M., et al., *Efficient and selective carbonyl hydroboration catalyzed by a lithium NCN-Pincer magnesiate complex [Li (THF) 4][NCN-MgBr2].* Journal of Organometallic Chemistry, 2018. **868**: p. 31-35.
18. Bage, A.D., et al., *The Hidden Role of Boranes and Borohydrides in Hydroboration Catalysis.* ACS Catalysis, 2020. **10**(22): p. 13479-13486.

19. Stanford, M.W., A. Bismuto, and M.J. Cowley, *Silyl Anion Initiated Hydroboration of Aldehydes and Ketones.* Chemistry (Weinheim an der Bergstrasse, Germany), 2020. **26**(44): p. 9855.
20. Peddarao, T., N. Sarkar, and S. Nembenna, *Mono-and Bimetallic Aluminum Alkyl, Alkoxide, Halide and Hydride Complexes of a Bulky Conjugated Bis-Guanidinate (CBG) Ligand and Aluminum Alkyls as Precatalysts for Carbonyl Hydroboration.* Inorganic chemistry, 2020. **59**(7): p. 4693-4702.
21. Fohlmeister, L. and A. Stasch, *Ring-Shaped Phosphinoamido-Magnesium-Hydride Complexes: Syntheses, Structures, Reactivity, and Catalysis.* Chemistry–A European Journal, 2016. **22**(29): p. 10235-10246.
22. Banerjee, S., A. Andrews, and A. Venugopal, *A disguised hydride in a butylmagnesium cation.* Chemical Communications, 2018. **54**(45): p. 5788-5791.
23. Perdew, J.P. and Y. Wang, *Accurate and simple analytic representation of the electron-gas correlation energy.* Physical review B, 1992. **45**(23): p. 13244.
24. Becke, A.D., *Density-functional thermochemistry. II. The effect of the Perdew–Wang generalized-gradient correlation correction.* The Journal of chemical physics, 1992. **97**(12): p. 9173-9177.
25. Blaudeau, J.-P., et al., *Extension of Gaussian-2 (G2) theory to molecules containing third-row atoms K and Ca.* The Journal of chemical physics, 1997. **107**(13): p. 5016-5021.

General Conclusion

Generally speaking, compounds with relative molecular mass less than 500 are collectively referred to as small molecules. Small molecules are found in all corners of life. Because of the specificity of the d orbital valence electrons, chemists once thought that the activation of small molecules had to be done by d/f-block metal compounds. The first reports of activation of small molecules by the main group elements were decades behind the transition metal elements. How to activate very strong bonds in small molecules is a continuous challenge for organometallic and coordination chemists. Thus, the design of diverse ligands for coordination of metals in different blocks has greatly enriched the field of organic chemistry and offers a wealth of possibilities for catalytic small molecule activation. Therefore, this thesis focuses on the theoretical mechanisms of small molecule activation catalyzed by several d-block, f-block, and s-block metal complexes, which are summarized below for each chapter.

Chapter 1 mainly introduces the background of the thesis. The development and research process of several elementary reactions involved in the activation of small molecules and the complex catalysts involved in the thesis are mainly introduced.

Chapter 2 focuses on some theoretical background knowledge involved in the computational approach. For example, the formulation of DFT, the definition of computational basis sets, the concept of transition states, and the theory of natural bond orbitals and frontier molecular orbitals.

Chapter 3 focuses on the d-block metal complexes. Firstly, a pentadentate ligand is proposed that can adjust the charge of the ligand by adding or subtracting boron atoms, namely B_2Pz_4Py and BPz_2Py_3. The reactions of interconversion of scandium hydroxo bridged complexes and oxo bridged complexes supported by the dianionic ligand B_2Pz_4Py by adding or subtracting water are firstly calculated DFT calculations demonstrate the thermodynamic stability of the dimeric hydroxyl scandium and that its hydrolytic conversion to oxo complexes only requires overcoming a low energy barrier of 13.2 kcal/mol. Thus the two can be easily transformed into each other. Next, the

catalytic activation of ammonia and hydrazine by iron complexes supported by the same double anionic ligands was calculated. The calculations verify the validity of t activation of ammonia and explain why the coupling of the para-C to NH_2 could not be observed experimentally. And in the activation of hydrazine, a reaction mechanism in which hydrogen transfer occurs within hydrazine was proposed. A mechanistic study has also been done for the synthesis process of scandium forming a double bond with a main group element at the terminal of a coordination metal. A perfect mechanism for the generation of Sc=O double bond from a scandium complex with a monoanion *BPz_2Py_3* coordination found in the experiment is verified and explained by calculations. This leads to the study of the properties of Sc=P and Sc=N double bonds. It was demonstrated computationally that the Sc=P double bond can induce the breakage of the C-C bond in the ligand to produce the phosphido-pyridyl complex. At the same time we also calculated the reaction mechanism of $[Fe_2(\mu^2\text{-NP (pip)}_3)_2(\text{NP (pip)}_3)_2]$ catalyzing the reduction of N_2O to N_2. A thermodynamically very favorable pathway and stable μ^2-O product were obtained. And in this product $[Fe_2(\mu^2\text{-O})(\mu_2\text{-NP(pip)}_3)_2(\text{NP(pip)}_3)_2]$ was shown to possess the shortest Fe-Fe distance comparing with other reports.

Chapter 4 deals with the reactions involving f-block metal complexes. There are three main systems: The first one is the mechanism of the regioselective addition reaction of benzaldehyde and pentadienyl lanthanum metal complex. Several phenomena in the experiment were explained :(1) In the La/I_2 system, the addition of benzaldehyde only produces linear products. Since the formation of branched products on $[(pdl)LaI_2(THF)]$ is thermodynamically unfavorable, it is a reversible reaction. (2) In the La/I_2 system, the addition of p-EWG-benzaldehyde can generate linear products and unexpected ipso products. The introduction of electron-withdrawing p-NO_2-benzaldehyde lowers the energy barrier of epsilon attack, and the ε addition transition state is more favorable from a kinetic point of view. (3) In the $La/I_2/AlCl_3$ system, the addition of benzaldehyde can generate branched products. That is because from the perspective of kinetics and thermodynamics, γ addition is more likely to occur in the aluminum metal center. The second system is the mechanism of direct coupling of benzophenone and N-heterocycle (such as pyridine and phenanthroline) to form methanol by DFT. The reaction mechanism is divided into two parts. The first step is the formation of C-C bond, and the second step is the transfer of H atoms as the speed

determining step. Finally, compared with pyridine, it was verified that the addition of phenanthroline in the experiment can make the coupling reaction occur under mild conditions. The third system is the reduction mechanism of CO_2 and CS_2 on a bimetallic coordination compound of a multidentate tris(tertbutoxy)siloxide ligand with samarium or ytterbium. In $[Sm_2L_4]$, the calculation results support the bimetallic synergistic effect observed in the experiment, which is more conducive to the production of oxalate. In $[Yb_2L_4]$, we verified the bonding mode of a new key intermediate found in the experiment, and because of this unique intermediate, the reaction experienced a different cycloaddition mechanism, causing the transition state to appear sulfur-to-sulfur , carbon to carbon four-membered ring.

Chapter 5 focuses on the small-molecule activation reactions of s-block metals Mg and Ca supported by N heterocyclic polydentate ligands. Firstly, for the calcium hydride catalyzed CO reduction reaction, we propose a new reaction pathway in which the dimeric calcium hydride under NNNN-type macrocyclic ligands first dissociates into the monomer $[CaH]^+$ possessing high reactivity. CO can be inserted between the metal-hydrogen to generate a monomeric intermediate, which dimerizes via a C=C double bond into the final cis- ethenediolate product. This new reaction pathway is mainly based on the generation of monomers, thus the thermodynamically favorable dissociation of the 15-membered macrocyclic dimeric calcium hydroxide possessing more N to monomers in THF leads to a higher catalytic activity of this macrocyclic ligand-supported calcium. Secondly, the mechanism of ketone hydroboration catalyzed by magnesium alkoxide was introduced. the process of Ph_2CHO-Bpin generation from benzophenone has a higher energy barrier, while MenPrCHO-Bpin generation from 2-pentanone is more stable. Thus the reaction of 2-pentanone is thermodynamically and kinetically more favorable than that of benzophenone. This is consistent with the experiment. At the same time we also proposed a simple catalyst $Mg(OCHPh_2)_2$, which proved to be more favorable for the reduction of benzophenone.

In summary, we provide mechanisms for the activation reactions of inorganic/organic small molecules catalyzed by metal complexes of d/f/s-blocks in the periodic table of elements using DFT calculations, respectively. To some extent, the experimental phenomena of activation of small molecules catalyzed by several catalysts are explained separately. For example, the d-block metal di-iron complexes supported by dianionic pentadentate ligand B_2Pz_4Py were considered as a good catalyst for the

activation of ammonia and hydrazine reactions, as well as the reduction reaction with nitrous oxide was used to examine the reactivity of di-iron imidophosphorane complexes as catalysts. Also for example, DFT calculations were used to explain the selectivity of aldehyde addition involving f-block metal lanthanide complexes and the mechanism of samarium/ytterbium-mediated reductive coupling of CO_2 and CS_2. Finally for s-block metals, we used the reduction of CO to verify the reactivity of Ca complexes and we also verified the mechanism of ketone hydroboration catalyzed by magnesium alkoxide complexes. These work could provide ideas on the mechanism of catalytic small molecule activation for future complexes formed by various ligands combined with metal centers, and could serve as a comparable example. Currently, each of the ligands we calculated is restricted to the same block of the periodic table, and it would be interesting to extend them to the application of different blocks of metal centers in the future.

List of Abbreviations:

DFT: Density Functional Theory

B3PW91: Becke, 3-parameter, Perdew-Wang

HOMO: Highest Occupied Molecular Orbital

LUMO: Lowest Unoccupied Molecular Orbital

RECP: Relativistic Effective Core Potential

TS: transition state

NBO: natural bond orbital

Å: Angstrom

HBpin: pinacolborane

THF: tetrahydrofuran

Py: pyridyl

Pz: pyrazolyl

Ph: phenyl

tBu: tert-butyl

Activation de molécules par des complexes mono et multimétalliques ! Une approche théorique

résumé

On trouve des petites molécules dans tous les coins de la vie. En raison de la spécificité des électrons de valence de l'orbitale d, les chimistes pensaient autrefois que l'activation des petites molécules devait se faire par des composés métalliques à blocs d/f. Les premiers rapports sur l'activation de petites molécules par les éléments du groupe principal avaient des décennies de retard sur les éléments des métaux de transition. La manière d'activer les liaisons très fortes dans les petites molécules est un défi permanent pour les chimistes organométalliques et de coordination. Ainsi, la conception de divers ligands pour la coordination des métaux dans différents blocs a considérablement enrichi le domaine de la chimie organique et offre une multitude de possibilités pour l'activation catalytique de petites molécules. Par conséquent, cette thèse se concentre sur les mécanismes théoriques de l'activation de petites molécules catalysée par plusieurs complexes métalliques d-block, f-block et s-block, qui sont résumés ci-dessous pour chaque chapitre.

Le chapitre 1 présente principalement le contexte de la thèse. Le développement et le processus de recherche de plusieurs réactions élémentaires impliquées dans l'activation de petites molécules et les catalyseurs complexes impliqués dans la thèse sont principalement présentés.

Le chapitre 2 se concentre sur certaines connaissances théoriques de base impliquées dans l'approche computationnelle. Par exemple, la formulation de la DFT, la définition des ensembles de base de calcul, le concept des états de transition, et la théorie des orbitales de liaison naturelle et des orbitales moléculaires de frontière.

Le chapitre 3 se concentre sur les complexes métalliques à bloc d. Des recherches sur les complexes de métaux d supportés par des ligands pentadentate B_2Pz_4Py ou

BPz_2Py_3 ont été étudiées. La première rangée de métaux de transition a été coordonnée et synthétisée par de tels ligands pentadentate. Cette section traite principalement des différentes propriétés réactionnelles apportées par la diversité des groupes de liaison métalliques terminaux des complexes de fer et des complexes de scandium et des dérivés du mode multiliaison[1-4]. Tout d'abord, un ligand pentadentate est proposé qui peut ajuster la charge du ligand en ajoutant ou en soustrayant des atomes de bore, à savoir B_2Pz_4Py et BPz_2Py_3[5-7].

Les réactions d'interconversion des complexes pontés hydroxyle de scandium et des complexes pontés oxo supportés par le ligand dianionique B_2Pz_4Py en ajoutant ou en soustrayant de l'eau sont tout d'abord calculées. Les calculs DFT démontrent la stabilité thermodynamique du scandium hydroxyle dimérique et que sa conversion hydrolytique en complexes oxo ne nécessite que de surmonter une faible barrière énergétique de 13,2 kcal/mol. Les deux peuvent donc être facilement transformés l'un en l'autre(Figure 1).

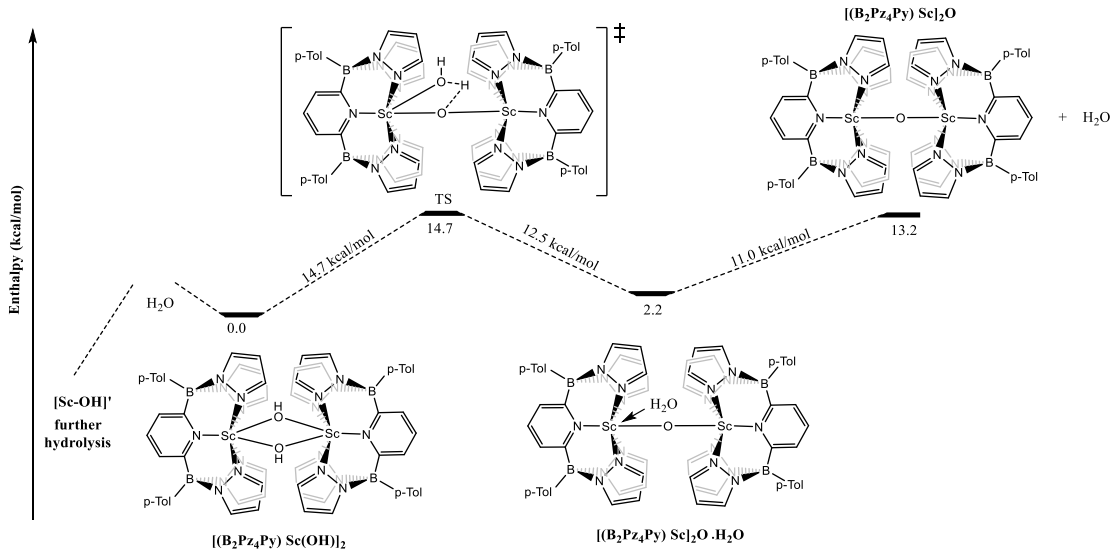

Figure 1 Profil enthalpique calculé pour l'interconversion d'hydroxo et oxo

Ensuite, l'activation catalytique de l'ammoniac et de l'hydrazine par les complexes de fer supportés par les mêmes doubles ligands anioniques a été calculée. En raison de l'énergie de dissociation élevée de la liaison N-H dans le NH_3 (107,6 kcal/mol)[8], il

n'est pas si facile d'activer le NH_3. Professor Warren E. Piers [9] ont également utilisé le ligand pentadentate dianionique B_2Pz_4Py pour la coordination des atomes de fer afin d'activer le NH_3. Les calculs vérifient la validité de l'activation de l'ammoniac et expliquent pourquoi le couplage du para-C au NH_2 n'a pas pu être observé expérimentalement. Comme la génération du produit para est un processus endothermique, alors que le produit ortho est exothermique, la génération du produit para est thermodynamiquement plus favorable(Figure 2).

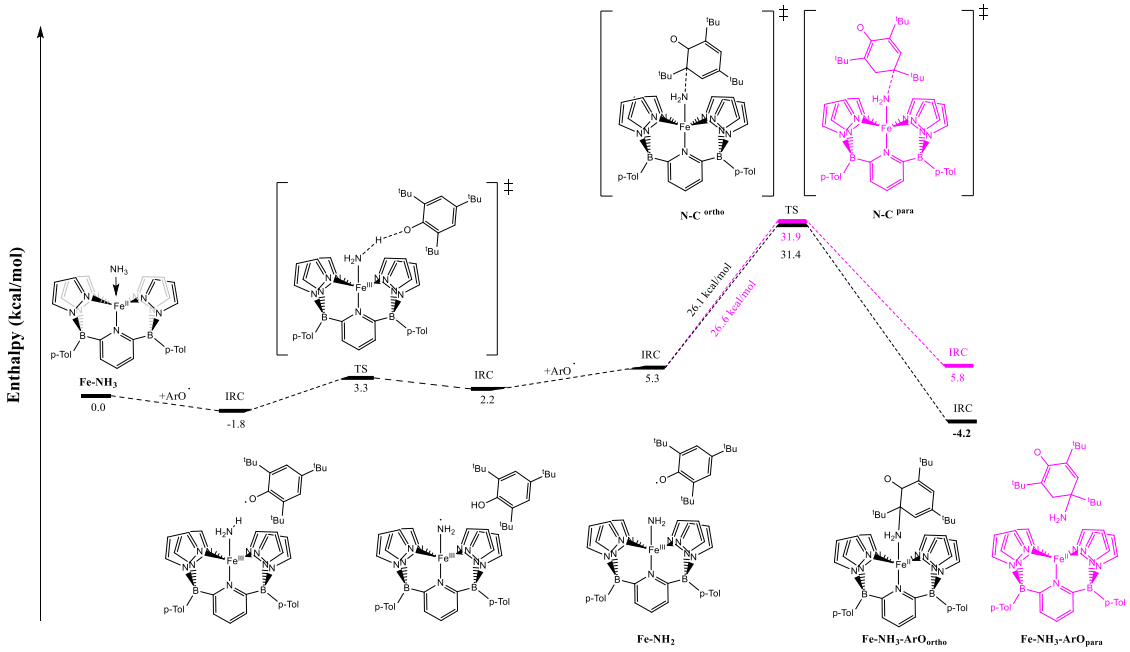

Figure 2 Profil enthalpique calculé pour l'activation de l'ammoniac

En raison de la nature dianionique du ligand B_2Pz_4Py, le composé de fer divalent peut être un agent réducteur fort qui peut induire le clivage de la liaison azote-azote dans l'hydrazine. Par conséquent, lorsque H_2N-NH_2 a été ajouté à (B_2Pz_4Py) Fe, deux produits ont été obtenus, le dimère trans-diazène $[(B_2Pz_4Py)Fe(NH_2)]_2$ et (B_2Pz_4Py)Fe-NH_3 dans les expériences. Et dans l'activation de l'hydrazine, un mécanisme de réaction dans lequel le transfert d'hydrogène se produit au sein de l'hydrazine a été proposé. Lorsque Fe-NH_2NH_2-Fe subit un transfert d'hydrogène entre les hydrazines internes pour donner l'espèce imido, ce Fe-NH se polymérise très rapidement en un dimère(Figure 3).

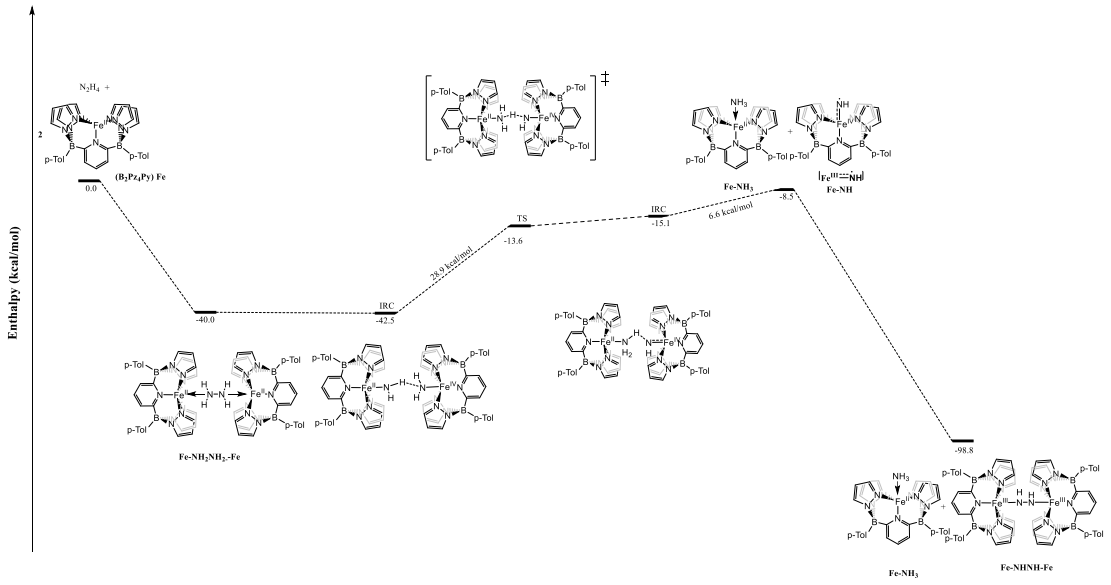

Figure 3 Profil enthalpique calculé pour l'activation de l'hydrazine

Une étude mécanistique a également été réalisée pour le processus de synthèse du scandium formant une double liaison avec un élément du groupe principal à l'extrémité d'un métal de coordination[6]. Ici, un nouveau ligand BPz_2Py_3 avec un monoanion est proposé pour réduire la forte basicité que l'anion double confère au complexe Sc=E. Professor Warren E. Piers ont travaillé sur la préparation de $(BPz_2Py_3)Sc=O$ et $(BPz_2Py_3)Fe=O$, et ont récemment découvert une excellente voie de synthèse en trois étapes. Le ligand libre protoné BPz_2Py_3-H réagit avec ScR_3-THF_2 ($R=CH_2SiMe_2Ph$), et un RH est retiré pour former $(BPz_2Py_3)ScR_2$. Après avoir ajouté du $B(C_6F_5)_3$ hydraté, les deux équivalents restants de RH sont éliminés, obtenant ainsi une liaison Sc-O-B.La voie de synthèse parfaite trouvée dans les expériences est corroborée par le fait qu'il n'y a pas de barrières énergétiques élevées à surmonter tout au long de la réaction exothermique pour la formation de la double liaison(Figure 4).

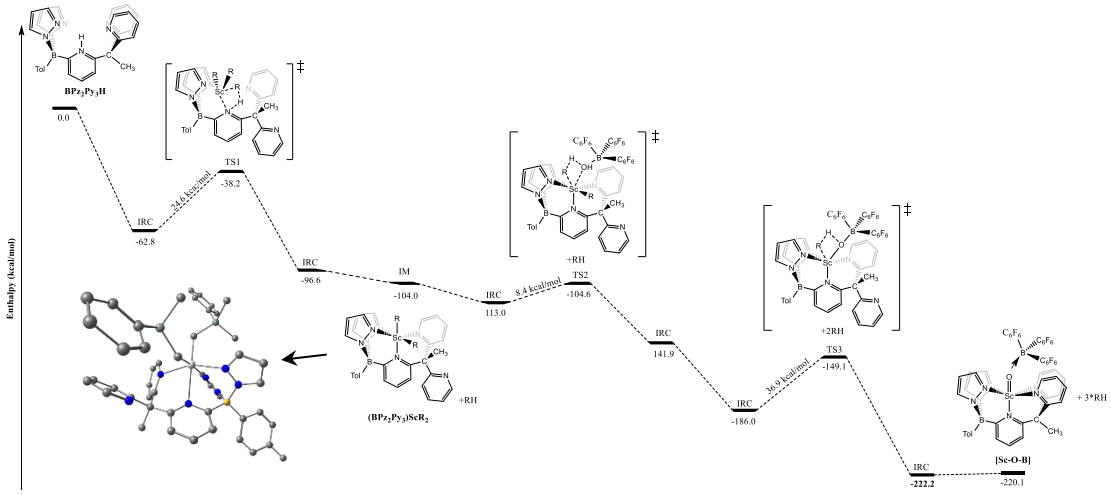

Figure 4 Profil enthalpique calculé pour la formation de la double liaison scandium-oxygène

Lorsque le $(BPz_2Py_3)ScR_2$ est généré puis que la 2,6-di-iso-propylaniline est ajoutée, il subit encore deux équivalents d'élimination de RH, et obtient finalement le complexe imido de scandium terminal. En utilisant la même voie de préparation, la 2,6-di-iso-propylphényl phosphine peut être ajoutée au terminal Sc. A ce moment, cependant, des changements inattendus sont apparus dans le produit. Grâce à la caractérisation expérimentale, il a été découvert que dans le complexe phosphoalkyle, la caractéristique de la double liaison du phosphore de scandium a été perdue, et le groupe pyridyle a été transféré au groupe P par le clivage de la liaison C-C, formant ainsi un nouveau ligand tétradentate[10]. On a constaté que les produits de réaction de la double liaison Sc=P présentaient un changement distinctif. Il a été démontré par calcul que la double liaison Sc=P peut induire la rupture de la liaison C-C dans le ligand pour produire le complexe phosphido-pyridyle. Et pour Sc=N, la barrière énergétique requise pour cette étape de l'état de transition est encore plus grande, de sorte que cette étape n'est pas facile à mettre en œuvre de manière dynamique(Figure 5).

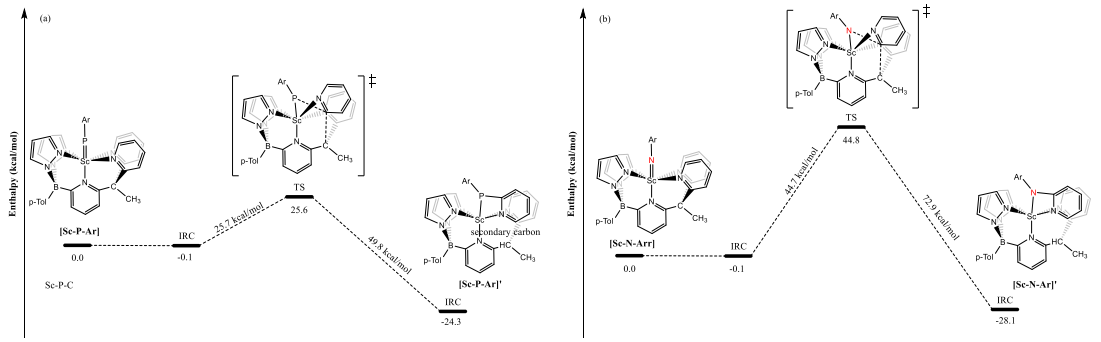

Figure 5 Profil enthalpique calculé d'une autre voie pour la formation d'un nouveau produit [Sc-P-Ar]' à partir du phosphinidène [Sc-P-Ar].

Parallèlement, le groupe d' Professeur La Pierre HS a expérimenté l'utilisation de ligands monodentés à champ faible pour la construction de composés à liaison métal-métal. Ils ont étudié la réaction de complexes de fer(II) supportés par ce ligand à champ faible tris(dialkylamido)-imidophosphoranes avec l'oxyde nitreux, qui a été utilisé pour étudier la réactivité de ce complexe bimétallique. L'oxyde nitreux est un gaz à effet de serre et son utilisation potentielle comme oxydant vert est devenue une cible technologique importante[7, 11-13]. Nous avons également calculé le mécanisme de réaction de $[Fe_2(\mu^2\text{-NP (pip)}_3)_2(\text{NP (pip)}_3)_2]$ catalysant la réduction de N_2O en N_2 . Une voie thermodynamiquement très favorable et un produit μ2-O stable ont été obtenus. Et dans ce produit, $[Fe_2(\mu^2\text{-O})(\mu^2\text{-NP(pip)}_3)_2(\text{NP(pip)}_3)_2]$ s'est avéré posséder la plus courte distance Fe-Fe par rapport à d'autres rapports(Figure 6). Et dans ce produit, $[Fe_2(\mu^2\text{-O})(\mu^2\text{-NP(pip)}_3)_2(\text{NP(pip)}_3)_2]$ s'est avéré posséder la plus courte distance Fe-Fe par rapport à d'autres rapports[14, 15].

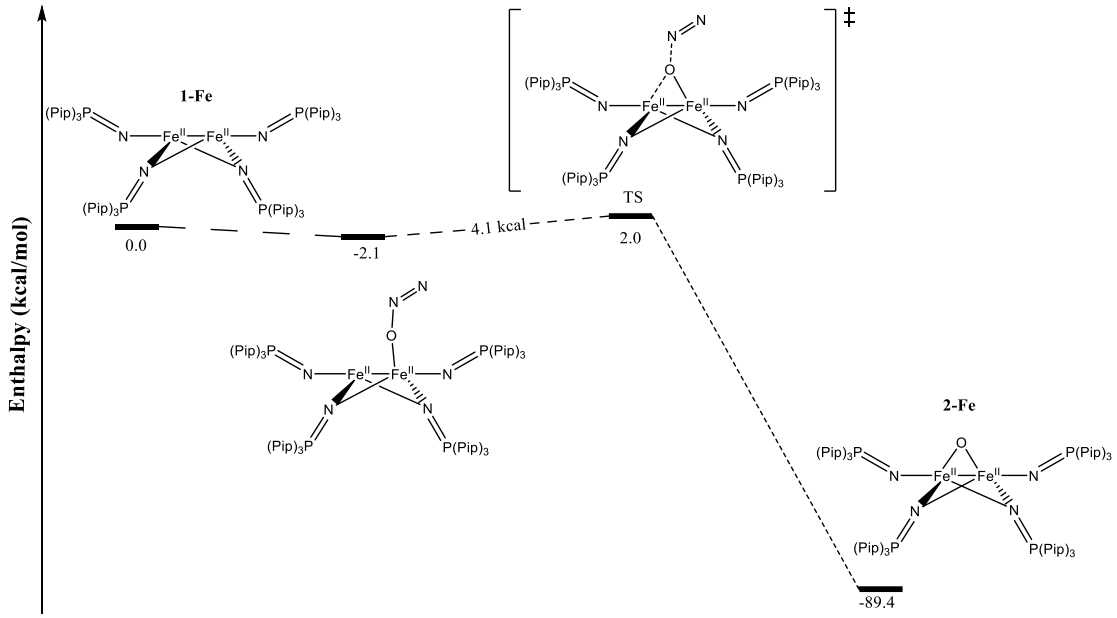

Figure 6 Profil enthalpique calculé pour la réaction de [1-Fe] avec N_2O

Dans le chapitre 4, nous utilisons une approche computationnelle pour étudier mécaniquement l'activation de petites molécules organiques et inorganiques catalysée par trois complexes métalliques de type f-block. Il y a trois systèmes principaux : Le premier est le mécanisme de la réaction d'addition régiosélective du benzaldéhyde et du complexe métallique pentadiényle du lanthane. Plusieurs phénomènes de l'expérience ont été expliqués :(1) Dans le système La/I_2, l'addition du benzaldéhyde ne donne que des produits linéaires. Comme la formation de produits ramifiés sur [(pdl)LaI_2(THF)] est thermodynamiquement défavorable, il s'agit d'une réaction réversible. (2) Dans le système La/I_2, l'addition de p-EWG-benzaldéhyde peut générer des produits linéaires et des produits ipso inattendus. L'introduction de p-NO_2-benzaldéhyde attracteur d'électrons abaisse la barrière énergétique de l'attaque epsilon, et l'état de transition d'addition ε est plus favorable d'un point de vue cinétique(Figure 7). (3) Dans le système La/I_2/$AlCl_3$, l'addition de benzaldéhyde peut générer des produits ramifiés. C'est parce que du point de vue de la cinétique et de la thermodynamique, l'addition γ est plus susceptible de se produire dans le centre métallique de l'aluminium(Figure 8).

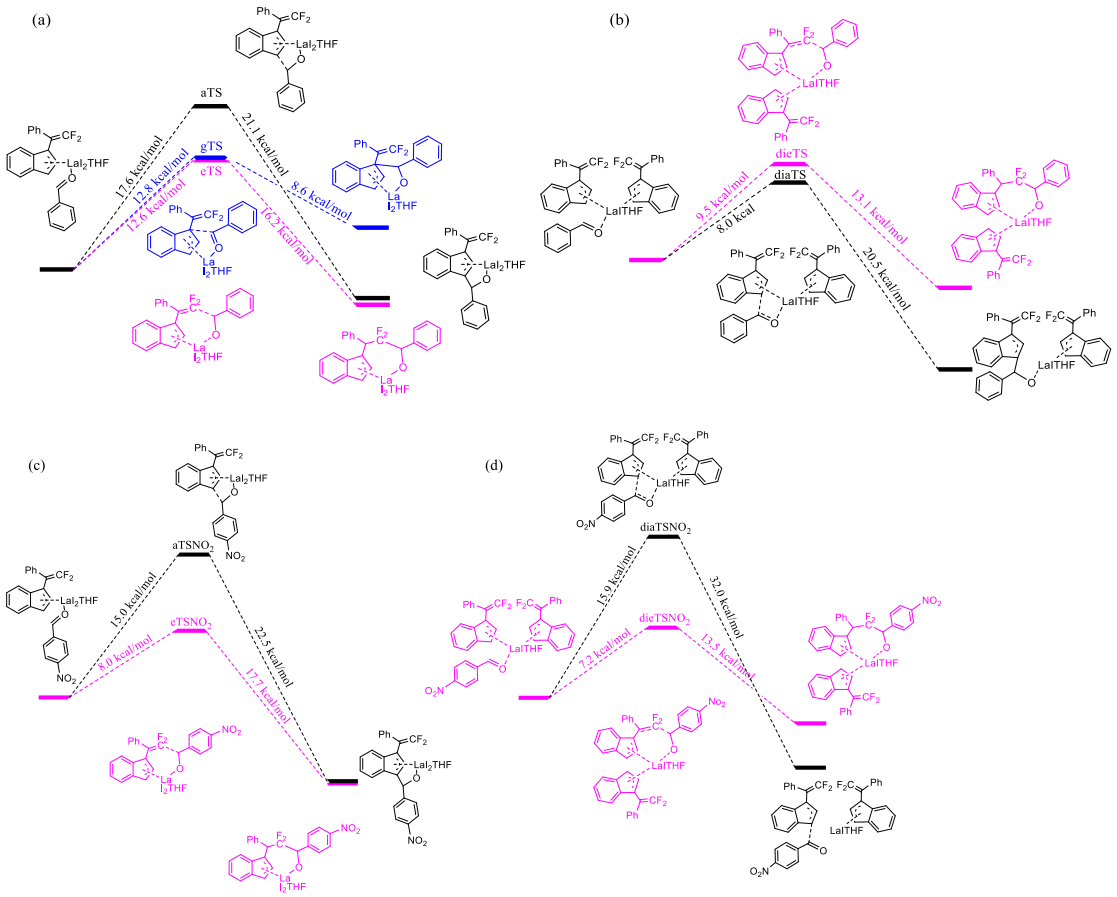

Figure 7 Mécanisme de réaction de l'addition du benzaldéhyde avec (a)[(pdl)LaI_2(THF)], (b)[$(pdl)_2$LaI(THF)]. Et mécanisme de réaction de l'addition p-NO_2-benzaldéhyde avec (c)[(pdl)LaI_2(THF)], (d)[$(pdl)_2$LaI(THF)].

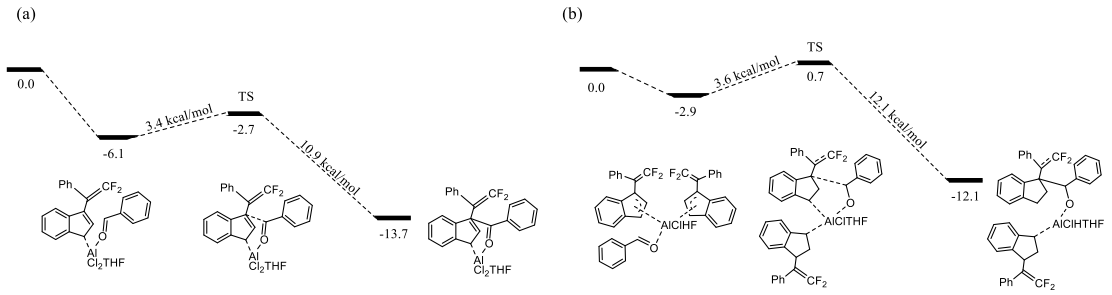

Figure 8 Mécanisme d'addition γ du benzaldéhyde avec (a) [(pdl)$AlCl_2$(THF)] et (b) [$(pdl)_2$AlCl(THF)].

Le deuxième système est le mécanisme de couplage direct de la benzophénone et du N-hétérocycle (comme la pyridine et la phénanthroline) pour former du méthanol par DFT. La formation de liaisons C-C est la base de la synthèse organique et de la

construction de composés organiques colorés[16]. Le diiodure de samarium joue un rôle important dans la synthèse des liaisons carbone-carbone en tant qu'excellent réactif de transfert d'électron unique [17]. Cette section s'appuie sur les expériences du professeur Grégory Nocton [18-20] qui ont utilisé la pyridine, la bipyridine, la phénanthroline et d'autres composés aromatiques hétérocycliques de type N pour réagir avec des aldéhydes ou des cétones afin de produire des substituants hydroxyle en position α.

Dans cette réaction, aucun autre agent de couplage n'a participé à l'exception du SmI_2. L'arrangement électronique du radical cétyle est vérifié par l'analyse de la densité de spin. En utilisant le radical cétyle comme point de départ du calcul du mécanisme, le mécanisme de réaction est divisé en deux parties. La première étape est la formation de la liaison C-C, et la deuxième étape est le transfert des atomes H comme étape déterminant la vitesse. Enfin, par rapport à la pyridine, il a été vérifié que l'ajout de phénanthroline dans l'expérience peut faire se produire la réaction de couplage dans des conditions douces(Figure 9).

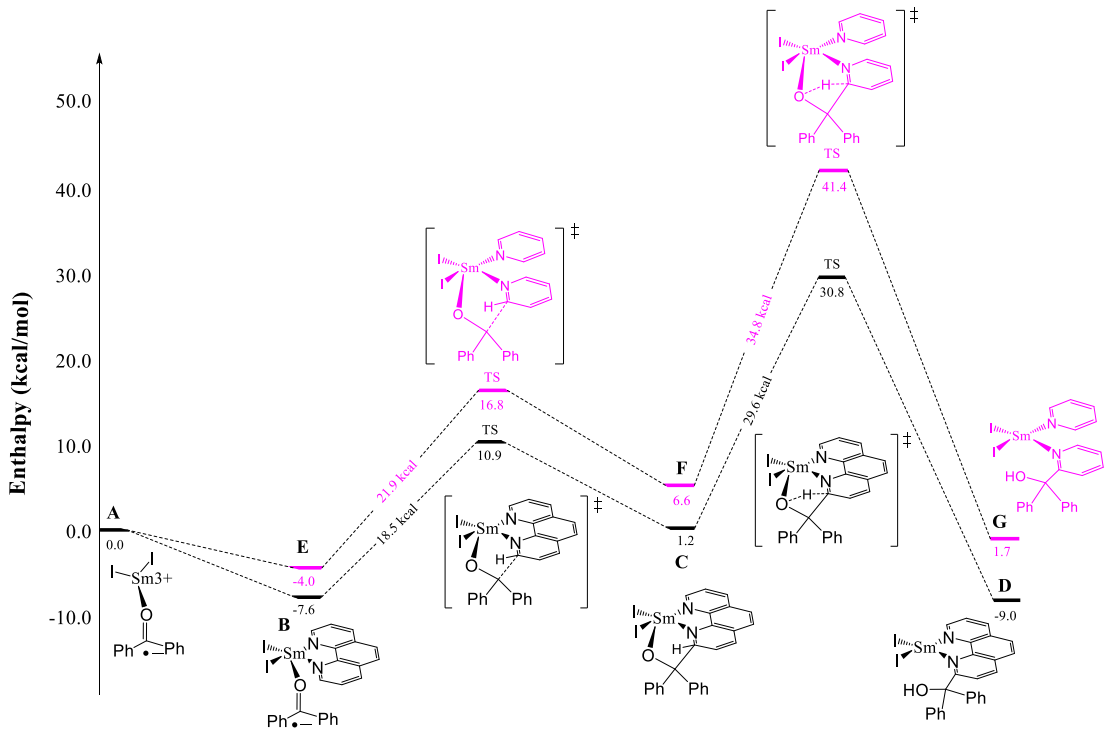

Figure 9 Profil enthalpique calculé pour la formation de D (noir) et G (rose).

Le troisième système est le mécanisme de réduction du CO_2 et du CS_2 sur un composé de coordination bimétallique d'un ligand tris(tertbutoxy)siloxyde multidenté avec le samarium ou l'ytterbium. Professor Marinella Mazzanti[21] ont rapporté un composé de coordination bimétallique d'un ligand tris (tertbutoxy) siloxyde multidenté avec le samarium ou l'ytterbium, qui est $[Yb_2L_4]$ et $[Sm_2L_4]$ (L=$(O^tBu)_3SiO^-$), respectivement. Ces deux complexes réagissent avec le dioxyde de carbone pour produire de l'oxalate et du carbonate, et des expériences ont confirmé que les espèces qui existent sous forme de dimères dans des solutions non polaires sont favorables à la formation d'oxalate. Professor Marinella Mazzanti [22] ont obtenu un produit acétylènedithiolate ($C_2S_2^{2-}$) sans précédent par le couplage réducteur de $[Yb_2L_4]$ et de CS_2. Nous allons étudier le mécanisme de la DFT à partir de ces deux réactions.

Dans $[Sm_2L_4]$, les résultats des calculs confirment l'effet synergique bimétallique observé dans l'expérience, ce qui est plus favorable à la production d'oxalate(Figure 10). Dans $[Yb_2L_4]$, nous avons vérifié le mode de liaison d'un nouvel intermédiaire clé trouvé dans l'expérience, et à cause de cet intermédiaire unique, la réaction a connu un mécanisme de cycloaddition différent, faisant apparaître l'état de transition soufre à soufre, carbone à carbone dans un cycle à quatre membres(Figure 11).

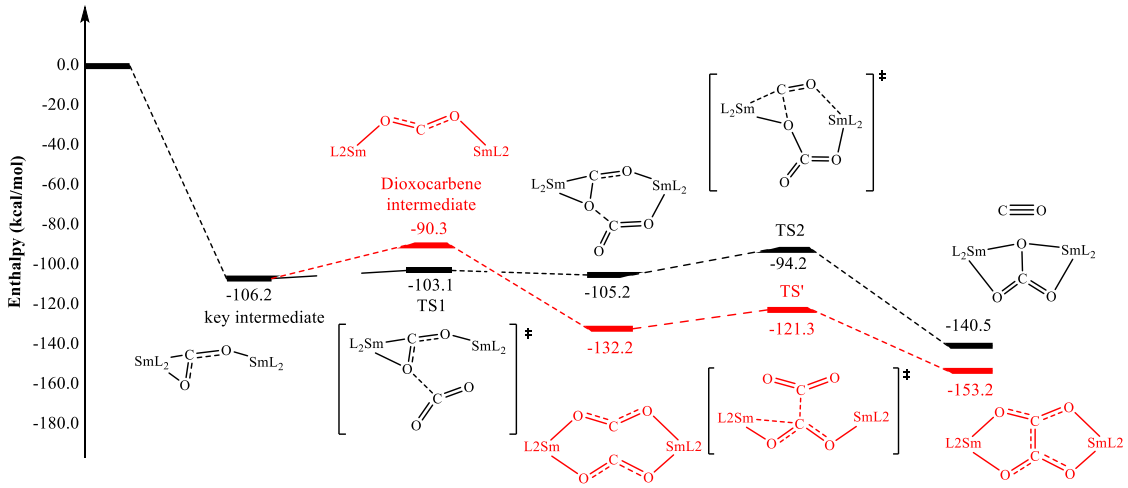

Figure 10 Profil enthalpique calculé pour la réaction de $[Yb_2L_4]$ avec le CO_2. Le profil noir est la voie de formation du carbonate et le profil rouge est la voie de formation de l'oxalate.

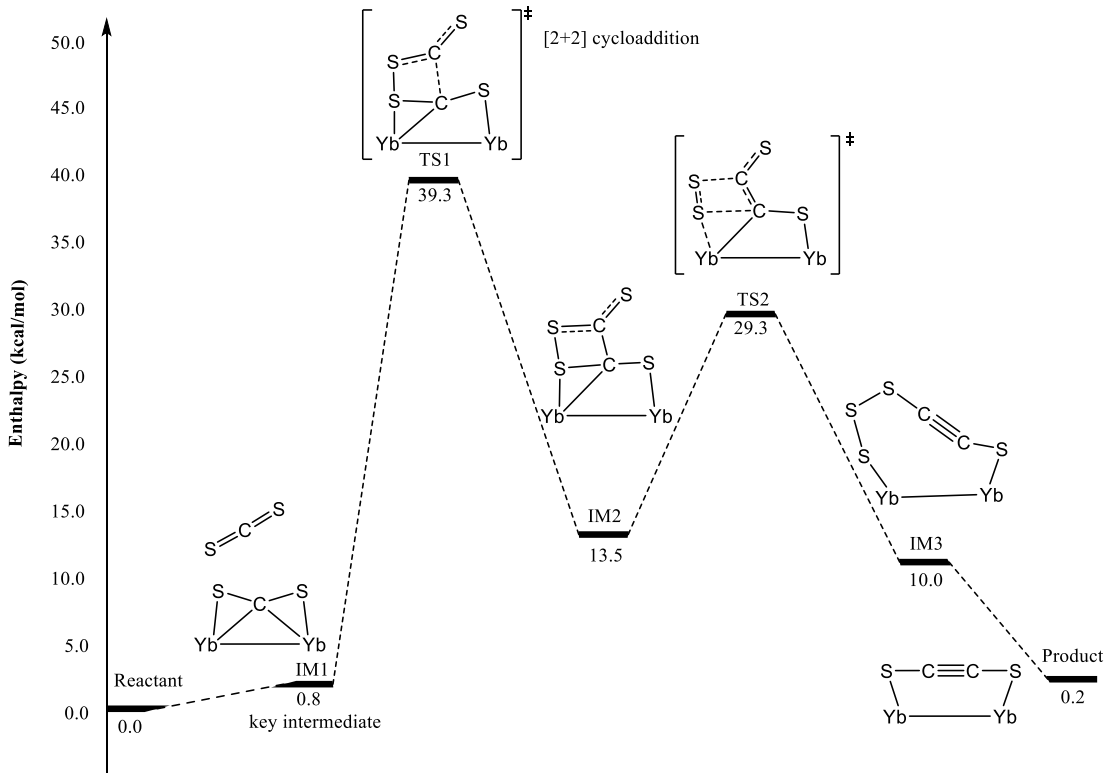

Figure 11 Profil enthalpique calculé pour la réaction de $[Yb_2L_4]$ avec CS_2

Le chapitre 5 se concentre sur les réactions d'activation des petites molécules des métaux du bloc s, Mg et Ca, supportés par des ligands polydentés hétérocycliques de type N.

Tout d'abord, l'hydrure de calcium moléculaire contient une variété de co-ligands et a montré une activité dans de nombreuses réactions catalytiques pertinentes telles que l'hydrogénation des oléfines et la réduction du CO [23-30]. Comme exemple d'hydrure de calcium mononucléaire avec une liaison Ca-H terminale, $[(Tp^{Ad,iPr})Ca(H)(thp)]$ ($Tp^{Ad,iPr}$=borate d'hydrotris(3-adamantyl-5-isopropyl-pyrazolyl) a été signalé plus récemment pour catalyser l'hydrogénation des oléfines [31]. Ces hydrures de calcium mononucléaires réactifs peuvent généralement être conçus comme les espèces actives dans les réactions catalytiques impliquant des substrats oléfiniques.

L'hydrure de calcium cationique supporté par des ligands macrocycliques à 12 et 15 chaînons a été étudié par le groupe de Professor Jun Okuda [32, 33]. Le premier fait référence à un macrocycle de type NNNN $[(Me_4TACD)_2Ca_2(\mu\text{-}H)_2]^{2+}$

(Me_4TACD=1,4,7,10-tétraméthyl-1,4,7,10-tétraazacyclododécane) ; et le dernier fait référence à un macrocycle de type NNNNN $[(Me_5PACP)_2Ca_2(\mu\text{-}H)_2]^{2+}$ (Me_5PACP=1,4,7,10,13-pentaméthyl-1,4,7,10,13-pentaazacyclopentadecane). Le schéma de réactivité d'un hydrure de calcium cationique supporté par un macrocycle NNNN a été sondé avec du CO. Les hydrures de calcium ont subi une réaction avec le CO dans le THF pendant 5 minutes et ont abouti à un complexe cis-éthénediolate incolore $[(Me_4TACD)_2Ca_2(\mu\text{-}OCH{=}CHO)]^{2+}$. La structure monocristalline démontre que le complexe cis-éthènediolate est un dimère non symétrique, et que le centre calcique est à sept coordinations. Le mécanisme computationnel de cette réactivité de l'hydrure de calcium macrocyclique avec le CO a été rapporté dans ce chapitre.

Pour la réaction de réduction du CO catalysée par l'hydrure de calcium, nous proposons une nouvelle voie de réaction dans laquelle l'hydrure de calcium dimère sous des ligands macrocycliques de type NNNN se dissocie d'abord en le monomère $[CaH]^+$ possédant une grande réactivité. Le CO peut être inséré entre le métal et l'hydrogène pour générer un intermédiaire monomère, qui se dimérise via une double liaison C=C dans le produit final cis-éthénediolate. Cette nouvelle voie de réaction est principalement basée sur la génération de monomères, ainsi la dissociation thermodynamiquement favorable de l'hydroxyde de calcium dimérique macrocyclique à 15 membres possédant plus de N aux monomères dans le THF conduit à une activité catalytique plus élevée de ce calcium macrocyclique supporté par un ligand(Figure 12).

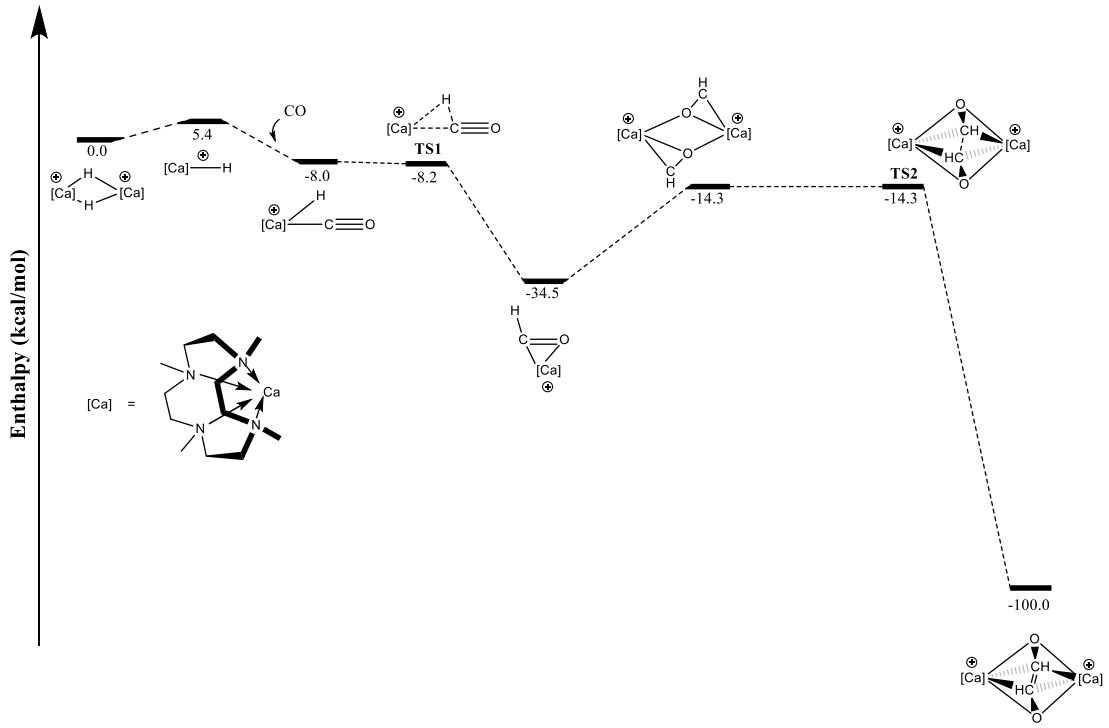

Figure 12 Profil enthalpique calculé pour la formation du complexe cis-éthènediolate de calcium

Deuxièmement, Le groupe d'Ajay a étudié l'hydroboration de la benzophénone par le complexe butylmagnésium $[(Me_6Tren)MgOCHPh_2]^+$ (Me_6Tren=tris[2-(diméthylamino)-éthyl]amine) et a trouvé un état de transition à six membres impliquant Mg-$OCHPh_2$, H-Bpin et $O=CR_2$ [34]. Leur rapport fournit une nouvelle idée pour l'étude récente de l'hydroboration des cétones sans l'implication des hydrures métalliques. Ensuite, ils ont effectué la réaction en quantité équimolaire de PhMeCO et HBpin dans le toluène et ont observé les produits $[(Me_6Tren)MgOCHMePh]^+$ et $Ph_2C(H)OBpin$. nous pouvons voir que dans cette réaction, l'acétophénone muette PhCOMe est réduite au groupe alcoxy PhMeC(H)O, tandis qu'en même temps le groupe alcoxy du complexe métallique terminal est substitué au pinacol.ici $Ph_2C(H)O$ est considéré comme un ligand sacrificiel. Dans leurs expériences, ils ont étendu les aldéhydes pour générer le produit d'hydroboration (R_1R_2) CHO-Bpin, comme le dibenzaldéhyde et la 2-pentanone. Pour la cétone alkyl-substituée 2-pentanone, des rendements de 95 % ont pu être obtenus en une demi-heure. Mais pour la benzophénone, la réaction prend 14 heures et le rendement n'est que de 65%. Par conséquent, nous allons étudier ce phénomène d'un point de vue mécanique.

Le mécanisme d'hydroboration des cétones catalysé par l'alcoxyde de magnésium a été présenté. Le processus de génération de Ph_2CHO-Bpin à partir de la benzophénone a une barrière énergétique plus élevée, tandis que la génération de Me^nPrCHO-Bpin à partir de la 2-pentanone est plus stable. Ainsi, la réaction de la 2-pentanone est thermodynamiquement et cinétiquement plus favorable que celle de la benzophénone. La barrière énergétique de TS2' est seulement de 1,7kcal/mol et le produit est stable (-58,5kcal/mol). Par conséquent, le borohydrure de la 2-pentanone est plus favorable du point de vue cinétique et thermodynamique, ce qui est cohérent avec l'expérience. Ceci est cohérent avec l'expérience(Figure 13).

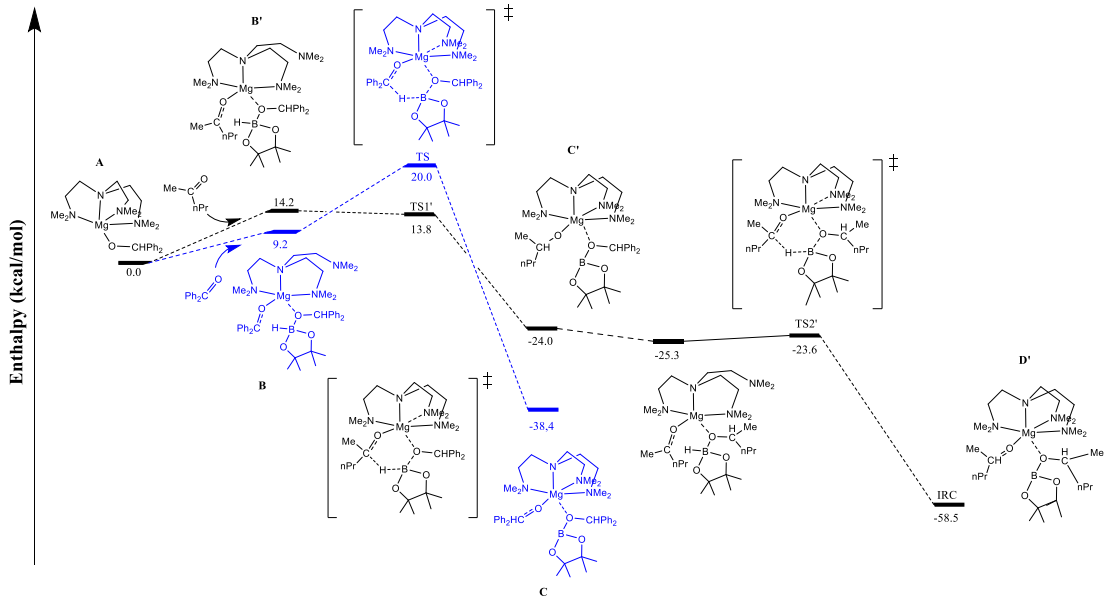

Figure 13 Profil enthalpique calculé pour l'hydroboration de la benzophénone catalysée par (Me_6Tren)MgOCHMePh, où la ligne bleue représente la réaction de la benzophénone et la ligne noire celle de la 2-pentanone.

Le mécanisme du borohydrure de cétone synergique catalysé par le magnésium et soutenu par des ligands N-polydentés nous a incités à étudier l'activité catalytique des simples alcoxydes de magnésium homoleptiques $Mg(OR)_2$. Par exemple, $Mg(OCHPh_2)_2$ agit comme un catalyseur pour la réaction avec la benzophénone et la HBpin pour produire des esters de bore dans des conditions sans solvant. Le rendement a atteint 90 %. Ce catalyseur facilement disponible s'est avéré posséder une

performance catalytique très efficace. Nous avons calculé ce processus à l'aide de la DFT. Initialement, la coordination de HBpin à $Mg(OR)_2$ a produit l'intermédiaire I. Ce processus est exothermique 24.3 kcal/mol. La réaction a continué exothermiquement après l'addition de benzophénone, produisant ainsi un intermédiaire II stable, dans lequel la benzophénone substitue les deux ligands HBpin sur Mg. L'hydrure du centre de bore interagit ensuite avec le carbone du carbonyle dans le Ph_2CO pour former l'état de transition III à six chaînons, qui présente une barrière énergétique très faible de 3,1 kcal/mol. L'intermédiaire IV est produit après l'état de transition III, où la benzophénone réduite et l'ester d'acide boronique restent liés au centre Mg. Le processus exotherme 27,6 kcal/mol. Le deuxième transfert de H sur l'épingle à cheveux se produit sur l'intermédiaire IV, avec une barrière énergétique de 9,6 kcal/mol pour l'état de transition à six chaînons V. Cela conduit ensuite à un intermédiaire stable, dans lequel les deux esters boroniques se lient à Mg(Figure 14).

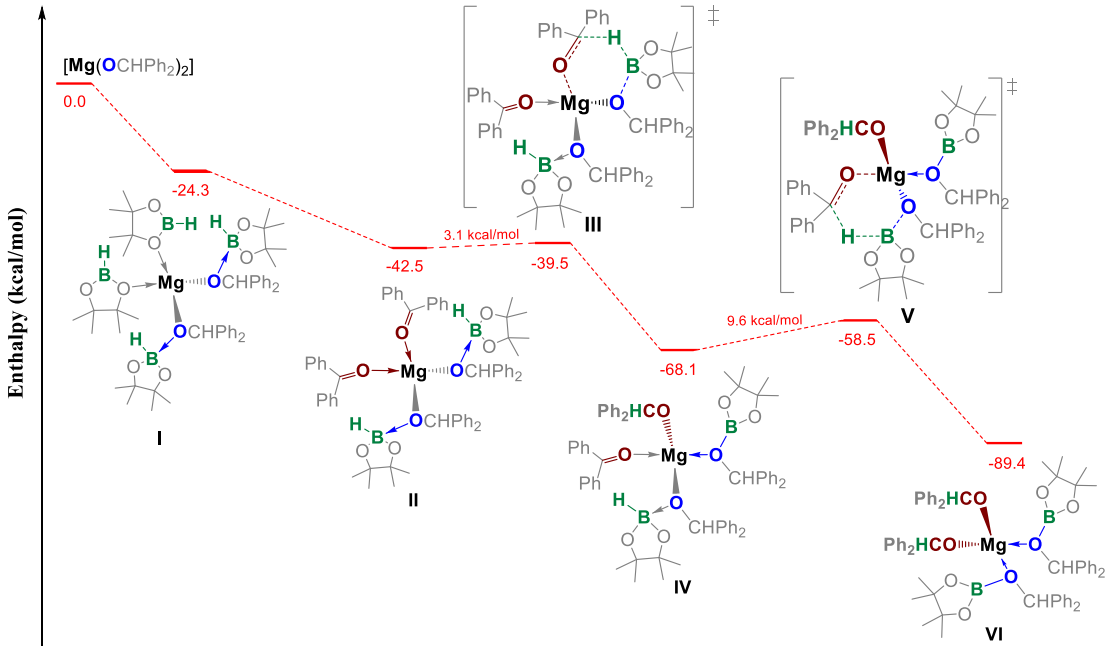

Figure 14 Profil enthalpique calculé pour l'hydroboration de la benzophénone catalysée par $Mg(OCHPh_2)_2$

La théorie informatique a démontré que la réaction utilisant l'hydroboration simple catalysée par $Mg(OCHPh_2)_2$ était cinétiquement et thermodynamiquement plus

favorable par rapport à $[(Me_6Tren)MgOCHPh_2]^+$, avec un exotherme de réaction final de 89,4 kcal/mol.

En résumé, nous fournissons des mécanismes pour les réactions d'activation de petites molécules inorganiques/organiques catalysées par des complexes métalliques des blocs d/f/s du tableau périodique des éléments en utilisant respectivement des calculs DFT. Dans une certaine mesure, les phénomènes expérimentaux d'activation de petites molécules catalysées par plusieurs catalyseurs sont expliqués séparément. Par exemple, les complexes de di-fer à bloc d supportés par le ligand pentadentate dianionique B_2Pz_4Py ont été considérés comme un bon catalyseur pour l'activation des réactions de l'ammoniac et de l'hydrazine, ainsi que la réaction de réduction avec l'oxyde nitreux a été utilisée pour examiner la réactivité des complexes d'imidophosphorane de di-fer comme catalyseurs. Par exemple, des calculs DFT ont également été utilisés pour expliquer la sélectivité de l'addition d'aldéhydes impliquant des complexes de lanthanides métalliques du bloc f et le mécanisme du couplage réducteur du CO_2 et du CS_2 médié par le samarium/ytterbium. Enfin, pour les métaux du bloc s, nous avons utilisé la réduction du CO pour vérifier la réactivité des complexes de Ca et nous avons également vérifié le mécanisme de l'hydroboration des cétones catalysée par les complexes d'alcoxyde de magnésium. Ces travaux pourraient fournir des idées sur le mécanisme d'activation catalytique de petites molécules pour les futurs complexes formés par divers ligands combinés à des centres métalliques, et pourraient servir d'exemple comparable. Actuellement, chacun des ligands que nous avons calculés est limité au même bloc du tableau périodique, et il serait intéressant de les étendre à l'application de différents blocs de centres métalliques à l'avenir.

---

1. Beh, D.W., et al., *Tandem deoxygenative hydrosilation of carbon dioxide with a cationic scandium hydridoborate and B (C 6 F 5) 3.* Dalton Transactions, 2020. **49**(1): p. 95-101.
2. Beh, D.W., et al., *Scandium alkyl and hydride complexes supported by a pentadentate diborate ligand: reactions with CO 2 and N 2 O.* Dalton

Transactions, 2018. **47**(38): p. 13680-13688.

3. Nurdin, L., et al., *Oxygen–oxygen bond cleavage and formation in Co (II)-mediated stoichiometric O2 reduction via the potential intermediacy of a Co (IV) oxyl radical.* Journal of the American Chemical Society, 2018. **140**(47): p. 16094-16105.
4. Nurdin, L., et al., *Reactions of Neutral Cobalt (II) Complexes of a Dianionic Tetrapodal Pentadentate Ligand: Cobalt (III) Amides from Imido Radicals.* Inorganic chemistry, 2017. **56**(7): p. 4157-4168.
5. Beh, D.W., et al., *Hydrolysis of scandium alkyl derivatives supported by a pentadentate diborate ligand: Interconversion of hydroxo and oxo complexes.* Polyhedron, 2020. **179**: p. 114410.
6. Lu, E., J. Chu, and Y. Chen, *Scandium terminal imido chemistry.* Accounts of chemical research, 2018. **51**(2): p. 557-566.
7. Rice, N.T., et al., *Homoleptic imidophosphorane stabilization of tetravalent cerium.* Inorganic chemistry, 2019. **58**(8): p. 5289-5304.
8. Warren, J.J., T.A. Tronic, and J.M. Mayer, *Thermochemistry of proton-coupled electron transfer reagents and its implications.* Chemical reviews, 2010. **110**(12): p. 6961-7001.
9. Nurdin, L., et al., *Activation of ammonia and hydrazine by electron rich Fe (ii) complexes supported by a dianionic pentadentate ligand platform through a common terminal Fe (iii) amido intermediate.* Chemical Science, 2021. **12**(6): p. 2231-2241.
10. Patrick, E.A., et al., *A monoanionic pentadentate ligand platform for scandium–pnictogen multiple bonds.* Chemical Communications, 2021. **57**(69): p. 8640-8643.
11. Gompa, T.P., et al., *The chemical and physical properties of tetravalent lanthanides: Pr, Nd, Tb, and Dy.* Dalton Transactions, 2020. **49**(45): p. 15945-15987.
12. Rice, N.T., et al., *Comparison of tetravalent cerium and terbium ions in a conserved, homoleptic imidophosphorane ligand field.* Chemical science, 2020.

11(24): p. 6149-6159.

13. Quintana, L.M.A., et al., *Chalcogen-Atom Abstraction Reactions of a Di-Iron Imidophosphorane Complex.* Chemical Communications, 2021.
14. Delabie, A., et al., *Evaluating the activation barriers for transition metal N2O reactions.* The Journal of Physical Chemistry A, 2001. **105**(22): p. 5479-5485.
15. Zhao, L., et al., *Theoretical investigation of the Fe+-catalyzed oxidation of acetylene by N2O.* The Journal of Physical Chemistry A, 2008. **112**(25): p. 5676-5683.
16. Li, C.-J., *Organic reactions in aqueous media with a focus on carbon− carbon bond formations: a decade update.* Chemical Reviews, 2005. **105**(8): p. 3095-3166.
17. Price, K., *Reductive Cyclisation Cascades of Lactones Using SmI 2-H 2 O*. 2011: The University of Manchester (United Kingdom).
18. Weitgenant, J.A., J.D. Mortison, and P. Helquist, *Samarium-promoted coupling of pyridine-based heteroaryl analogues of benzylic acetates with carbonyl compounds.* Organic letters, 2005. **7**(17): p. 3609-3612.
19. Weitgenant, J.A., et al., *Samarium-promoted coupling of 1, 10-phenanthroline with carbonyl compounds for synthesis of new ligands.* The Journal of organic chemistry, 2004. **69**(8): p. 2809-2815.
20. Jaoul, A., et al., *Atom economical coupling of benzophenone and N-heterocyclic aromatics with SmI 2.* Chemical Communications, 2020. **56**(79): p. 11875-11878.
21. Willauer, A.R., et al., *Carbon dioxide reduction by dinuclear Yb (ii) and Sm (ii) complexes supported by siloxide ligands.* Dalton Transactions, 2019. **48**(18): p. 6100-6110.
22. Mazzanti, M., et al., *CS2 Reductive Coupling to Acetylenedithiolate by a Dinuclear Ytterbium (II) Complex*. 2019.
23. Causero, A., et al., *Stabilization of calcium hydride complexes by fine tuning of amidinate ligands.* Organometallics, 2016. **35**(19): p. 3350-3360.
24. Jochmann, P., et al., *A Cationic Calcium Hydride Cluster Stabilized by Cyclen-*

Derived Macrocyclic N, N, N, N Ligands. Angewandte Chemie International Edition, 2012. **51**(18): p. 4452-4455.

25. Harder, S. and J. Brettar, *Rational Design of a Well-Defined Soluble Calcium Hydride Complex.* Angewandte Chemie, 2006. **118**(21): p. 3554-3558.
26. Leich, V., et al., *Molecular Calcium Hydride: Dicalcium Trihydride Cation Stabilized by a Neutral NNNN-Type Macrocyclic Ligand.* Angewandte Chemie International Edition, 2016. **55**(15): p. 4794-4797.
27. Shi, X., et al., *Super-Bulky Penta-arylcyclopentadienyl Ligands: Isolation of the Full Range of Half-Sandwich Heavy Alkaline-Earth Metal Hydrides.* Angewandte Chemie, 2019. **131**(13): p. 4400-4404.
28. Mukherjee, D., D. Schuhknecht, and J. Okuda, *Hydrido Complexes of Calcium: A New Family of Molecular Alkaline-Earth-Metal Compounds.* Angewandte Chemie International Edition, 2018. **57**(31): p. 9590-9602.
29. Hill, M.S., D.J. Liptrot, and C. Weetman, *Alkaline earths as main group reagents in molecular catalysis.* Chemical Society Reviews, 2016. **45**(4): p. 972-988.
30. Harder, S., *From limestone to catalysis: application of calcium compounds as homogeneous catalysts.* Chemical reviews, 2010. **110**(7): p. 3852-3876.
31. Shi, X., et al., *Mononuclear calcium complex as effective catalyst for alkenes hydrogenation.* Chemical Communications, 2020. **56**(38): p. 5162-5165.
32. Schuhknecht, D., et al., *Reactivity of a Molecular Calcium Hydride Cation ([CaH]+) Supported by an NNNN Macrocycle.* Inorganic Chemistry, 2020. **59**(13): p. 9406-9415.
33. Höllerhage, T., et al., *Calcium Hydride Catalysts for Olefin Hydrofunctionalization: Ring-Size Effect of Macrocyclic Ligands on Activity.* Chemistry (Weinheim an der Bergstrasse, Germany), 2021. **27**(9): p. 3002.
34. Banerjee, S., A. Andrews, and A. Venugopal, *A disguised hydride in a butylmagnesium cation.* Chemical Communications, 2018. **54**(45): p. 5788-5791.